SAR COMPLIANCE TESTING OF RF MICRO DEVICES 802.11a CARDBUS CARD MODEL DK5405 WITH TOSHIBA MODEL 1415-S173 HOST COMPUTER

FCC ID# RFN5405RDK0401

Host Computer: Toshiba Model 1415-S173
S/N: 9207316P

October 15, 2003

Prepared for: RF Micro Devices, Inc.
7628 Thorndike Road
Greenboro, NC 27409, U.S.A.

Prepared by: Om P. Gandhi
Professor of Electrical and Computer Engineering
University of Utah
50 S Central Campus Dr., Rm. 3280
Salt Lake City, UT 84112-9206

TABLE OF CONTENTS

SAR COMPLIANCE TESTING OF RF MICRO DEVICES 802.11a CARDBUS CARD MODEL DK5405 WITH TOSHIBA MODEL 1415-S173 HOST COMPUTER

FCC ID# RFN5405RDK0401

Host Computer: Toshiba Model 1415-S173
S/N: 9207316P

I. Introduction

We have used the measurement procedures outlined in FCC Supplement C (Edition 97-01) to OET Bulletin 65 [1] and an updated version of the same [2] for evaluating compliance of the RF Micro Devices Cardbus Card Model DK5405 (FCC ID# RFN5405RDK0401) inserted into Toshiba Model 1415-S173 Host Computer. Three photographs of the Toshiba Model 1415-S173 Host Computer with RF Micro Devices Cardbus Card Model DK5405 are given in Figs. 1a-c respectively. The RF Micro Devices Cardbus Card Model DK5405 uses two identical antennas that operate over the frequency band 5.18 to 5.32 GHz in the normal mode with conducted powers that are given in Table 1.

For SAR measurements, two configurations of the wireless PC relative to the experimental phantom have been used. These are as follows:

a. **Configuration 1** is for the wireless PC placed on a user's lap. For this configuration, a planar phantom model with inside dimensions 12" × 16.5" (30.5 × 41.9 cm) and a base thickness of 2.0 ± 0.2 mm (recommended in [2]) was used for SAR measurements and the bottom side of the laptop computer shown in Fig. 1 was pressed against it (see Fig. 2).

b. **Configuration 2** – Edge-on position. This configuration corresponds to a bystandar close to the outer edge of the Cardbus Card. For this configuration, the PC is placed at 90º with the edge of the RF Micro Devices Model DK5405 Cardbus Card pressed against the bottom of the planar phantom. A photograph for this edge-on position for SAR testing is given in Fig. 3.

II. The SAR Measurement System

The University of Utah SAR Measurement System has been described in peer-reviewed literature [3]. A photograph of the SAR Measurement System is given in Fig. 4. This SAR Measurement System uses a computer-controlled 3-D stepper motor system (Arrick Robotics MD-2A). A triaxial Narda Model 8021 E-field probe is used to determine the internal electric fields. The positioning repeatability of the stepper motor system moving the E-field probe is within ± 0.1 mm. Outputs from the three channels of the E-field probe are dc voltages, the sum of which is proportional to the square of the internal electric fields $\left(|E_i|^2\right)$ from which the SAR can be obtained from the equation SAR = $\sigma\left(|E_i|^2\right)/\rho$, where σ and ρ are the conductivity and mass density of the tissue-simulant materials, respectively [4]. The dc voltages for the three channels of the E-field probe are read by three HP 34401A multimeters and sent to the computer via an HPIB interface. The setup is carefully grounded and shielded to reduce the noise due to the electromagnetic interference (EMI). A cutout in a wooden table allows placement of a plastic holder (shown in Fig. 5) on which the laptop computer with the 802.11a wireless antennas (see Fig. 1) is supported. The plastic holder (see Fig. 5) can be moved up or down so that the base of the PC (for Configuration 1) is pressed against the base of the flat phantom for determination of SAR for Above-lap position (see Fig. 2). Similarly, for "Edge-On" SAR determination, Configuration 2, the laptop computer is mounted sideways (at 90°) on the plastic holder and moved up so that the edge of the RF Micro Devices Model DK5405 Cardbus Card is pressed against the bottom of the flat phantom (see Fig. 3).

The Flat Phantom

As recommended in Supplement C Edition 01-01 to OET Bulletin 65 [2], a planar phantom model with inside dimensions 12" × 16.5" (30.5 × 41.9 cm) and base thickness 2.0 ± 0.2 mm was used for SAR measurements (see Figs. 2, 3).

III. Calibration of the E-Field Probe

The IEEE Standard P1528 [5] suggests a recommended procedure for probe calibration (see Section 4.4.1 of [5]) for frequencies above 800 MHz where waveguide size is manageable. Calibration using an appropriate rectangular waveguide is recommended. As in some previously reported SAR measurements at 6 GHz [4], we have calibrated the Narda Model 8021 Miniature Broadband Electric Field Probe of tip diameter 4 mm (internal dipole dimensions on the order of 2.5 mm) using a rectangular waveguide WR 159 (of internal dimensions 1.59 × 0.795 inches) that was filled with the tissue-simulant fluid of composition given in Section V (see Figs. 2, 3). The triaxial (3 dipole) E-field probe shown in Fig. 7 was originally developed by Howard Bassen and colleagues of FDA and has been manufactured under license by Narda Microwave Corporation, Hauppage, New York. The probe is described in detail in references 6 and 7. It uses three orthogonal pick up dipoles each of length about 2.5 mm offset from the tip by 3 mm, each with its own leadless zero voltage Schottky barrier diode operating in the square law region. The sum of the three diode outputs read by three microvoltmeters [3] gives an output proportional to E^2. By rotating the probe around its axis, the isotropy of the probe was measured to be less than ± 0.23 dB and the deviation of the probe from the square law behavior was less than ± 3%.

As suggested in the IEEE Standard P1528, the waveguide (WR 159) filled with the tissue-simulant fluid was maintained vertically. From microwave field theory [see e.g. ref. 8], the transverse field distribution in the liquid corresponds to the fundamental mode (TE_{10}) with an exponential decay in the vertical direction (z-axis). The liquid level was 15 cm deep which is deep enough to guarantee that reflections from the top liquid surface do not affect the calibration. By comparing the square of the decaying electric fields expected in the tissue from the analytical expressions for the TE_{10} mode of the rectangular waveguide, we obtained a calibration factor of 2.98 (mW/kg)/μV with a variability of less than ± 2% for measurement frequencies of 5.25 and 5.8 GHz, respectively. This is no doubt due to a fairly limited frequency band of only 0.55 GHz out of a recommended bandwidth of 2.2 GHz for the TE_{10} mode for the WR159 waveguide (recommended band of 4.9-7.1 GHz -- see e.g. ref. 8) and the fact that the bandwidth of 550 MHz for the entire set of measurements is on the order of ± 5% of the midband frequencies.

The date for the calibration of the E-field probe closest to the SAR tests given here was October 10, 2003.

To verify that the probe calibration conducted for the 802.11a band with CW signals is also valid for modulated signals used for the Cardbus Card, two procedures have been used. These are described in Appendix A.

IV. SAR System Verification

It is very difficult to develop half wave dipole antennas for use in the 5.2 to 5.8 GHz band both because of fairly small dimensions and the resulting dimensional tolerances, and relatively narrow bandwidths of the required baluns – balanced-to-unbalanced transformers. On the other hand, waveguides are broadband with simultaneous bandwidths larger than 1-2 GHz and fairly easy to use for frequencies in excess of 3 GHz. As shown in Fig. 8, we have, therefore, developed a system verification system by using an open-ended, air-filled waveguide as an irradiation system placed at a distance of 8 mm below the base of the planar phantom (10 mm from the lossy fluid in the phantom). For this application, we have set up a WR 187 rectangular waveguide of internal dimensions 1.872" × 0.872" that is fed with microwave power from a Hewlett Packard Model 83620A Synthesized Sweeper (10 MHz-20 GHz). The operating (TE_{10} mode) band of this waveguide is from 3.95 to 5.85 GHz. The microwave circuit arrangement used for system verification is sketched in Fig. 9. When placed at a distance of 8 mm from the base of the planar phantom, the reflection coefficient is about 10-20%. As seen in Fig. 8, even this relatively small amount of reflection has been reduced to less than 0.5% by using a movable slide-screw waveguide tuner (Narda Model 22CI). The measured SAR distribution for peak 1-g SAR region using this system at 5.25 GHz for the day of the SAR measurements October 10, 2003, is given in Appendix B. Also given in Appendix B is the waveguide SAR plot for this date of SAR measurements. The peak 1-g SARs measured for 100 mW of radiated power for 5.25 GHz was 3.593 W/kg. The measured 1-g SAR is in excellent agreement with the FDTD-calculated 1-g SAR for this waveguide of 3.580 W/kg at 5.25 GHz. Also as expected, the measured SAR plot in Appendix B is quite symmetric at the irradiation frequency.

For FDTD-calculations of the SAR distributions for the WR187 rectangular waveguide irradiation system, we have used the dielectric properties for the phantom given in Table 2 that have been taken from [2]. Using a resolution of 0.5 mm for the FDTD cells, the calculated variations of the SAR distributions are given in Figs. 10a, b as a function of height above the bottom surface of the phantom. From Figs. 10a, b, it is obvious that the penetration of electromagnetic fields in the 5.2-5.8 GHz range is extremely shallow. The calculated depths of penetration corresponding to $1/e^2$-reduction of SAR (13.5% of the SAR at the surface) are only 6.85 and 5.95 mm at 5.25 and 5.8 GHz, respectively. Both of these depths of penetration for this near-field exposure system are very similar to those obtained for plane wave irradiation at these frequencies (7.15 mm for 5.25 GHz and 6.25 mm for 5.8 GHz).

Also shown in Figs. 10a, b are the SAR variations measured for this waveguide exposure system at depths of 4, 6, 8, 10, 12, and 14 mm in the tissue-simulant fluid. We tried second-, third-, fourth-, and fifth-order polynomial least-square fits to extrapolate the measured SARs to depths of 1, 3, 5, 7, and 9 mm. As seen in Figs. 10a, b, the fourth-order polynomial provides an excellent agreement with the FDTD-calculated in-depth variation of SAR both at 5.25 and 5.8 GHz. Also as aforementioned, the peak 1-g SARs thus obtained for 100 mW of radiated power for 5.25 and 5.80 GHz of 3.593 and 4.020 W/kg are extremely close to the FDTD-calculated 1-g SARs for this waveguide of 3.580 and 3.946 W/kg at the two frequencies, respectively.

V. Tissue Simulant Fluid for the Frequency Band 5.2 to 5.8 GHz

In OET 65 Supplement C [2], the dielectric parameters suggested for body phantom are given only for 3000 and 5800 MHz. These are listed in Table 2 here. Using linear interpolation, we can obtain the dielectric parameters to use for the frequency band between 5.25 to 5.8 GHz.

The desired dielectric properties thus obtained are also given in Table 2. From Table 2, it can be noticed that the desired dielectric constant ε_r varies from 48.2 to 49.0 which is a variation of less than ± 1% from the average value of 48.6 for this band. Also the conductivity σ varies linearly with frequency from 5.3 to 6.00 S/m.

No tissue-simulant fluids have been suggested in any of the existing standards or draft standards [2, 5, 9, 10]. Because of this limitation, some of the standards are only written for frequencies up to 3 GHz [e.g. refs. 5, 9]. During the last several months, we have looked at over 40 liquid mixtures of the following broad categories to decide on a fluid that would give the peak 1-g SAR for 802.11a antennas operating at frequencies 5.15 to 5.35 and 5.745 to 5.845 GHz that are comparable to those obtained for the FCC-recommended dielectric properties [2]. The categories of fluids studied for determination of dielectric properties $(\varepsilon', \varepsilon'')$ using Hewlett Packard Model 85070B Dielectric Probe and the latest software 85070d provided by the company are:

a. Deionized water.
b. Deionized water and HEC mixtures (with HEC being 1-4%).
c. Deionized water, polyethylene powder (PEP) and HEC mixtures.
d. Mannitol, deionized water, HEC mixtures.
e. Sugar, deionized water, HEC mixtures.

The screen-dumps for some of the representative fluids studied are given in Appendix C, Figs. C.1-C.5, respectively. For each of the cases, the conductivity σ for the fluid may be obtained by multiplying ε'' by $\omega\varepsilon_o$ where $\omega = 2\pi f$ and ε_o is the permittivity of free space, 8.854×10^{-12} F/m. The measured ε', σ thus determined for frequencies of 5.25 and 5.8 GHz typical of 802.11a band are given in Table 3. Looking at Table 3, it is clear that the dielectric properties for pure deionized water are undesirable (the dielectric constant is too high even though the conductivities σ are no more than 10% larger than the desired values); the deionized water/PEP/HEC mixture and mannitol/water/HEC combinations are quite acceptable with dielectric constants within 1-3% and conductivities within 6-12% of the desired values. However, these two fluids have an undesirable feature that they are not transparent. The sugar/water/HEC mixture, on the other hand, is transparent. While giving the dielectric constants ε' that are within 1-3% of the desired values, the conductivity of this otherwise desirable fluid is about 27-30% higher than the desired values.

It was decided to determine SAR distributions and peak 1-g SARs for the three somewhat desirable fluids marked 3, 4, and 5 using an open-ended waveguide (WR187) as an irradiator that has been proposed for SAR system validation [11, attached as Appendix D]. Given in Table 4 are the peak 1-g SARs determined for fluids 3, 4, and 5 (of Table 3). Also given for comparison is the FDTD-calculated values both at 5.25 and 5.8 GHz using an FDTD-grid size of 0.5 mm for the dielectric properties recommended by FCC ($\varepsilon' = 48.9$, $\sigma = 5.36$ S/m for 5.25 GHz; $\varepsilon' = 48.2$, $\sigma = 6.00$ S/m at 5.8 GHz). It is most interesting to note that in spite of up to 30% higher conductivity for the sugar/water/HEC fluid 5 (of Table 3), the peak 1-g SAR is within ± 1.5% of that for the FCC-recommended dielectric properties [2] both at 5.25 and 5.86 Hz. This result was most surprising and led us to a detailed study of the effect of dielectric properties on the peak 1- and 10-g SAR for the 802.11a frequencies described as a part of the paper that has been accepted for publication in *IEEE Transactions on Electromagnetic Compatibility* [12, attached as Appendix E]. In this study, we have taken conductivities that are up to 150% of the values recommended by FCC [2] at 5.25 and 5.8 GHz to show that the peak 1-g SARs vary by no more than ± 2% for typical near-field sources such as a waveguide and a microstrip antenna of dimensions typical of 802.11a antennas (see Tables 1, 2 of Appendix E). As explained in [12], this is due to higher surface SAR but shallower depth of penetration of EM fields for the higher conductivity media resulting in nearly identical SARs for cubical volumes associated with 1- or 10-g of tissue, respectively. This point is illustrated in Figs. 11 and 12 for 5.25 and 5.8 GHz, respectively.

VI. The Measured SAR Distributions

The RF power outputs measured for the RF Micro Devices Model DK5405 Cardbus Card for the normal mode are given in Table 1. For SAR measurements, we selected frequencies of

5.18, 5.26, and 5.32 GHz. The various frequencies were selected both for their highest power outputs as well as to cover the frequency band planned for this PC. As recommended in Supplement C, Edition 01-01 [2], the stability of the conducted power was determined by repeated SAR measurements at the same location for each of the selected channels. The variability of the SAR thus determined for three repeated measurements over a 60-minute time period was within ± 0.1 dB (± 2.5%).

The highest SAR region for each of the measurement frequencies was identified in the first instance by using a coarser sampling with a step size of 8.0 mm over three overlapping areas for a total scan area of 11.2 × 19.2 cm. The data thus obtained was resolved into a 4 × 4 times larger grid i.e. a grid involving 56 × 96 points by linear interpolation using a 2 mm step size. After thus identifying the region of the highest SAR, the SAR distribution was then measured with a resolution of 2 mm in order to obtain the peak 1 cm^3 or 1-g SAR. The SAR measurements were performed at 4, 6, 8, 10, 12 mm height from the bottom surface of the body-simulant fluid. The SARs thus measured were extrapolated using a fourth-order least-square fit to the measured data to obtain the SAR variation correctly for the 802.11a frequencies of 5.2 to 5.8 GHz [11, attached as Appendix D]. This allowed us to obtain SAR values at 1, 3, 5, 7 and 9 mm height that were used to obtain 1-g SARs. The uncertainty analysis of the University of Utah SAR measurement system is given in Appendix F. The combined standard uncertainty is ± 8.3%.

As determined by the coarse scans, the highest SAR region was invariably found for the 11.2 × 19.2 cm area immediately below the Cardbus Card for the "Above-lap" Configuration 1 and above the projected area of the antenna for the "Edge-on" Configuration 2. The coarse scans for these highest SAR regions are given in Appendix G, Figs. G.1 to G.6. In these figures, the two axes are marked in units of step size of 8 mm. Also shown in these figures are the respective antenna outlines overlaid on the SAR contours. It is interesting to note that the highest SAR regions are immediately above the two antennas used for this Cardbus Card. Also given in Appendix G as Tables G.1 to G.6 are the SAR distributions for the highest SAR region of volume 10 × 10 × 10 mm for which the coarse scans are given in Figs. G.1 to G.6, respectively. The SARs are given for xy planes at heights Z of 1, 3, 5, 7, and 9 mm from the bottom of the flat phantom. The individual SAR values for this grid of 5 × 5 × 5 or 125 points are averaged to obtain peak 1-g SAR values (for a volume of 1 cm^3). The temperature variation of the tissue-simulant fluid measured with a Bailey Instruments Model BAT 8 Temperature Probe for measurements at the various frequencies was $23.0 \pm 0.2^{\circ}C$.

The z-axis scan plots taken at the highest SAR locations for each set of tests are given in Appendix H. As discussed in Section IV, the SARs drop off fairly rapidly with depth in the phantom.

The SAR measurement results for the RF Micro Devices Cardbus Card Model DK5405 (FCC ID# RFN5405RDK0401) inserted into Toshiba Model 1415-S173 Host Computer are summarized in Table 5. All of the measured 1-g SARs are less than the FCC 96-326 guideline of 1.6 W/kg.

VII. Comparison of the Data with FCC 96-326 Guidelines

According to the FCC 96-326 Guideline, the peak SAR for any 1-g of tissue should not exceed 1.6 W/kg. For the RF Micro Devices Cardbus Card Model DK5405 (FCC ID# RFN5405RDK0401) inserted into Toshiba Model 1415-S173 Host Computer, the measured peak 1-g SARs vary from 0.122 to 0.610 W/kg which are smaller than 1.6 W/kg.

REFERENCES

1. K. Chan, R. F. Cleveland, Jr., and D. L. Means, "Evaluating Compliance With FCC Guidelines for Human Exposure to Radiofrequency Electromagnetic Fields," Supplement C (Edition 97-01) to OET Bulletin 65, December, 1997. Available from Office of Engineering and Technology, Federal Communications Commission, Washington D.C., 20554.

2. Federal Communications Commission "Supplement C Edition 01-01 to OET Bulletin 65 Edition 97-01" June 2001.

3. Q. Yu, O. P. Gandhi, M. Aronsson, and D. Wu, "An Automated SAR Measurement System for Compliance Testing of Personal Wireless Devices," *IEEE Transactions on Electromagnetic Compatibility,* Vol. 41(3), pp. 234-245, August 1999.

4. O. P. Gandhi and J-Y. Chen, "Electromagnetic Absorption in the Human Head from Experimental 6-GHz Handheld Transceivers," *IEEE Transactions on Electromagnetic Compatibility*, Vol. 39(4), pp. 547-558, 1995.

5. IEEE Standard P1528, "Recommended Practice for Determining the Peak Spatial-Average Specific Absorption Rate (SAR) in the Human Body Due to Wireless Communication Devices: Experimental Techniques," 2003.

6. H. Bassen. M. Swicord, and J. Abita, "A Miniature Broadband Electric Field Probe," Ann. New York Academy of Sciences, Vol. 247, pp. 481-493, 1974.

7. H. Bassen and T. Babij, "Experimental Techniques and Instrumentation," Chapter 7 in *Biological Effects and Medical Applications of Electromagnetic Energy*, O. P. Gandhi, Editor, Prentice Hall Inc., Englewood Cliffs, NJ, 1990.

8. O. P. Gandhi, *Microwave Engineering and Applications,* Pergamon Press, New York, 1981.

9. European Standard EN50361, "Basic Standard for the Measurement of Specific Absorption Rate Related to Human Exposure to Electromagnetic Fields from Mobile Phones (300 MHz-3 GHz)," CENELEC, Central Secretariat: rue de Stassart 35, B-1050, Brussels.

10. Draft IEC PT62209 Part 2, "Procedure to Measure the Specific Absorption Rate (SAR) for Two-Way Radios, Palmtop Terminals, Laptop Terminals, Desktop Terminals, and Body-Mounted Devices Including Accessories and Multiple Transmitters (30 MHz to 6 GHz)," Draft version 0.6.

11. Q. Li, O. P. Gandhi, and G. Kang, "An Open-Ended Waveguide System for SAR System Validation and/or Probe Calibration for Frequencies above 3 GHz," submitted for publication to *IEEE Transactions on Microwave Theory and Techniques*, June 2003 (attached here as Appendix D).

12. G. Kang and O. P. Gandhi, "Effect of Dielectric Properties on the Peak 1- and 10-g SAR for 802.11 a/b/g Frequencies 2.45 and 5.15 to 5.85 GHz," accepted for publication in *IEEE Transactions on Electromagnetic Compatibility* (attached here as Appendix E).

Table 1. Peak conducted RF power outputs measured at various frequencies for the RF Micro Devices Model DK5405 Cardbus Card inserted into Toshiba Model 1415-S173 Host Computer for the normal mode used for this PC.

Frequency MHz	Conducted RF Power (dBm)
5180	16.5
5260	14.6
5320	15.1

Table 2. Dielectric parameters for body phantom for the frequency band 5.2 to 5.8 GHz [2].

Frequency (GHz)	ε_r	σ (S/m)	Reference
3.0	52.0	2.73	Ref. 2
5.8	48.2	6.00	Ref. 2
5.25	49.0	5.30	Interpolated
5.3	48.9	5.42	Interpolated
5.4	48.7	5.53	Interpolated
5.6	48.5	5.77	Interpolated
5.7	48.3	5.88	Interpolated

Table 3. The measured dielectric constants and conductivities σ for some fluids for frequencies 5.25 and 5.8 GHz.

Fluid	5.25 GHz		5.8 GHz	
	ε′	σ S/m	ε′	σ S/m
1. Deionized water	72.97	5.54	71.82	6.61
2. Deionized water (96%), HEC (4%)	68.89	5.81	67.78	6.90
3. Deionized water (82%), polyethylene powder (16%), HEC (2%)	49.31	4.77	47.99	5.64
4. Mannitol (31.5%), deionized water (67.5%), HEC (1%)	47.59	5.80	47.30	6.74
5. Sugar (31%), deionized water (68.0%), HEC (1%)	48.79	6.82	46.86	7.83

Table 4. Comparison of the measured and calculated peak 1-g SAR at 5.25 and 5.8 GHz.

	5.25 GHz			5.8 GHz		
	ε′	σ S/m	1-g SAR W/kg	ε′	σ S/m	1-g SAR W/kg
FCC body [2]; calculated	48.9	5.36	3.57	48.2	6.00	3.95
Fluid 3 of Table 3, water/PEP/HEC; measured	49.3	4.77	3.55	48.0	5.64	3.91
Fluid 4 of Table 3, Mannitol/water/HEC; measured	47.6	5.80	3.59	47.3	6.74	3.93
Fluid 5 of Table 3, sugar/water/HEC; measured	48.8	6.82	3.62	46.9	7.83	3.94

Table 5. The SAR measurement results for the normal mode for RF Micro Devices Model DK5405 Cardbus Card inserted into Toshiba Model 1415-S173 Host Computer (FCC ID# RFN5405RDK0401).

Liquid temperature = 23.0 ± 0.2°C
Measurement date: October 10, 2003

Configu -ration	Separation from Phantom (cm)	Frequency (GHz)	Conducted RF Output Power (dBm)		1-g SAR (W/kg)	See Appendix G Table	See Appendix G Figure
			Before	After			
1	0	5.18	16.50	16.52	0.122	G.1	G.1
	0	5.26	14.60	14.57	0.148	G.2	G.2
	0	5.32	15.10	15.14	0.157	G.3	G.3
2	0	5.18	16.47	16.51	0.491	G.4	G.4
	0	5.26	14.63	14.66	0.468	G.5	G.5
	0	5.32	15.12	15.11	0.610	G.6	G.6

a. Top cover with screen open.

Fig. 1. Photograph of the Toshiba Model 1415-S173 Host Computer with RF Micro Devices Cardbus Card Model DK5405 inserted in it.

b. View from the bottom side of the laptop computer.

Fig. 1. Photograph of the Toshiba Model 1415-S173 Host Computer with RF Micro Devices Cardbus Card Model DK5405 inserted in it.

c. Side view showing the Cardbus Card edge.

Fig. 1. Photograph of the Toshiba Model 1415-S173 Host Computer with RF Micro Devices Cardbus Card Model DK5405 inserted in it.

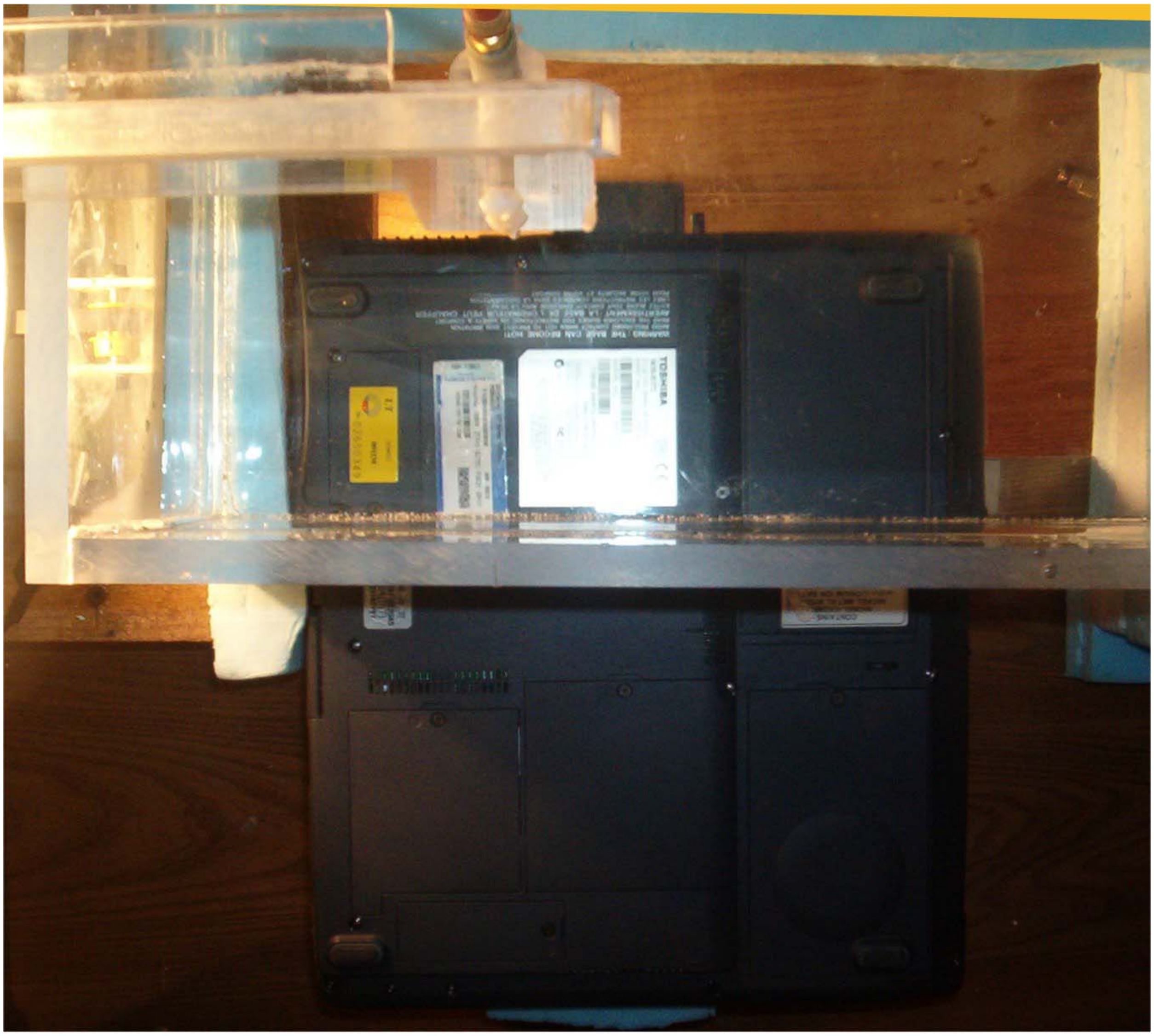

Fig. 2. Photograph of the bottom of the Toshiba Model 1415-S173 Host Computer with RF Micro Devices Cardbus Card Model DK5405 pressed against the bottom of the planar phantom. This is **Configuration 1 – Laptop position** for SAR testing.

Fig. 3. Photograph of the Toshiba Model 1415-S173 Host Computer at 90º with the edge of the RF Micro Devices Cardbus Card Model DK5405 pressed against the bottom of the planar phantom. This is **Configuration 2** for SAR testing and represents the case of a bystander at a distance of 0 cm from the edge of the Cardbus Card.

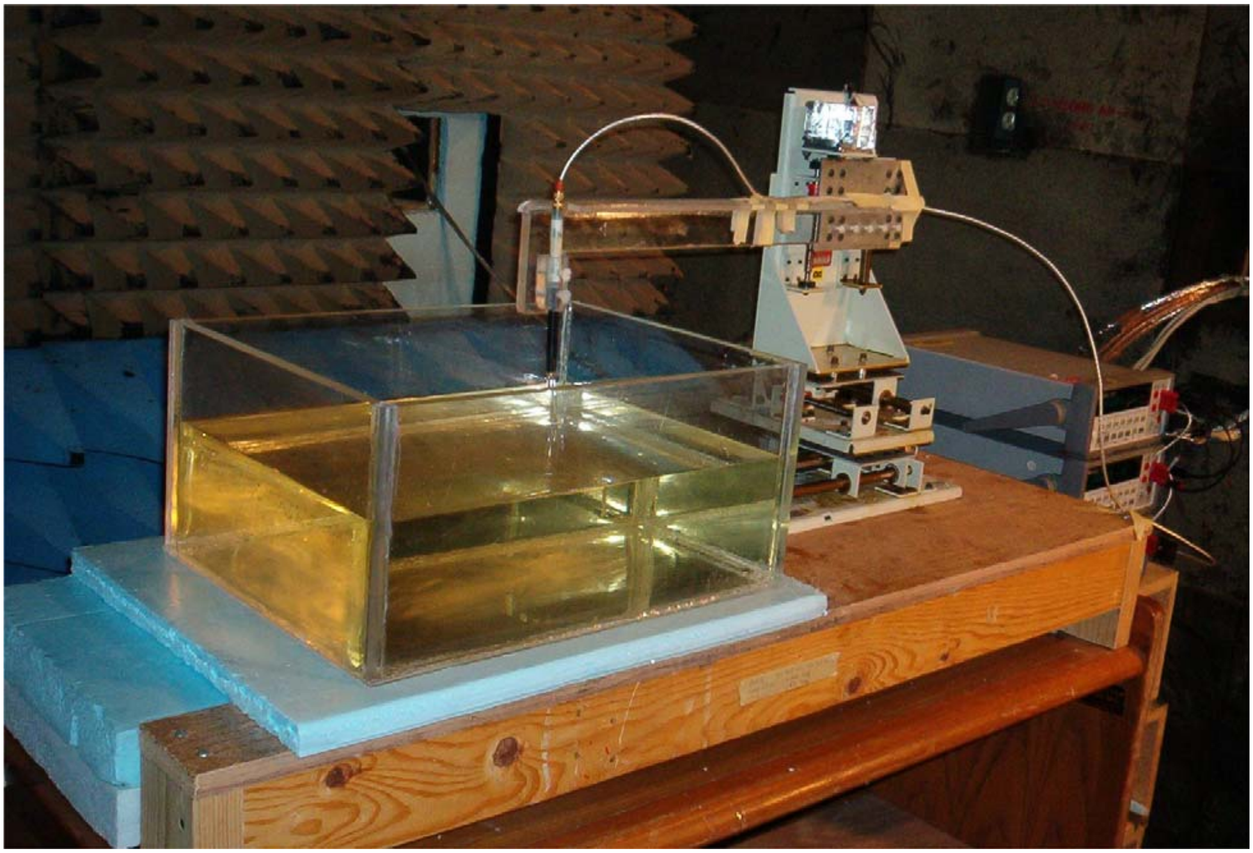

Fig. 4. Photograph of the three-dimensional stepper-motor-controlled SAR measurement system using a planar phantom.

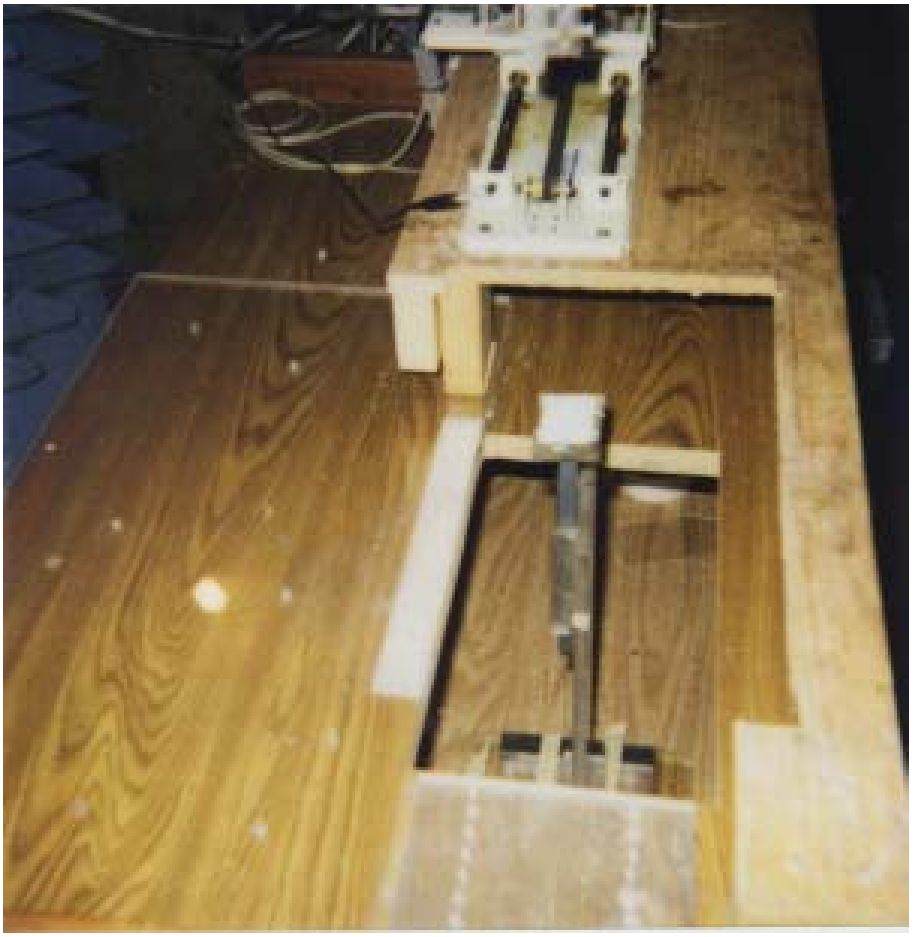

Fig. 5. The plastic holder used to support the portable PC for SAR measurements.

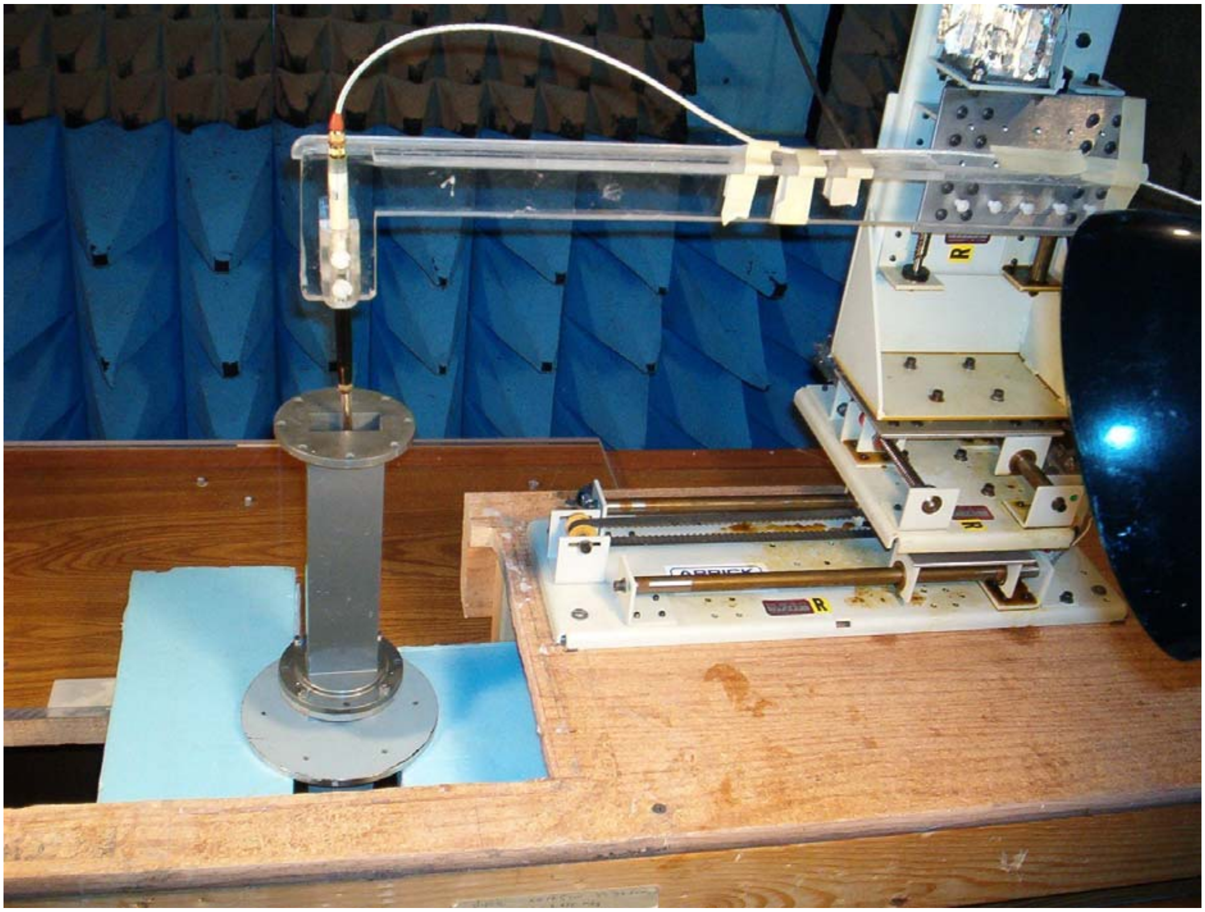

Fig. 6a. A photograph of the waveguide setup used for calibration of the Narda Model 8021 E-field probe in the frequency band 5.2-5.8 GHz.

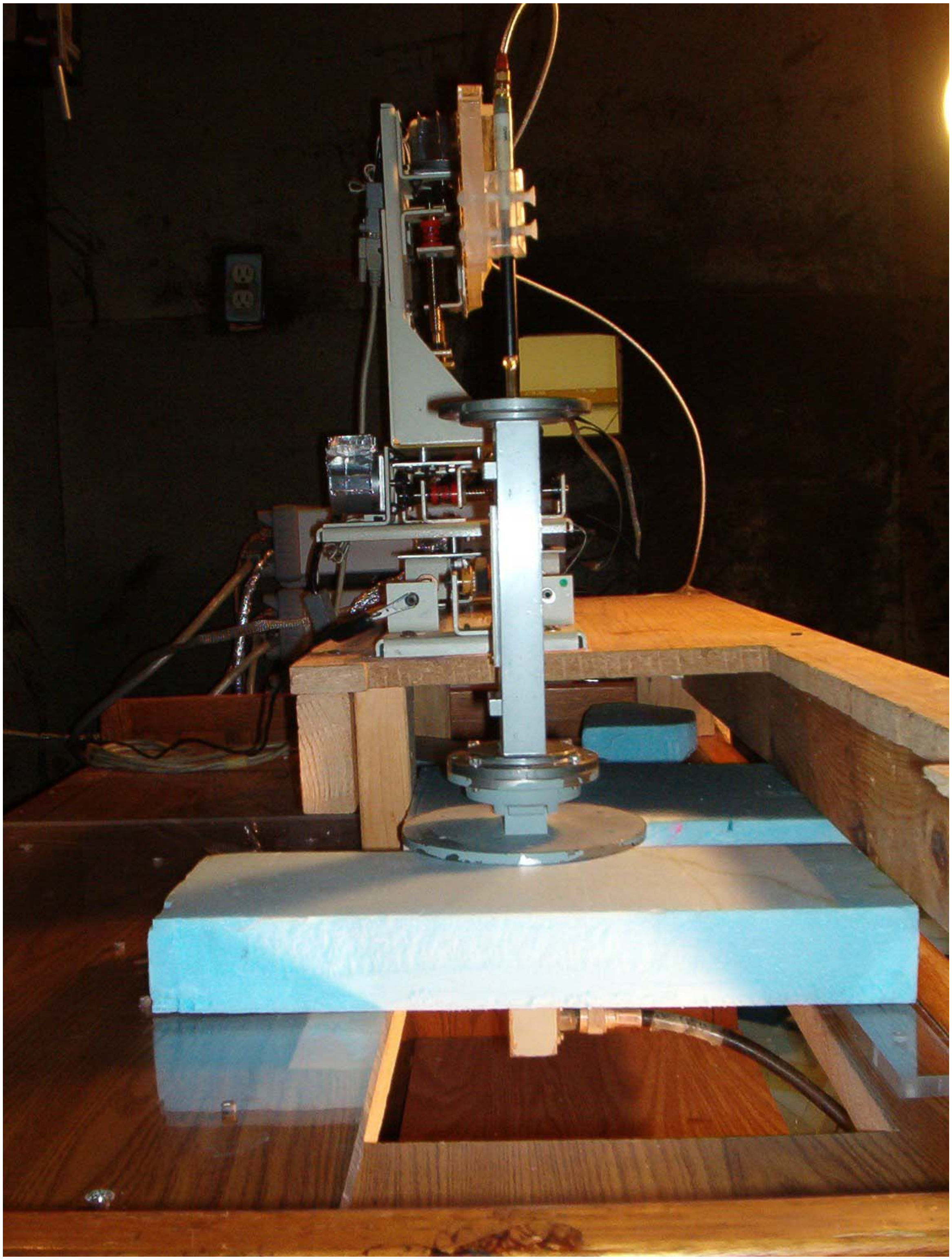

Fig. 6b. Photograph of the waveguide setup showing also the coax to waveguide coupler at the bottom used to feed power to the vertical waveguide containing the tissue-simulant fluid.

Fig. 7. Photograph of the Narda Model 8021 Broadband Electric Field Probe used for SAR measurements.

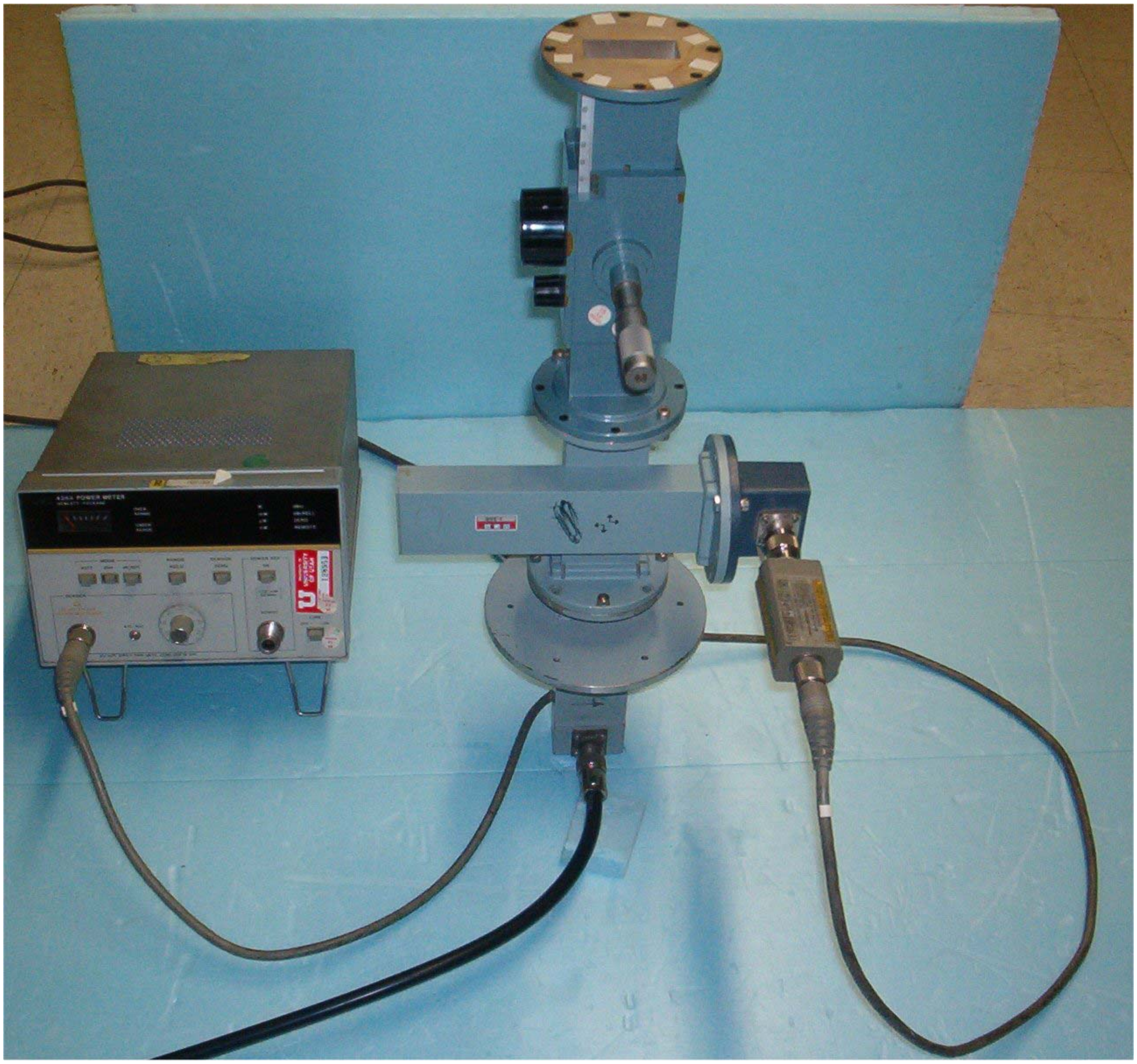

Fig. 8. Photograph of the rectangular waveguide radiator used for system verification for the 802.11a band. Also seen is the Narda Model 22CI movable slide screw tuner used to match the input power at 5.25 or 5.8 GHz to the planar phantom.

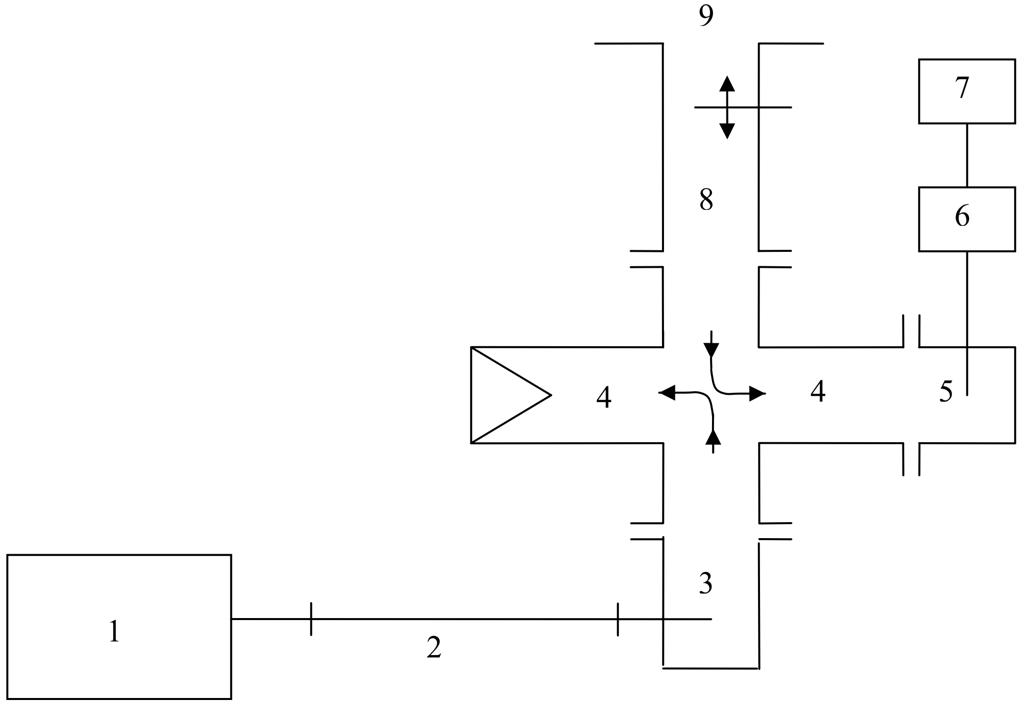

1. Hewlett Packard (HP) Model 83620A Synthesized Sweeper (10 MHz-20 GHz).
2. Coaxial line.
3. Coaxial to waveguide adapter.
4. 20 dB crossguide coupler (may be reversed to measure incident power).
5. HP Model G281A coaxial to waveguide adapter
6. HP Model 8482A power sensor.
7. HP Model 436A power meter.
8. Narda Microline® Slide Screw Tuner Model 22CI.
9. Radiating open end of the waveguide.

Fig. 9. The microwave circuit arrangement used for SAR system verification for the 802.11a band.

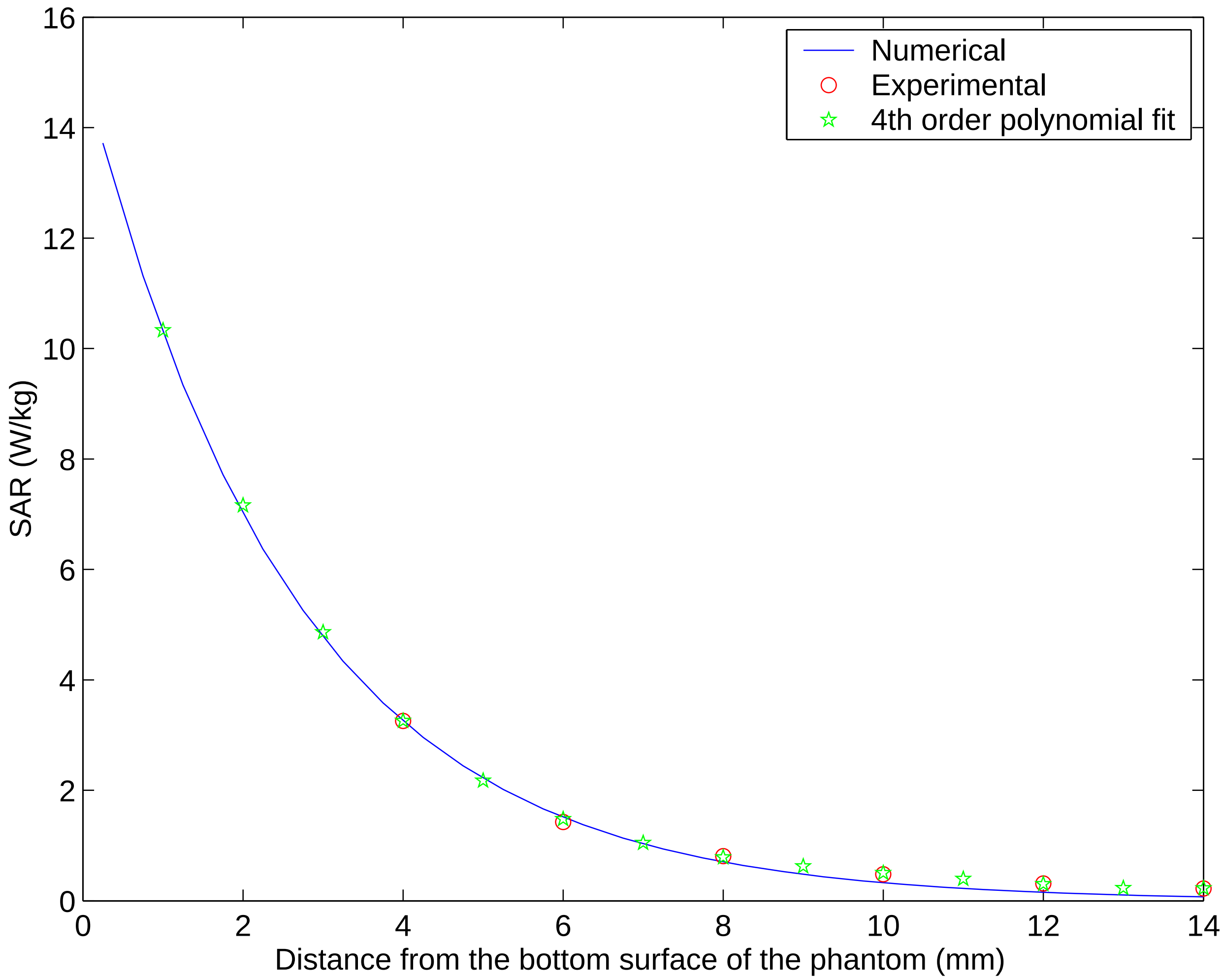

a. 5.25 GHz.

Fig. 10. Experimentally measured, extrapolated and FDTD-calculated variation of the SAR with depth in the body-simulant planar phantom. Radiated power = 100 mW.

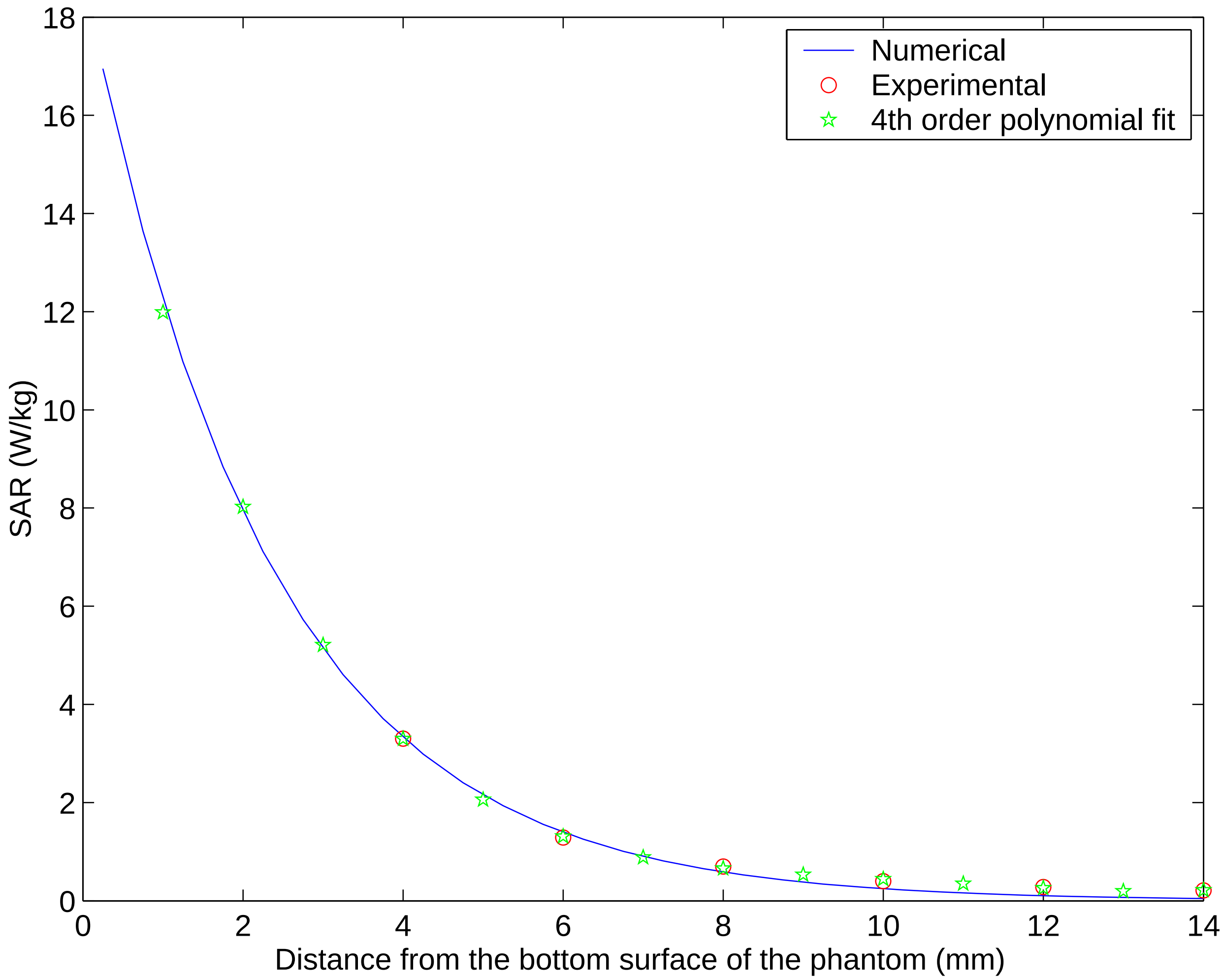

b. 5.80 GHz.

Fig. 10. Experimentally measured, extrapolated and FDTD-calculated variation of the SAR with depth in the body-simulant planar phantom. Radiated power = 100 mW.

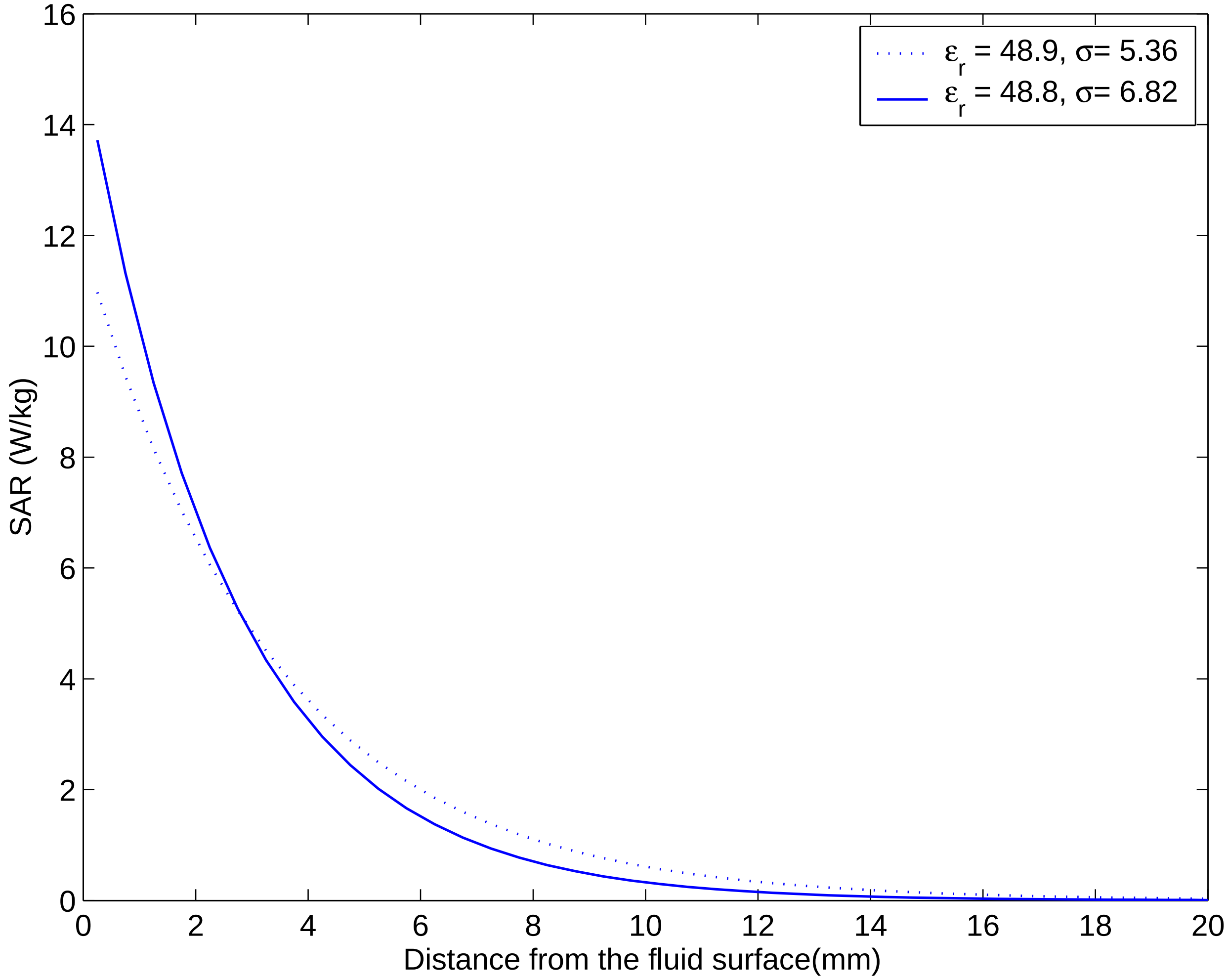

Fig. 11. Comparison of the FDTD-calculated variations of the SAR with depth for the FCC-recommended dielectric properties (ε' = 48.9, σ = 5.36 S/m) and the sugar/water/HEC fluid 5 (ε' = 48.8, σ = 6.82 S/m) at **5.25 GHz**. Assumed for calculations is the WR187 rectangular waveguide radiator placed 10 mm below the bottom surface of the tissue-simulant fluid in a flat phantom of base thickness 2 mm with ($\varepsilon_r = 2.56$). Radiated power = 100 mW.

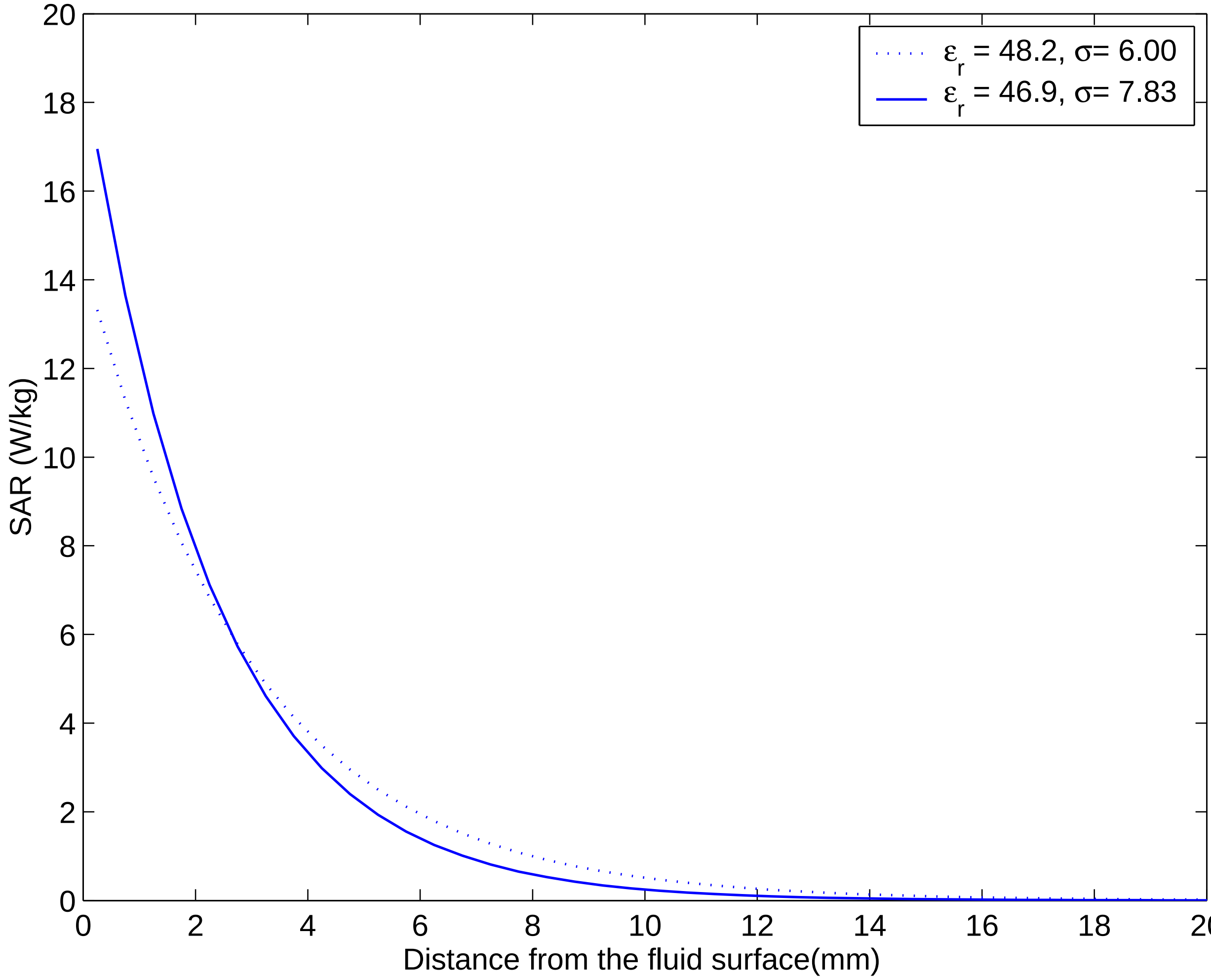

Fig. 12. Comparison of the FDTD-calculated variations of the SAR with depth for the FCC-recommended dielectric properties (ε' = 48.2, σ = 6.00 S/m) and the sugar/water/HEC fluid 5 (ε' = 46.9, σ = 7.83 S/m) at **5.8 GHz**. Assumed for calculations is the WR187 rectangular waveguide radiator placed 10 mm below the bottom surface of the tissue-simulant fluid in a flat phantom of base thickness 2 mm with ($\varepsilon_r = 2.56$). Radiated power = 100 mW.

APPENDIX A

Procedures to Demonstrate that E-Field Probe Calibration for CW Signals is Also Valid for Modulated Signals

Procedure 1

For the microvoltmeters in our SAR system (HP34401 multimeters), we use an AC signal filter with a passband of 20 Hz to 300 kHz (1 reading/second). This allows faithful readings of the rectified values of voltage outputs from the three pickup antennas (proportional to E^2) of the E-field probe used for SAR measurements. For a variety of modulated signals used for the 802.11a band, the multimeter passband of 20 Hz to 300 kHz is more than sufficient to read all of the frequency components. We have tested the validity of using this AC signal filter by applying signals from a Hewlett Packard Model 83620A Synthesized Sweeper operating at 5.25 and 5.8 GHz in the CW mode as well as the pulse mode with pulse repetition rates for the latter variable from 50 to 500 Hz and pulse duration variable from 0.5 to 1 msec. For a fixed location of the E-field probe, the SAR readings were proportional to the time-averaged radiated power (from 2.5 to 100 mW) from the WR187 rectangular waveguide at 5.25 and 5.8 GHz, respectively. Thus the probe calibration factors are no different for CW signals or for pulsed signals.

Procedure 2

As explained above, the passband of our SAR measurement system extends from 20 Hz to 300 kHz. This passband is more than sufficient to read all of the frequency components associated with OFDM or any of the other modulations that may be used for the 802.11a band.

Additional experiments have, however, been done to compare the SAR measured at one of the points in the planar phantom for OFDM modulated signals from the 802.11a Mini PCI and comparing the same with the CW signal of similar time-averaged power levels obtained from the Hewlett-Packard (HP) Model 83620A Synthesized Sweeper (10 MHz-20 GHz). For each of the two RF sources, the power output was measured using a microwave circuit arrangement similar to that of Fig. 11 of the SAR Report. As shown in this figure, the irradiation system uses a

WR187 rectangular waveguide (see Fig. 10 of the SAR Report) which is placed at a distance of 8 mm below the base of the planar phantom (10 mm from the lossy fluid in the phantom) used for SAR measurements.

Shown in Figs. A.1 and A.2 is a comparison of the SARs measured for a given location in the planar phantom for CW and 802.11a band modulated signals for the base mode at 5.32 GHz and 5.765 GHz, respectively. An excellent agreement in the SAR reading is observed whether CW or modulated signals are used. This is due to the broad bandwidth (20 Hz to 300 kHz) of the system used for measuring rectified signals from the E-field probe.

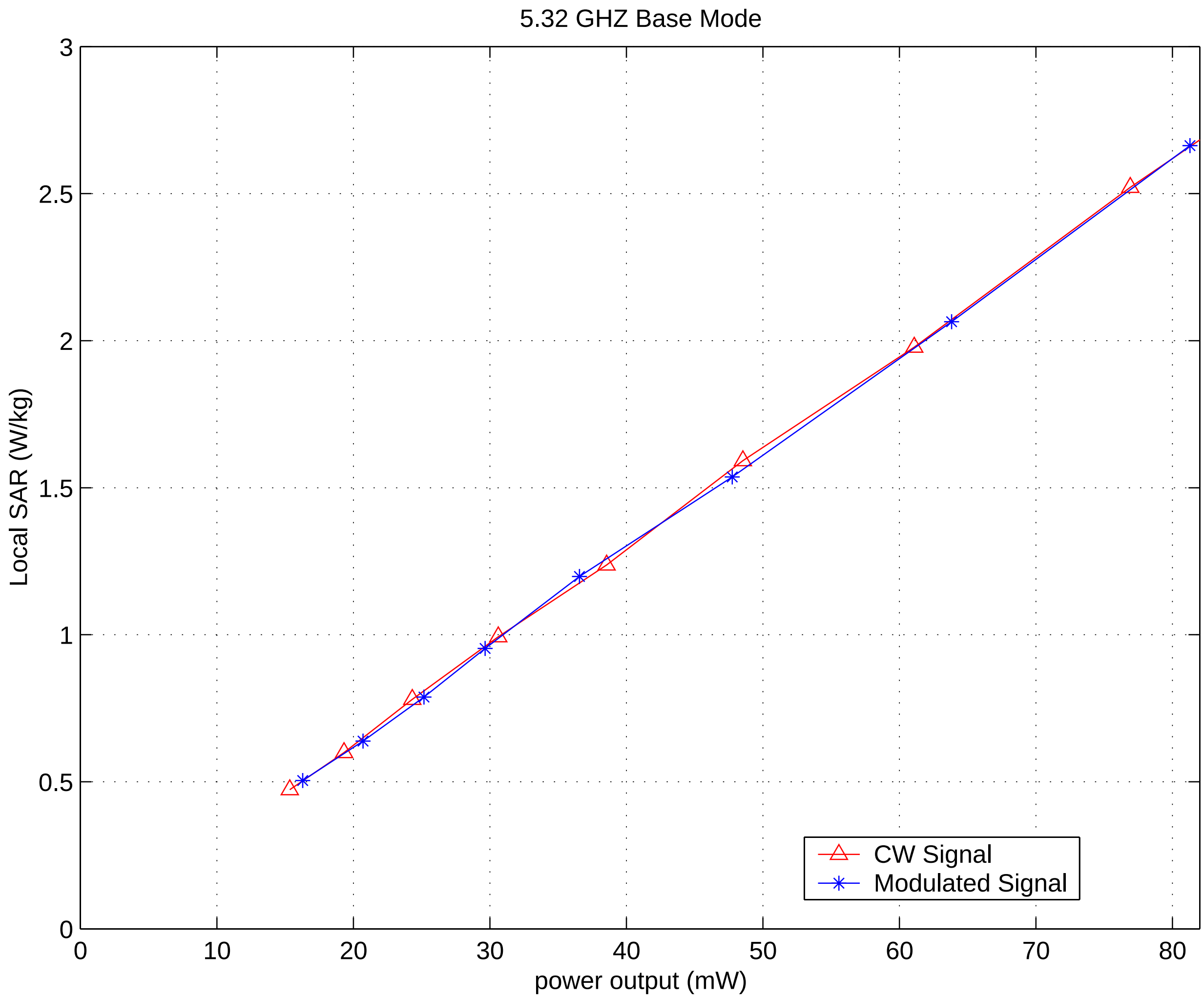

Fig. A.1. Comparison of the SAR for CW or OFDM modulated signals for the base mode at 5.32 GHz.

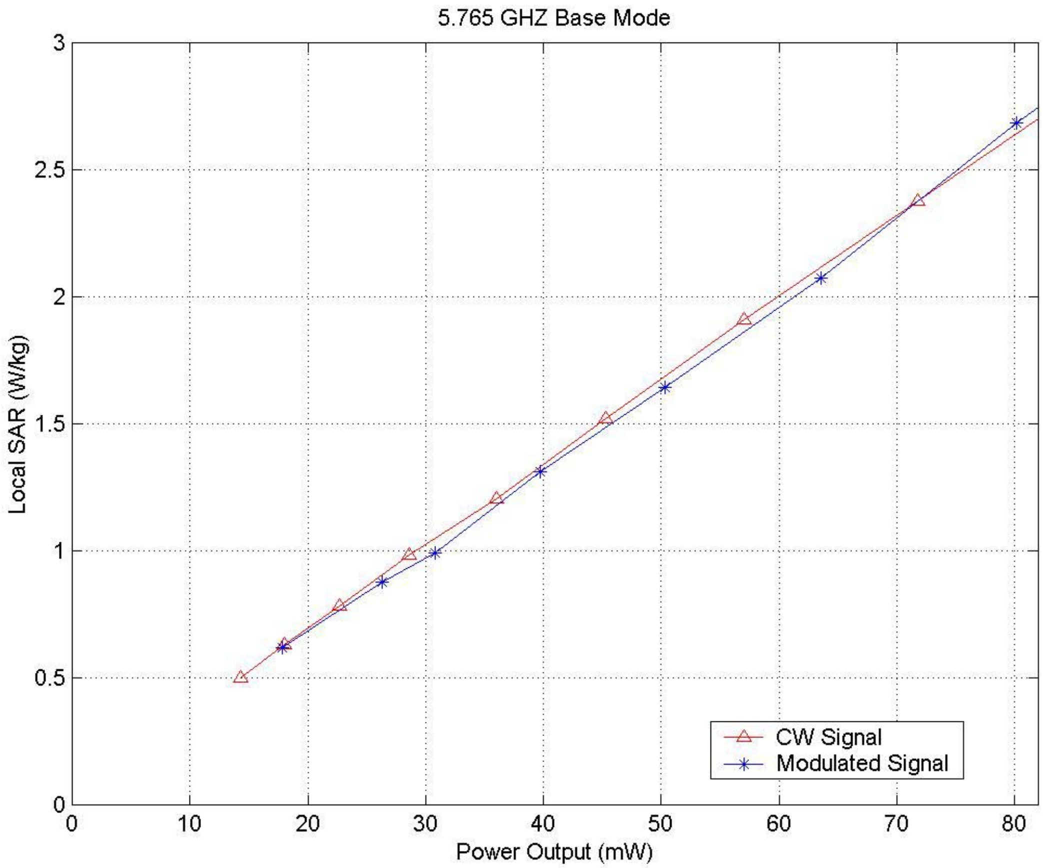

Fig. A.2. Comparison of the SAR for CW or OFDM modulated signals for the normal mode at 5.765 GHz.

APPENDIX B

SAR System Validation for the 802.11a Band

The measured SAR distribution for the peak 1-g SAR region using WR187 rectangular waveguide radiation system.

For October 10, 2003 – The SAR plot at 5.25 GHz

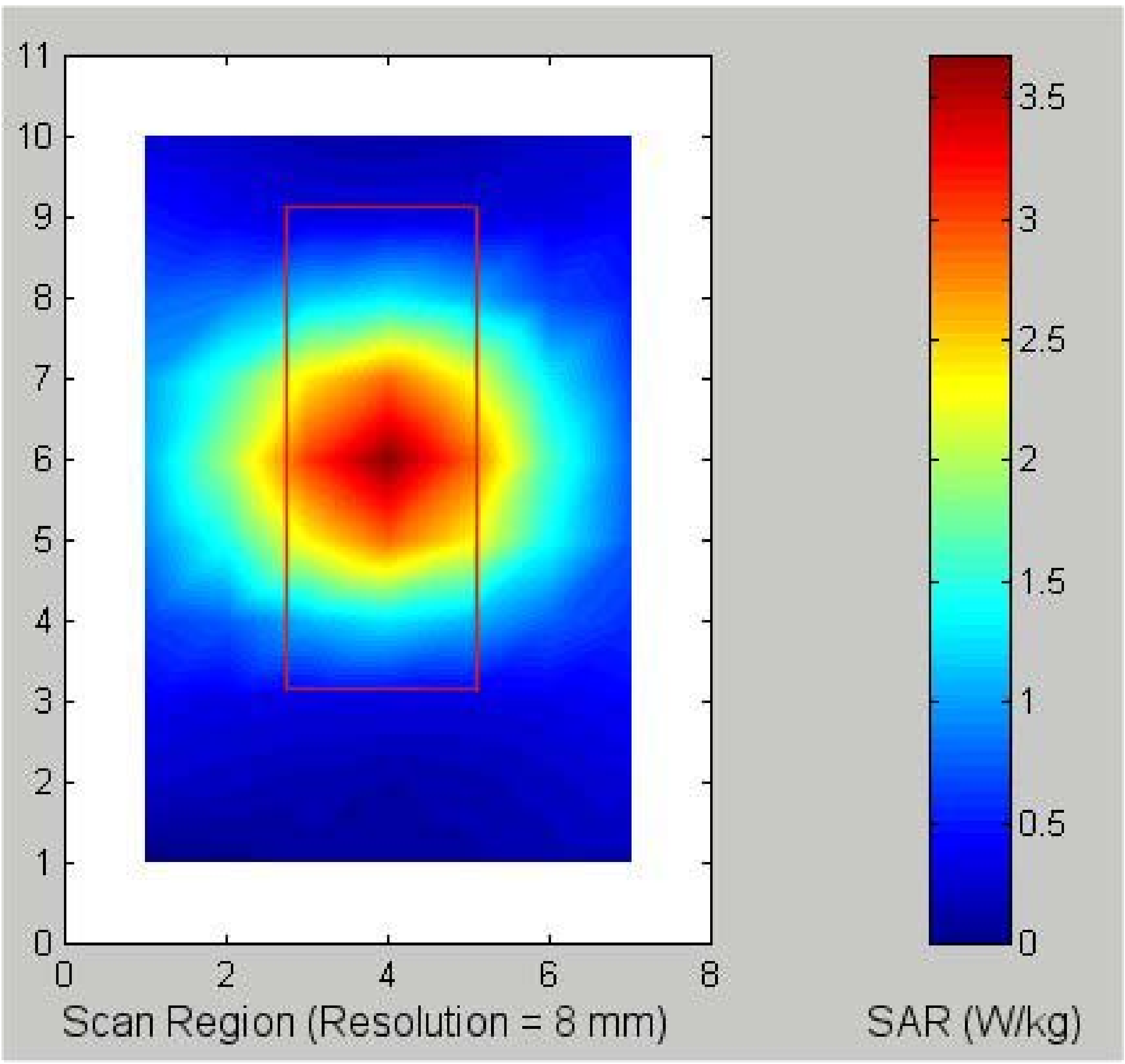

Fig. B.1. Coarse scans of the measured SAR distribution for the WR187 rectangular waveguide irradiation system for system verification at 5.25 GHz. Also shown is the outline of the rectangular waveguide overlaid on the SAR contours. Radiated power = 100 mW.

1-g SAR = 3.593 W/kg

a. At depth of 1 mm

8.804	9.478	9.650	9.027	8.525
9.385	9.938	10.272	10.030	9.265
9.634	10.225	10.382	10.241	9.365
9.124	9.845	10.062	9.699	9.117
8.483	9.052	9.444	9.229	8.439

b. At depth of 3 mm

4.308	4.652	4.749	4.522	4.263
4.576	4.905	5.053	4.903	4.571
4.644	4.982	5.111	4.990	4.626
4.457	4.826	4.968	4.773	4.478
4.128	4.460	4.607	4.476	4.160

c. At depth of 5 mm

2.028	2.195	2.252	2.175	2.051
2.139	2.310	2.376	2.297	2.154
2.144	2.315	2.401	2.324	2.184
2.078	2.264	2.342	2.244	2.096
1.907	2.096	2.148	2.076	1.961

d. At depth of 7 mm

1.010	1.092	1.125	1.082	1.023
1.054	1.127	1.163	1.127	1.051
1.047	1.121	1.170	1.131	1.069
1.012	1.110	1.143	1.098	1.018
0.915	1.020	1.049	1.015	0.964

e. At depth of 9 mm

0.578	0.627	0.640	0.598	0.565
0.601	0.623	0.645	0.626	0.576
0.590	0.619	0.646	0.627	0.590
0.566	0.622	0.629	0.611	0.563
0.506	0.561	0.588	0.576	0.545

APPENDIX C

SCREEN DUMPS FOR SOME OF THE FLUIDS STUDIED FOR DEVELOPMENT OF TISSUE-SIMULANT FLUID FOR THE FREQUENCY BAND 5.2 TO 5.8 GHz

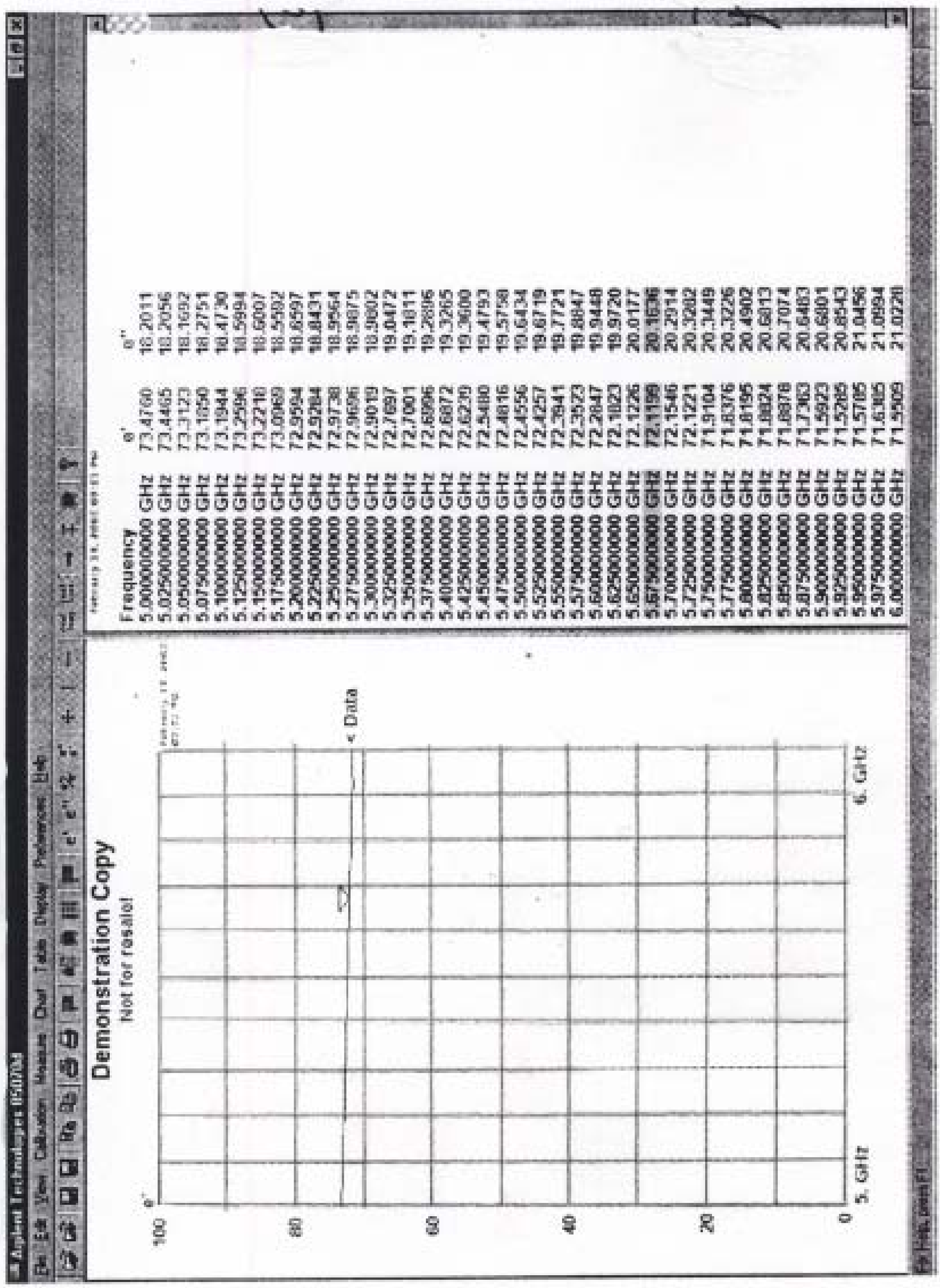

Fig. C.1. The output of the measured ε′, ε″ for deionized water for the frequency band 5 to 6 GHz.

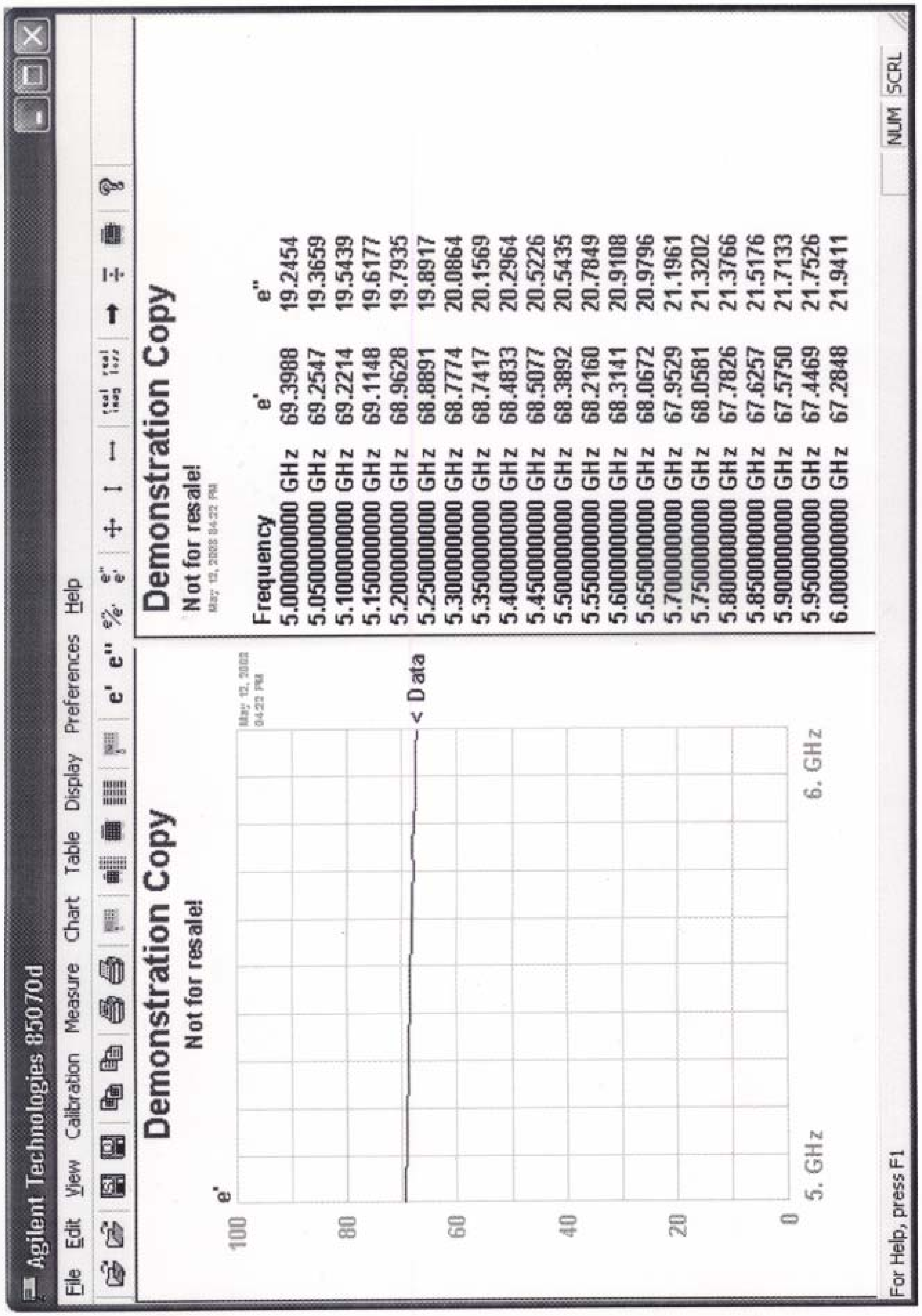

Frequency	e'	e''
5.000000000 GHz	69.3988	19.2454
5.050000000 GHz	69.2547	19.3659
5.100000000 GHz	69.2214	19.5439
5.150000000 GHz	69.1148	19.6177
5.200000000 GHz	68.9628	19.7935
5.250000000 GHz	68.8891	19.8917
5.300000000 GHz	68.7774	20.0864
5.350000000 GHz	68.7417	20.1569
5.400000000 GHz	68.4833	20.2964
5.450000000 GHz	68.5077	20.5226
5.500000000 GHz	68.3892	20.5435
5.550000000 GHz	68.2160	20.7849
5.600000000 GHz	68.3141	20.9108
5.650000000 GHz	68.0672	20.9796
5.700000000 GHz	67.9529	21.1961
5.750000000 GHz	68.0581	21.3202
5.800000000 GHz	67.7826	21.3766
5.850000000 GHz	67.6257	21.5176
5.900000000 GHz	67.5750	21.7133
5.950000000 GHz	67.4469	21.7526
6.000000000 GHz	67.2848	21.9411

Fig. C.2. The measured ε', ε'' for a composition of 96% deionized water and 4% HEC for the frequency band 5 to 6 GHz.

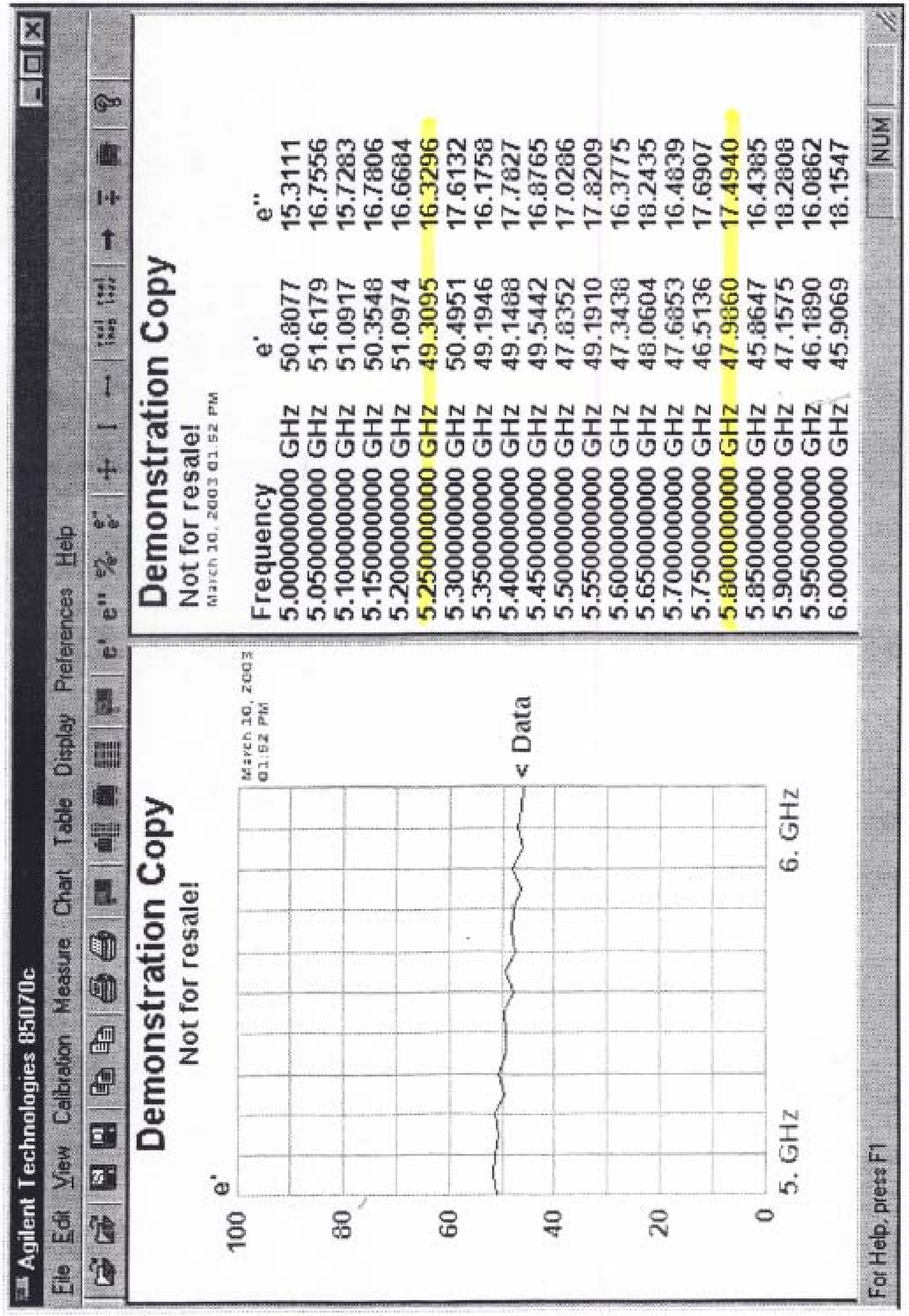

Frequency	e'	e''
5.000000000 GHz	50.8077	15.3111
5.050000000 GHz	51.6179	16.7556
5.100000000 GHz	51.0917	15.7283
5.150000000 GHz	50.3548	16.7806
5.200000000 GHz	51.0974	16.6684
5.250000000 GHz	49.3095	16.3296
5.300000000 GHz	50.4951	17.6132
5.350000000 GHz	49.1946	16.1758
5.400000000 GHz	49.1488	17.7827
5.450000000 GHz	49.5442	16.8765
5.500000000 GHz	47.6352	17.0286
5.550000000 GHz	49.1910	17.8209
5.600000000 GHz	47.3436	16.3775
5.650000000 GHz	48.0604	18.2435
5.700000000 GHz	47.6853	16.4839
5.750000000 GHz	46.5136	17.6907
5.800000000 GHz	47.9860	17.4940
5.850000000 GHz	45.8647	16.4385
5.900000000 GHz	47.1575	18.2808
5.950000000 GHz	46.1890	16.0862
6.000000000 GHz	45.9069	18.1547

Fig. C.3. The measured ε', ε'' for a composition of 82% deionized water, 16% polyethylene powder and 2% HEC for the frequency band 5 to 6 GHz.

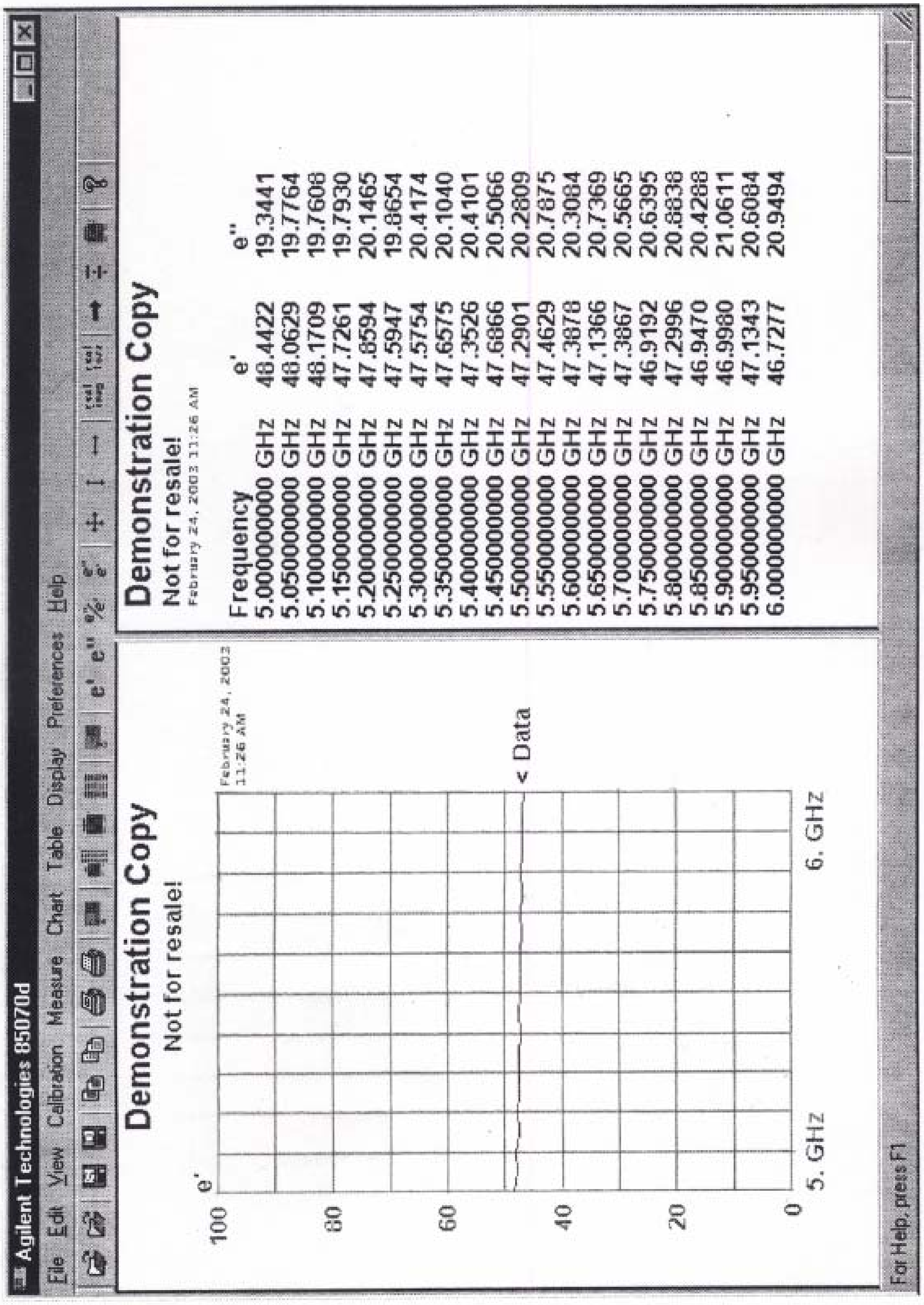

Frequency	e'	e''
5.000000000 GHz	48.4422	19.3441
5.050000000 GHz	48.0629	19.7764
5.100000000 GHz	48.1709	19.7608
5.150000000 GHz	47.7261	19.7930
5.200000000 GHz	47.8594	20.1465
5.250000000 GHz	47.5947	19.8654
5.300000000 GHz	47.5754	20.4174
5.350000000 GHz	47.6575	20.1040
5.400000000 GHz	47.3526	20.4101
5.450000000 GHz	47.6866	20.5066
5.500000000 GHz	47.2901	20.2809
5.550000000 GHz	47.4629	20.7875
5.600000000 GHz	47.3878	20.3084
5.650000000 GHz	47.1366	20.7369
5.700000000 GHz	47.3867	20.5665
5.750000000 GHz	46.9192	20.6395
5.800000000 GHz	47.2996	20.8838
5.850000000 GHz	46.9470	20.4288
5.900000000 GHz	46.9980	21.0611
5.950000000 GHz	47.1343	20.6084
6.000000000 GHz	46.7277	20.9494

Fig. C.4. The measured ε′, ε″ for a composition of 31.5% mannitol, 67.5% deionized water, and 1% HEC for the frequency band 5 to 6 GHz.

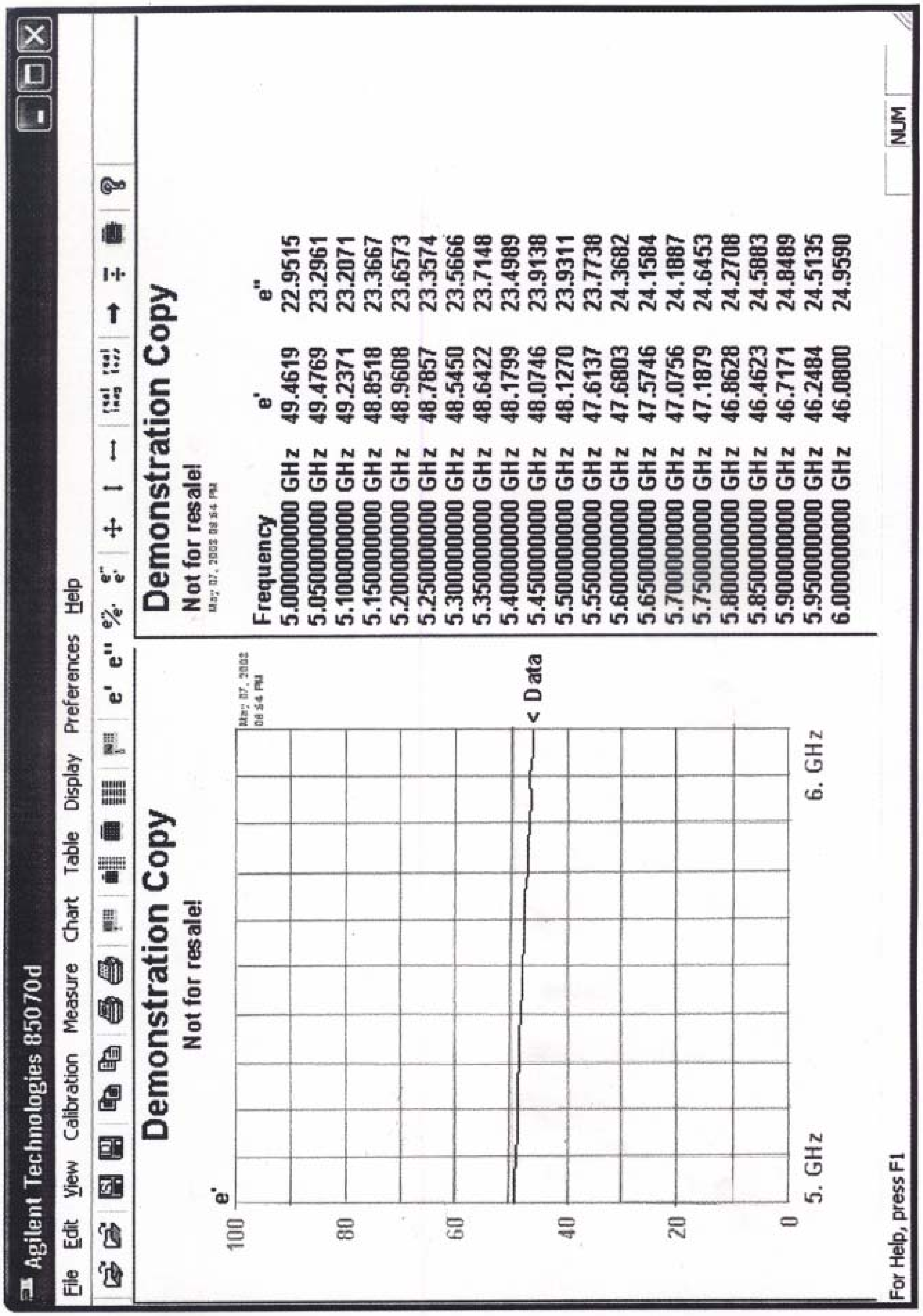

Demonstration Copy

Not for resale!

Frequency	e'	e"
5.000000000 GHz	49.4619	22.9515
5.050000000 GHz	49.4769	23.2961
5.100000000 GHz	49.2371	23.2071
5.150000000 GHz	48.8518	23.3667
5.200000000 GHz	48.9608	23.6573
5.250000000 GHz	48.7857	23.3574
5.300000000 GHz	48.5450	23.5666
5.350000000 GHz	48.6422	23.7148
5.400000000 GHz	48.1799	23.4989
5.450000000 GHz	48.0746	23.9138
5.500000000 GHz	48.1270	23.9311
5.550000000 GHz	47.6137	23.7738
5.600000000 GHz	47.6803	24.3682
5.650000000 GHz	47.5746	24.1584
5.700000000 GHz	47.0756	24.1887
5.750000000 GHz	47.1879	24.6453
5.800000000 GHz	46.8628	24.2708
5.850000000 GHz	46.4623	24.5883
5.900000000 GHz	46.7171	24.8489
5.950000000 GHz	46.2484	24.5135
6.000000000 GHz	46.0800	24.9590

Fig. C.5. The measured ε', ε'' for a composition of 31% sugar, 68% deionized water, and 1% HEC for the frequency band 5 to 6 GHz.

APPENDIX D

AN OPEN-ENDED WAVEGUIDE SYSTEM FOR SAR SYSTEM VALIDATION AND/OR PROBE CALIBRATION FOR FREQUENCIES ABOVE 3 GHz

Qingxiang Li, Student Member, IEEE
Om P. Gandhi, Life Fellow, IEEE, and
Gang Kang, Senior Member, IEEE
Department of Electrical and Computer Engineering
University of Utah
Salt Lake City, Utah 84112, U.S.A.

Abstract

Compliance with safety guidelines prescribed in terms of maximum electromagnetic power absorption (specific absorption rate or SAR) for any 1- or 10-g of tissue is required for all newly-introduced personal wireless devices such as Wi-Fi PCs. The prescribed SAR measuring system is a planar phantom with a relatively thin base of thickness 2.0 mm filled with a lossy fluid to simulate dielectric properties of the tissues. A well-characterized, broadband irradiator is required for SAR system validation and/or submerged E-field probe calibration for the new 802.11a frequencies in the 5-6 GHz band. We describe an open-ended waveguide system that may be used for this purpose. Using a fourth-order polynomial least-square fit to the experimental data gives SAR variations close to the bottom surface of the phantom that are in excellent agreement with those obtained using the FDTD numerical method. The experimentally-determined peak 1-g SARs are within 1 to 2 percent of those obtained using the FDTD both at 5.25 and 5.8 GHz.

Index Terms – Broadband, electromagnetic exposure system, probe calibration, safety assessment, comparison with numerical calculations

Submitted to *IEEE Transactions on Microwave Theory and Techniques*, June 10, 2003.

AN OPEN-ENDED WAVEGUIDE SYSTEM FOR SAR SYSTEM VALIDATION AND/OR PROBE CALIBRATION FOR FREQUENCIES ABOVE 3 GHz

Qingxiang Li, Student Member, IEEE
Om P. Gandhi, Life Fellow, IEEE, and
Gang Kang, Senior Member, IEEE

I. Introduction

Compliance with the safety guidelines such as those proposed by IEEE [1] ICNIRP [2], etc. is required by regulatory agencies in the United States and elsewhere for all newly-introduced personal wireless devices such as Wi-Fi PCs, cellular telephones, etc. These safety guidelines are set in terms of maximum 1- or 10-g mass-normalized rates of electromagnetic energy deposition (specific absorption rates or SARs) for any 1- or 10-g of tissue. The two most commonly-used SAR limits today are those of IEEE [1] – 1.6 W/kg for any 1 g of tissue, and ICNIRP [2] – 2 W/kg for any 10 g of tissue, excluding extremities such as hands, wrists, feet, and ankles where higher SARs up to 4 W/kg for any 10 g of tissue are permitted in both of these standards. Experimental and numerical techniques using planar or head-shaped phantoms have been proposed for determining compliance with the SAR limits [3-5]. For frequencies above 800 MHz, the size of a rectangular waveguide is quite manageable and use of an appropriate waveguide filled with a tissue-simulant medium is recommended for calibration of an E-field probe in FCC Supplement C, Edition 01-01 to OET Bulletin 65 [6]. Even though no recommendation is made on choice of an irradiation system for frequencies above 3 GHz, balanced half-wave dipoles have been suggested for system validation for frequencies less than or equal to 3 GHz [6]. It is very difficult to develop half-wave dipole antennas for use in the 5.1 to 5.8 GHz band both because of fairly small dimensions and the resulting dimensional tolerances, and relatively narrow bandwidths of the required baluns – balanced to unbalanced transformers (typically less than 10-12% for VSWR < 2.0 and less than 5-6% for VSWR < 1.5). On the other hand, rectangular waveguides are broadband with simultaneous bandwidths larger than 1-2 GHz and are fairly easy to use for frequencies in excess of 3 GHz. We have, therefore, developed an open-ended waveguide system for SAR system validation and/or probe calibration in the frequency band 5 to 6 GHz. This is a band that is presently being used for 802.11a antennas of Wi-Fi PCs.

II. The Waveguide Irradiation System

For the 5-6 GHz band, we have used a WR187 rectangular waveguide of internal dimensions 4.75 × 2.21 cm. The operating (TE_{10} mode) band of this waveguide is from 3.95 to 5.85 GHz. This is considerably larger than the required overall bandwidth of 675 MHz for the IEEE 802.11a frequency bands of 5.15-5.35 and 5.745 to 5.825 GHz. The waveguide irradiation system used for SAR system validation is shown in Fig. 1. As recommended in [6], the open-ended waveguide irradiator is placed at a distance of 8 mm below the base of planar phantom with inside dimensions of 30.5 × 41.9 cm and a base thickness of 2.0 ± 0.2 mm. This results in the open end of the waveguide at a distance of 10 mm below the lossy tissue-simulant fluid in the phantom. The microwave circuit arrangement used for the waveguide irradiation system is shown in Fig. 2. As shown in Fig. 2, the WR187 waveguide is fed with microwave power from a

Hewlett Packard Model 83620A Synthesized Sweeper (10 MHz-20 GHz). When placed at a distance of 8 mm below the base of the planar phantom, the reflection coefficient is about 10-20%. Even this relatively small amount of reflection has been greatly reduced to less than 0.5% by using a movable slide-screw waveguide tuner (Narda Model 22CI). The planar phantom is filled to a depth of 15 cm with a fluid to simulate dielectric properties recommended for the body phantom in [6]. The dielectric constants ε_r and conductivities σ at the experimental frequencies of 5.25 and 5.8 GHz are similar to those recommended in the SAR Compliance Standards used in the U.S. and in Europe [3, 4]. For our experiments and calculations, $\varepsilon_r = 48.8$, $\sigma = 6.82$ S/m at 5.25 GHz; and $\varepsilon_r = 46.9$, $\sigma = 7.83$ S/m at 5.8 GHz.

Fig. 1. Photograph of the rectangular waveguide radiator used for system validation. Also seen is the Narda Model 22CI movable slide screw tuner used to match the input power at 5.25 or 5.8 GHz to the planar tissue-simulant phantom.

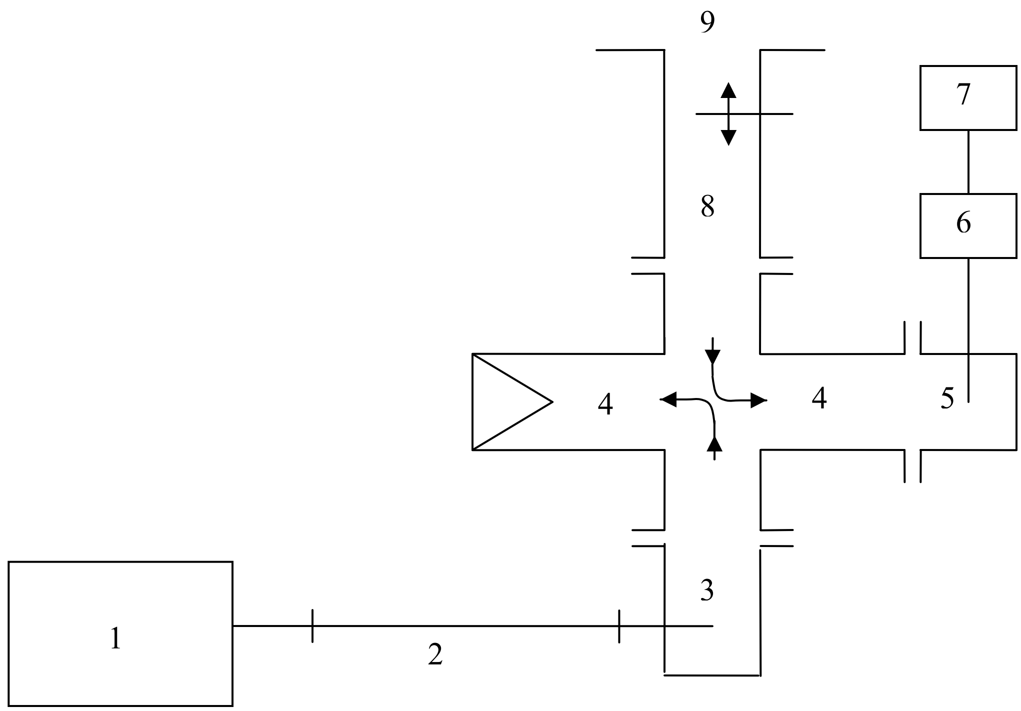

1. Hewlett Packard (HP) Model 83620A Synthesized Sweeper (10 MHz-20 GHz).
2. Coaxial line.
3. Coaxial to waveguide adapter.
4. 20 dB crossguide coupler (may be reversed to measure incident power).
5. HP Model G281A coaxial to waveguide adapter
6. HP Model 8482A power sensor.
7. HP Model 436A power meter.
8. Narda Microline® Slide Screw Tuner Model 22CI.
9. Radiating open end of the waveguide.

Fig. 2. The microwave circuit arrangement used for SAR system validation.

III. Calculation of the SAR Distributions

We have used the well-established finite-difference time-domain (FDTD) numerical electromagnetic method to calculate the electric fields and SAR distributions for the planar phantom of base thickness 2.0 mm of dielectric constant $\varepsilon_r = 2.56$ and dielectric properties of the tissue-simulant lossy fluid as given in Section II. The FDTD method described in several texts [7, 8] has been successfully used by various researchers [9-12] and, therefore, would not be described here. For the FDTD calculations, we have used a cell size $\delta = 0.5$ mm in order to meet the requirement $\delta \leq \lambda_\varepsilon / 10$ in the lossy fluid. The calculated variations of the SAR distribution at the experimental frequencies of 5.25 and 5.80 GHz are given in Figs. 3 a-c and 4 a-c, respectively. Also shown in the same figures are the experimental values of the SARs (shown by circles). From Figs. 3 and 4, it is obvious that the penetration of electromagnetic fields in the 5.1 to 5.8 GHz band is extremely shallow. The calculated depths of penetration corresponding to $1/e^2$-reduction of SAR (13.5% of the SAR at the surface) are only 6.85 and 5.985 mm at 5.25 and 5.8 GHz, respectively. Both of these depths of penetration are very similar to those obtained for plane-wave irradiation at these frequencies (7.15 mm for 5.25 GHz and 6.25 mm for 5.8 GHz).

IV. Experimental Setup and Measurements

A. *Experimental Setup*

As recommended in FCC Bulletin 65 [14], a planar phantom of fairly thin base thickness 2.0 mm of relatively low dielectric constant ($\varepsilon_r = 2.56$ in our case) is used for the determination of SAR distributions of wireless PCs and for the SAR system validation. The lateral dimensions of the planar phantom (in our case 30.5 × 41.9 cm) are large enough to ignore scattering from the edges of the rectangular box or the tissue-simulant lossy fluid used to fill this box to a depth of 10-15 cm (several times the depth of penetration of fields in the fluid so as to present a nearly infinitely deep medium to neglect reflections). A photograph of the phantom model together with a computer-controlled 3-D stepper motor system (Arrick Robotics MD-2A) is shown in Fig. 5.

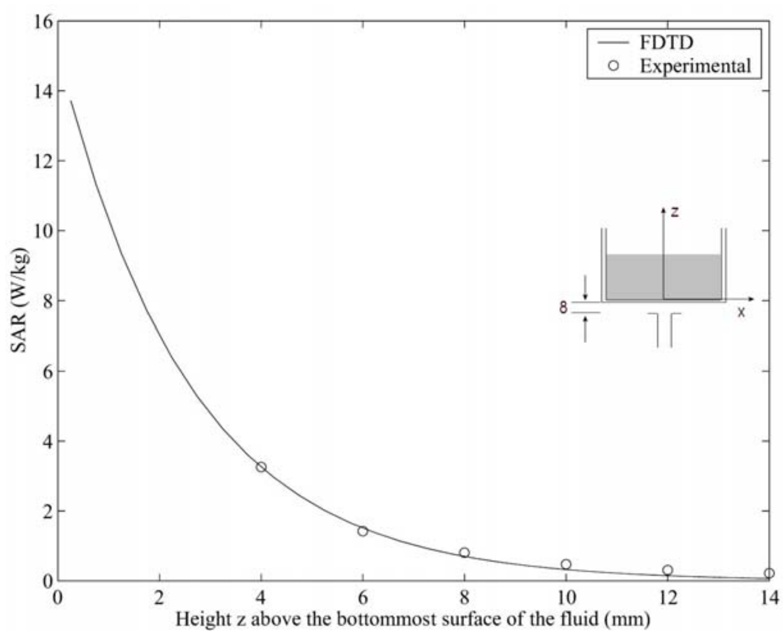

a. Variation of SAR along the z-axis.

Fig. 3. Comparison of the measured and calculated SAR variations for a planar phantom of base thickness 2.0 mm and internal dimensions 30.5 × 41.9 × 20 cm for a WR 187 open-ended waveguide radiator placed 10 mm below the bottommost surface of the lossy tissue-simulant phantom. Frequency = 5.25 GHz.

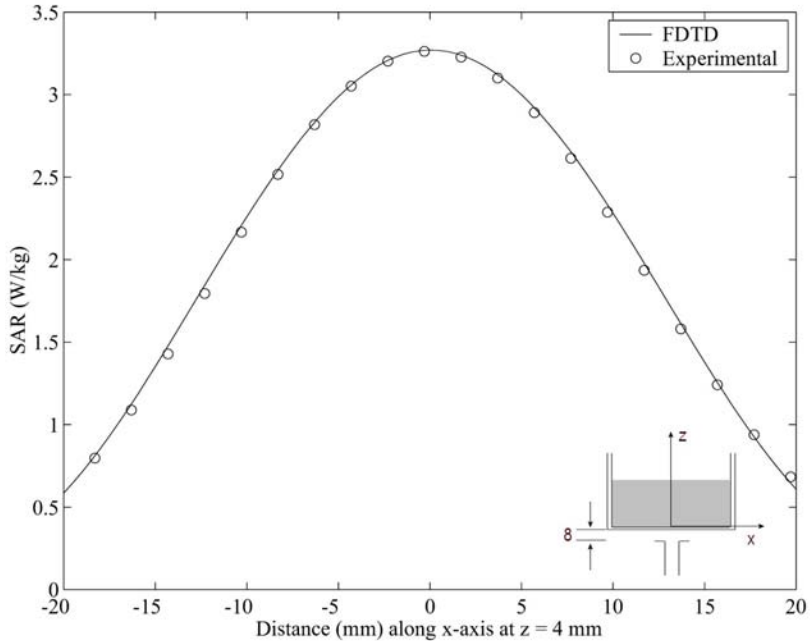

b. Variation of SAR along the x-axis parallel to the broader dimension of the waveguide at height z = 4 mm.

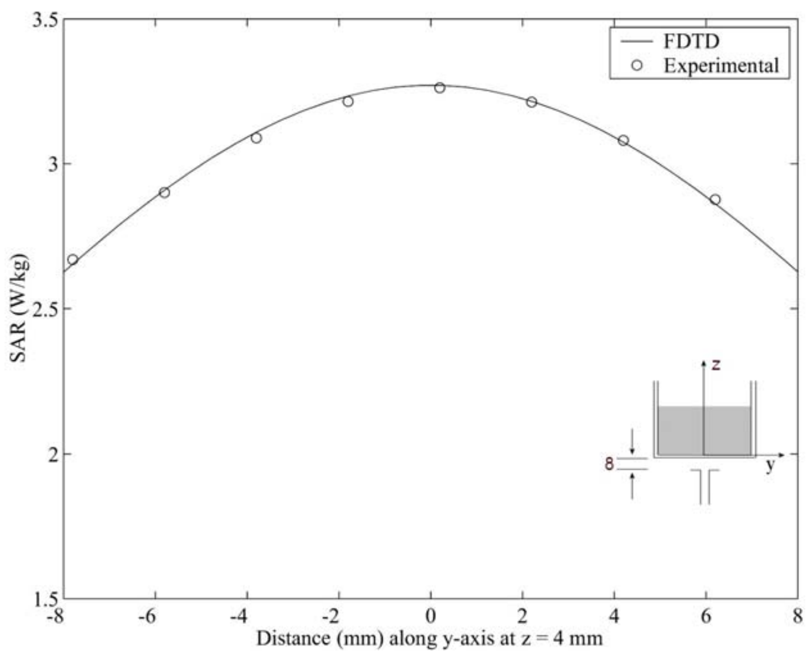

c. Variation of SAR along the y-axis parallel to the narrower dimension of the waveguide at height z = 4 mm.

Fig. 3. Comparison of the measured and calculated SAR variations for a planar phantom of base thickness 2.0 mm and internal dimensions 30.5 × 41.9 × 20 cm for a WR 187 open-ended waveguide radiator placed 10 mm below the bottommost surface of the lossy tissue-simulant phantom. Frequency = 5.25 GHz.

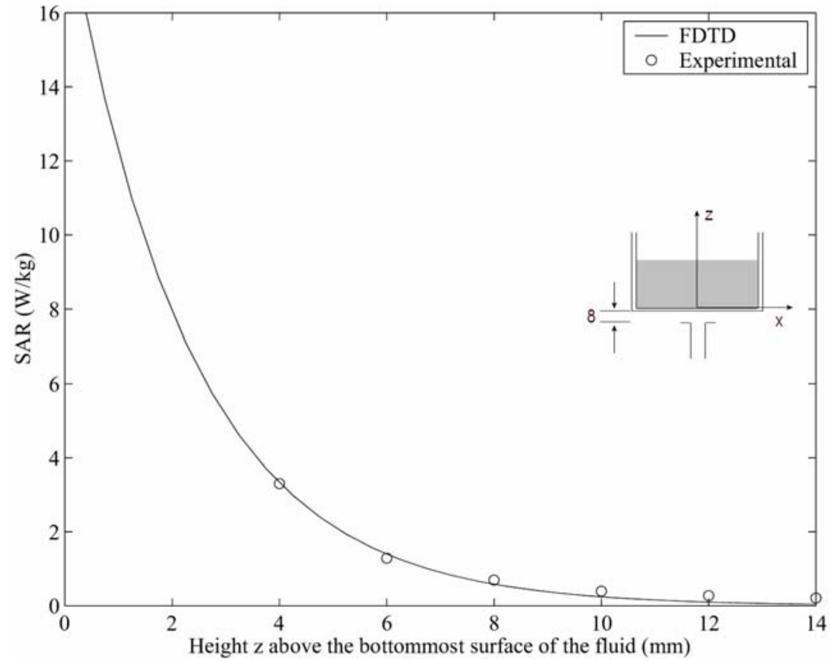

a. Variation of SAR along the z-axis.

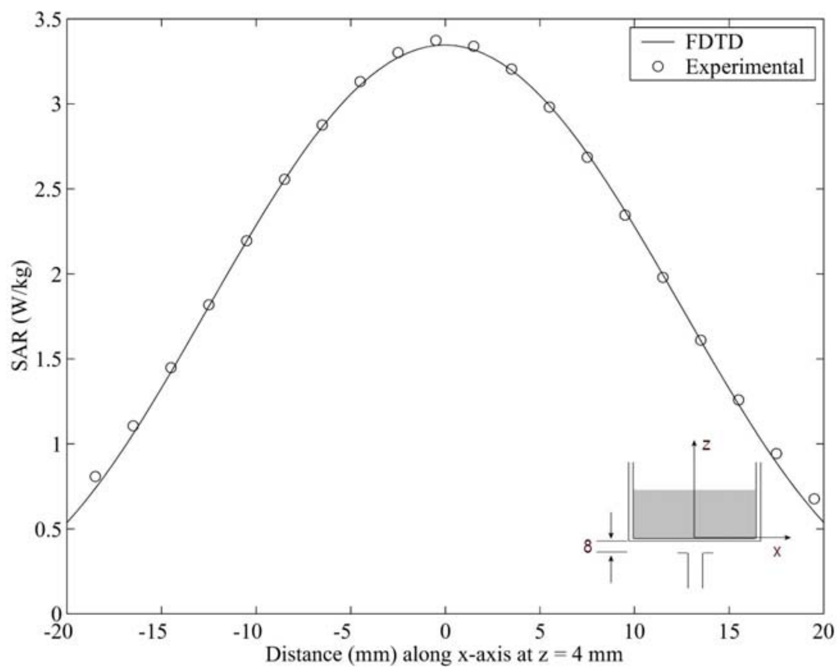

b. Variation of SAR along the x-axis parallel to the broader dimension of the waveguide at height z = 4 mm.

Fig. 4. Comparison of the measured and calculated SAR variations for a planar phantom of base thickness 2.0 mm and internal dimensions 30.5 × 41.9 × 20 cm for a WR 187 open-ended waveguide radiator placed 10 mm below the bottommost surface of the lossy tissue-simulant phantom. Frequency = 5.8 GHz.

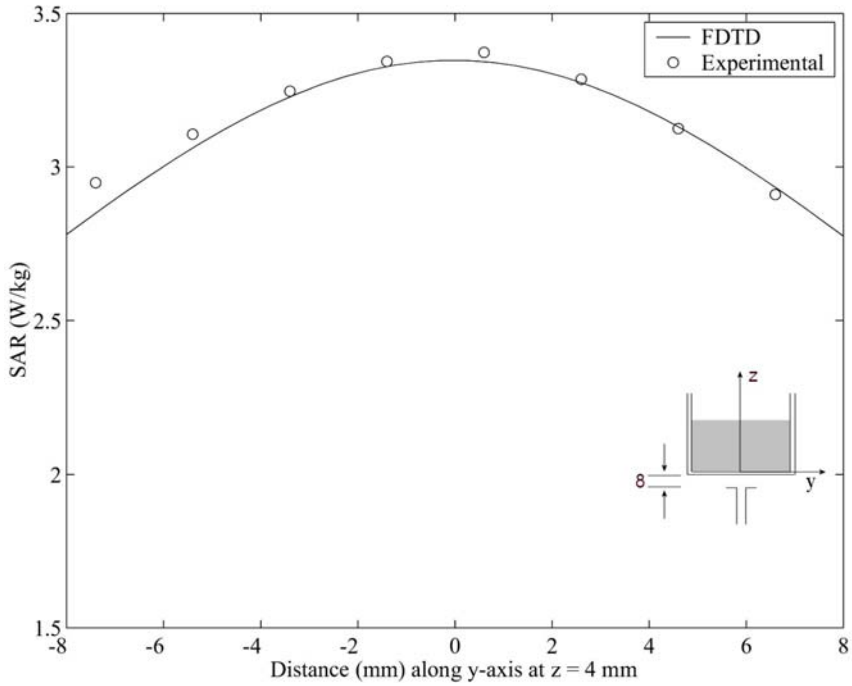

c. Variation of SAR along the y-axis parallel to the narrower dimension of the waveguide at height z = 4 mm.

Fig. 4. Comparison of the measured and calculated SAR variations for a planar phantom of base thickness 2.0 mm and internal dimensions 30.5 × 41.9 × 20 cm for a WR 187 open-ended waveguide radiator placed 10 mm below the bottommost surface of the lossy tissue-simulant phantom. Frequency = 5.8 GHz.

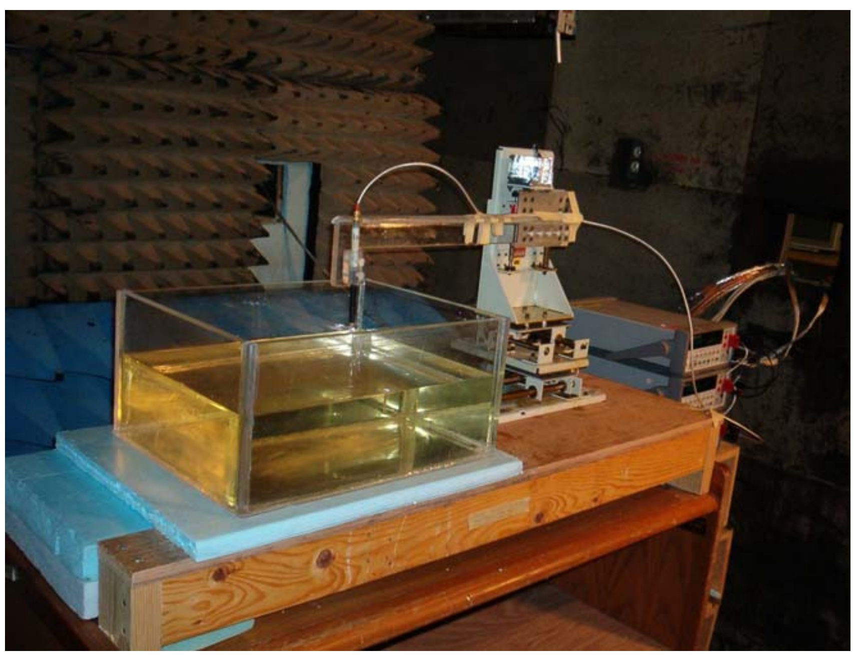

Fig. 5. Photograph of the planar model with the 3-D stepper motor system used for measurement of SAR variation for comparison with FDTD calculations.

A triaxial Narda Model 8021 E-field probe is used to determine the internal electric fields. The positioning repeatability of the stepper motor system moving the E-field probe is within ± 0.1 mm. Outputs from the three channels of the E-field probe are dc voltages, the sum of which is proportional to the square of the internal electric fields ($|E_i|^2$) from which the SAR can be obtained from the equation: $SAR = \sigma(|E_i|^2)/\rho$, where σ and ρ are the conductivity and mass density of the tissue-simulant material, respectively [13]. The dc voltages for the three channels of the E-field probe are read by three HP 34401A multimeters and sent to the computer via an HPIB interface. The setup is carefully grounded and shielded to reduce the noise due to the electromagnetic interference (EMI).

B. ***E-Field Probe***

The nonperturbing implantable E-field probe used in the setup was originally developed by Bassen et al. [14] and is manufactured by L3/Narda Microwave Corporation, Hauppauge, NY as Model 8021 E-field probe. In the probe, three orthogonal miniature dipoles each of length approximately 2.5 mm are placed on a triangular-beam substrate. Each dipole is loaded with a small Schottky diode and connected to the external circuitry by high resistance ($2\ M\Omega \pm 40\%$) leads to reduce secondary pickups. The entire structure is then encapsulated with a low dielectric constant insulating material. The probe thus constructed has a very small diameter (4 mm), which results in a relatively small perturbation of the internal electric field. The probe is rated for frequencies up to 3 GHz for tissue-simulant media, but is presently used for system validation at frequencies in the 5 to 6 GHz range. Consequently, the probe had to be checked for square-law performance, and isotropy for use at these higher frequencies.

1. **Test for Square-Law Region:** It is necessary to operate the E-field probe in the square-law region for each of the diodes so that the sum of the dc voltage outputs from the three dipoles is proportional to the square of the internal electric field ($|E_i|^2$). Fortunately, the personal wireless devices such as the PCs induce SARs that are generally less than 5-6 W/kg even for closest locations to the body. For SAR measurements, it is, therefore, necessary that the E-field probe be checked for square-law behavior for SARs up to such values that are likely to be encountered. Such a test may be conducted using a canonical lossy body such as a rectangular box used here. By varying the radiated power of the waveguide, the output of the probe should increase linearly with the applied power for each of the test locations.

   Shown in Fig. 6a and b are the results of the tests performed to check the square-law behavior of the E-field probe used in our setup at 5.25 and 5.8 GHz, respectively. Used as the radiator is the WR 187 waveguide placed at a distance of 8 mm below the base of the planar phantom (10 mm below the bottom surface of the tissue-simulant fluid as recommended in [6]).

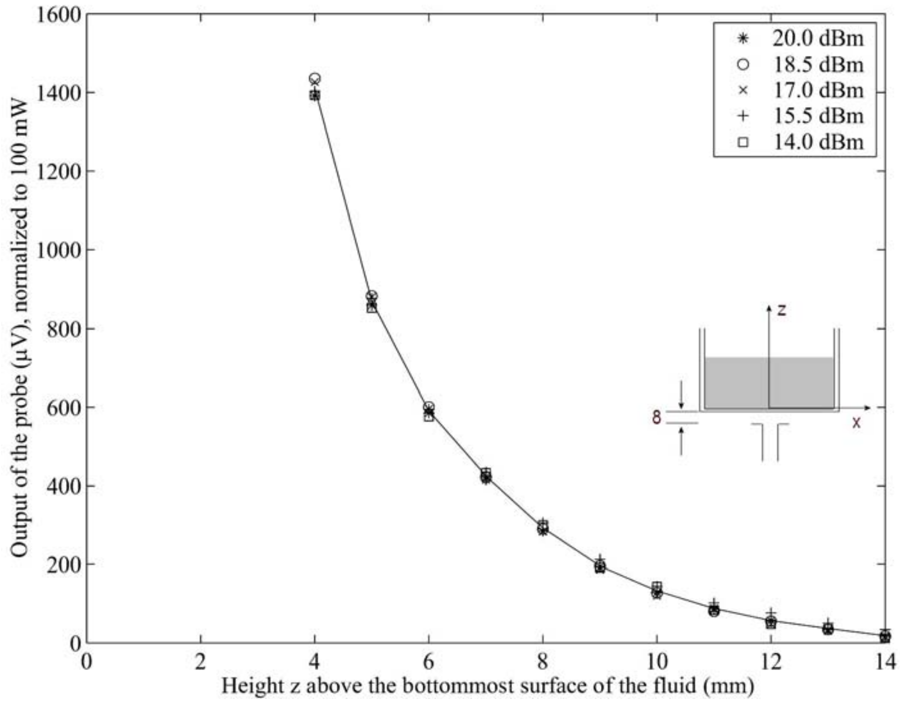

a. Test for square-law behavior at 5.25 GHz.

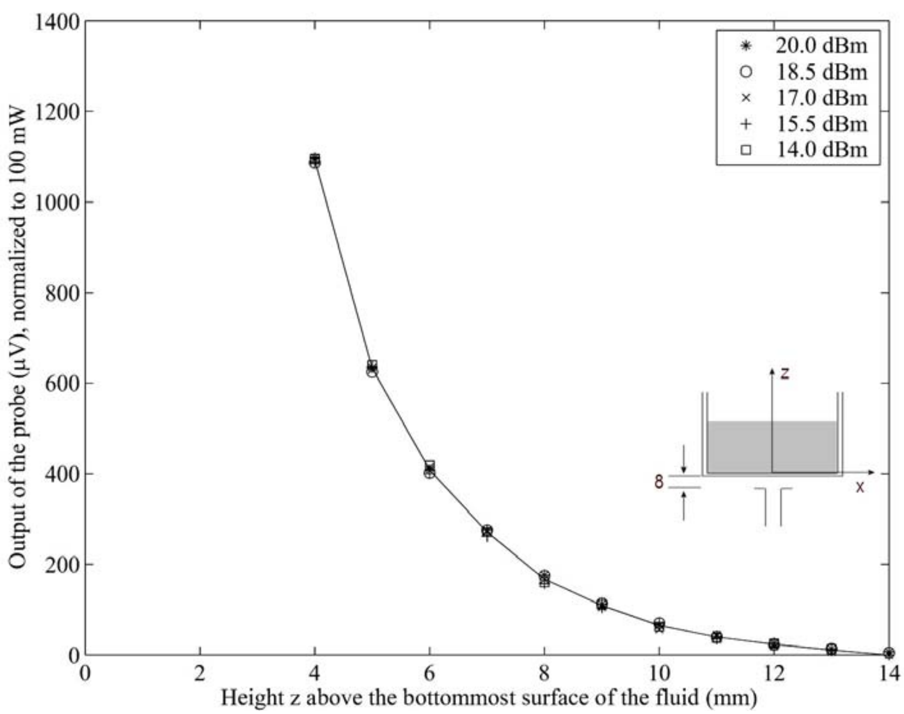

b. Test for square-law behavior at 5.8 GHz.

Fig. 6. Variation of the output voltage (proportional to $|E_i|^2$) for different radiated powers normalized to 100 mW (20 dBm).

Since the dc voltage outputs of the probe are fairly similar when normalized to a radiated power of 100 mW, the square-law behavior is demonstrated and an output voltage that is proportional to $|E_i|^2$ is obtained within ± 2.2% both at 5.25 and 5.8 GHz.

2. **Test for Isotropy of the Probe:** Another important characteristic of the probe that affects the measurement accuracy is its isotropy. Since the orientation of the induced electric field is generally unknown, the E-field probe should be relatively isotropic in its response to the orientation of the E-field. Shown in Fig. 7a and b are the test results of the E-field probe used in our setup at 5.25 and 5.8 GHz, respectively. The E-field probe was rotated around its axis from 0-180° in incremental steps of 15°. Because of the alternating nature of the fields, angles of θ and 180° + θ are identical, hence 0-165° rotation of the E-field probe was considered to be adequate to cover the entire 360° rotation of the probe. As seen in Fig. 7a and b, an isotropy of less than ± 0.18 dB (± 4.3%) was observed for this E-field probe both at 5.25 and 5.8 GHz.

3. **Calibration of the E-Field Probe:** Since the voltage output of the E-field probe is proportional to the square of the internal electric field ($|E_i|^2$), the SAR is, therefore, proportional to the voltage output of the E-field probe by a proportionality constant C. The constant C is defined as the calibration factor and is frequency and material dependent. It is measured to calibrate the probe at the various frequencies of interest using the appropriate tissue-simulating materials for the respective frequencies.

   Canonical geometries such as waveguides, rectangular slabs, and layered or homogeneous spheres have, in the past, been used for the calibration of the implantable E-field probe [15-17] albeit at lower frequencies. Since the FDTD method has been carefully validated to solve electromagnetic problems for a variety of near-field exposure geometries [18], we were able to calibrate the Narda E-field probe by comparing the measured variations of the probe voltage (proportional to $|E_i|^2$) against the FDTD-calculated variations of the SARs for the planar phantom of base thickness 2.0 mm ($\varepsilon_r = 2.56$) and internal dimensions 30.5 × 41.9 × 20 cm irradiated by the WR 187 waveguide placed below this phantom as previously described in Section. II. Shown in Figs. 6a, b and 7a, b are the comparisons between the experimentally measured and FDTD-calculated variations of the SAR distributions in the tissue-simulant fluid. Since there are excellent agreements between the calculated SARs and the measured variations of the voltage outputs of the E-field probe, it is possible to calculate the calibration factors at the respective frequencies by fitting the measured data to the FDTD-calculated results by means of the least mean-square error (LMSE) method. For the Narda Model 8021 E-field probe used in our setup, the calibration factor is determined to be 2.98 (mW/kg)/μV ± 5% both at 5.25 and 5.8 GHz, respectively.

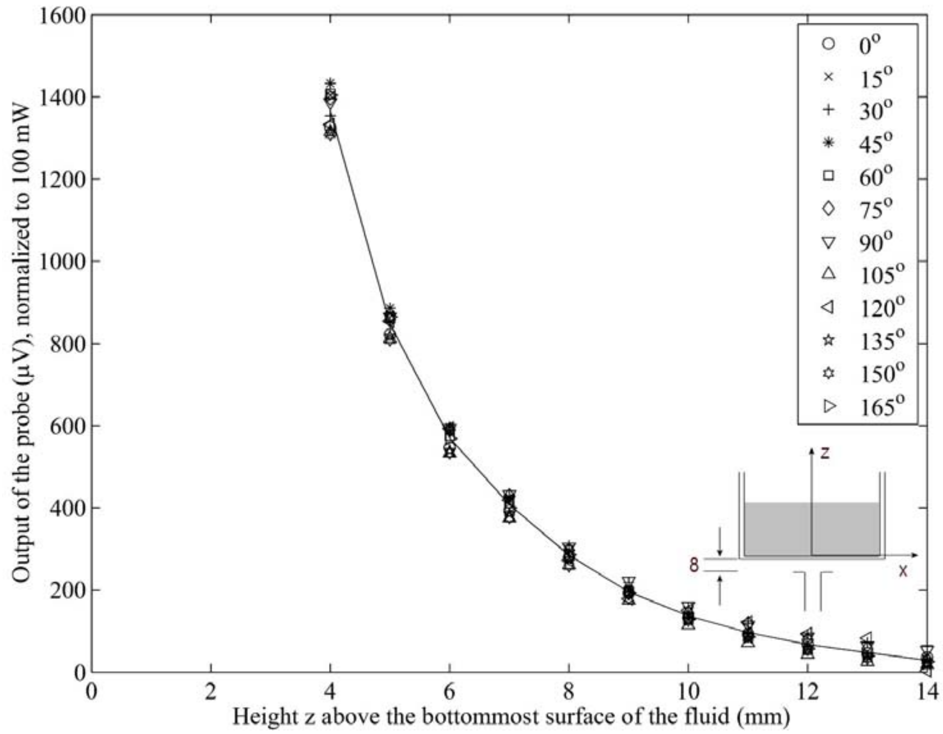

a. 5.25 GHz.

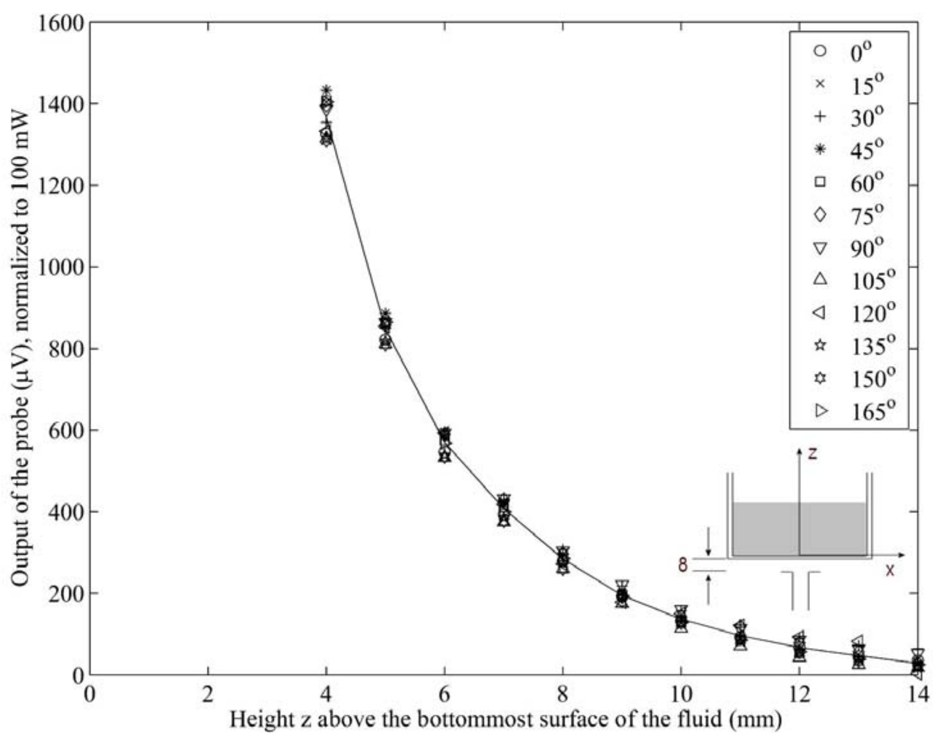

b. 5.8 GHz.

Fig. 7. Test for isotropy.

V. Need for Extrapolation

Because of the physical separation of the three orthogonal pickup dipoles from the tip of the E-field probe, the SAR measurements cannot be taken any closer than about 3 mm from the bottom surface of the phantom fluid. As given in Figs. 8 and 9, we have measured the SARs with 2 mm resolution at heights of 4, 6, 8, 10, 12 and 14 mm above the bottom surface of the phantom fluid. We have tried second-, third-, fourth-, and fifth-order polynomial least-square fits to extrapolate the measured data to obtain SARs closer to the bottom of the lossy fluid. As seen in Figs. 8 and 9, the second- and third-order polynomials underestimate the SARs while the fifth-order polynomial overestimates the SAR distribution. An excellent least-square fit to the numerically-calculated SAR variations is obtained by using a fourth-order polynomial to extrapolate the measured data both at 5.25 and 5.8 GHz.

After identifying the region of the highest SAR, the SAR distributions were measured with a finer resolution of 2 mm in order to obtain the peak $1\,cm^3$ or 1-g SAR. Here too, the SAR measurements were performed for the xy planes at heights z of 4, 6, 8, 10, 12, and 14 mm from the bottom surface of the body-simulant fluid. The SARs thus measured were extrapolated using a fourth-order least-square fit to the measured data to obtain values at 1, 3, 5, 7, and 9 mm height and used to obtain peak 1-g SARs. For a radiated power of 100 mW, the SARs thus obtained with 2 mm resolution for xy planes at heights z of 1, 3, 5, 7, and 9 mm for the peak SAR region of volume 10 ×10 × 10 mm were used to obtain peak 1-g SAR at 5.25 and 5.8 GHz, respectively. The experimentally-determined peak 1-g SARs for 100 mW of radiated power of 3.678 and 3.947 W/kg are extremely close to the FDTD-calculated 1-g SARs for this waveguide irradiator of 3.580 and 3.946 W/kg at 5.25 and 5.80 GHz, respectively.

V. Conclusions

We have developed an open-ended waveguide irradiation system for validation of the SAR measurement system and/or for E-field probe calibration in the 802.11a frequency band 5.15 to 5.825 GHz. A fourth-order polynomial least-square fit to the experimental data gives SAR variations close to the bottom surface of the phantom that are in excellent agreement with those obtained using the FDTD method. The experimentally-determined peak 1-g SARs are within 1 to 2 percent of those obtained using the FDTD numerical calculations.

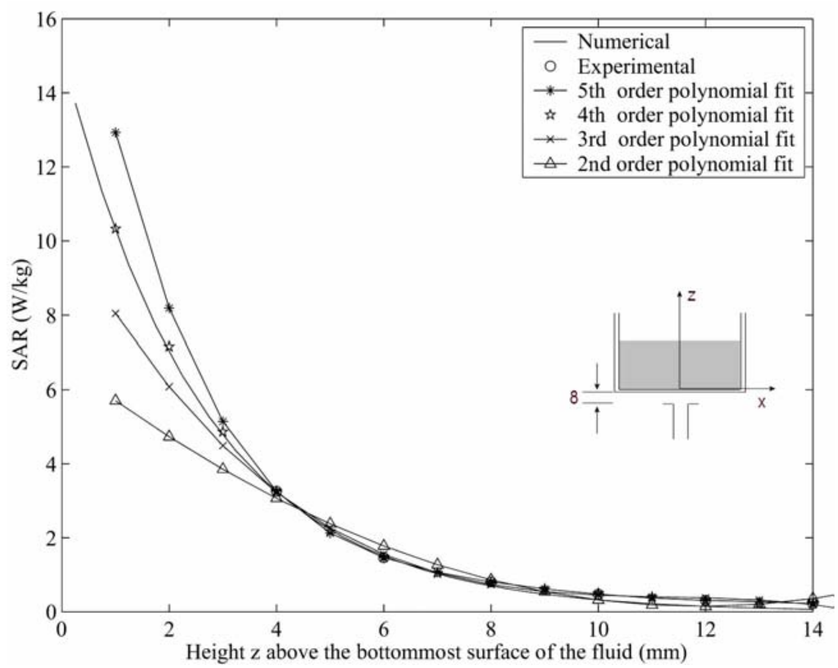

Fig. 8. Comparison of the experimentally measured and FDTD-calculated variation of the SAR with depth in the body-simulant planar phantom at 5.25 GHz. Also shown are the SARs extrapolated from experimental values to heights of 1, 3, 5, 7 and 9 mm above the bottom of the phantom using second-, third-, fourth-, and fifth-order least-square fit polynomials.

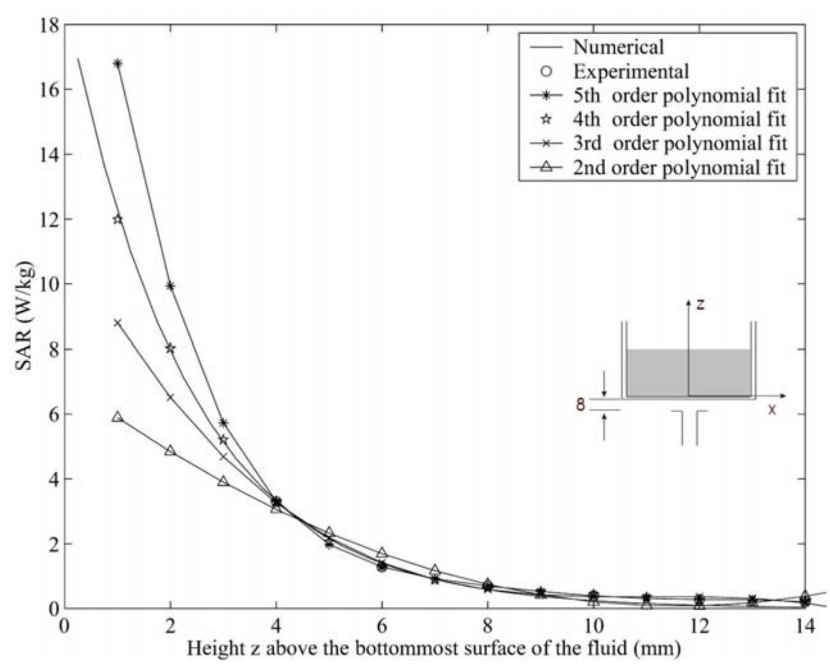

Fig. 9. Comparison of the experimentally measured and FDTD-calculated variation of the SAR with depth in the body-simulant planar phantom at 5.8 GHz. Also shown are the SARs extrapolated from experimental values to heights of 1, 3, 5, 7 and 9 mm above the bottom of the phantom using second-, third-, fourth-, and fifth-order least-square fit polynomials.

REFERENCES

1. IEEE Std. C95.1, "IEEE Standard for Safety Levels with Respect to Human Exposure to Radiofrequency Electromagnetic Fields, 3 kHz to 300 GHz," Institute of Electrical and Electronics Engineers, Piscataway, NJ, 1999.

2. ICNIRP (International Commission on Non-Ionizing Radiation Protection), "Guidelines for limiting exposure to time-varying electric, magnetic, and electromagnetic fields (up to 300 GHz)", *Health Physics*, Vol. 74, pp. 494-522, 1998.

3. IEEE Standards Coordinating Committee 34 Draft Standard, "Recommended Practice for Determining the Peak Spatial-Average Specific Absorption Rate (SAR) in the Human Body Due to Wireless Communications Devices: Experimental Techniques," Institute of Electrical and Electronics Engineers, 2002.

4. CENELEC EN50361, "Basic Standard for Measurement of Specific Absorption Rate Related to Human Exposure to Electromagnetic Fields from Mobile Telephones (300-MHz-3 GHz), CENELEC European Committee for Electrotechnical Standardization, rue de Stassart 35, B-1050, Brussels, Belgium.

5. IEC TC 106/PT62209, "Evaluation of Human Exposure to Radiofrequency Fields from Handheld and Body-Mounted Wireless Communications Devices in the Frequency Range of 30 MHz to 6 GHz: Human Models, Instrumentation Procedures," Draft Standard in preparation, 2003.

6. U.S. Federal Communications Commission (FCC), "Additional Information for Evaluating Compliance of Mobile and Portable Devices with FCC Limits for Human Exposure to Radiofrequency Emissions," Supplement C Edition 01-01 to OET Bulletin 65 Edition 97-01, June 2001.

7. A. Taflove (Ed.), *Advances in Computational Electrodynamics: The Finite-Difference Time-Domain Method,* Artech House, Boston, MA, 1998.

8. A. Taflove and S. C. Hagness, *Computational Electrodynamics: The Finite-Difference Time-Domain Method*, Artech House, Boston, MA, 2000.

9. P. J. Dimbylow and S. M. Mann, "SAR Calculations in an Anatomically-Based Realistic Model of the Head for Mobile Communication Transceivers at 900 MHz and 1.8 GHz," *Physics in Med. and Biol.,* Vol. 39**,** pp. 1537-1553, 1994.

10. O. P. Gandhi and J. Y. Chen, "Electromagnetic Absorption in the Human Head from Experimental 6 GHz Handheld Transceivers," *IEEE Trans. on Electromag. Compat.,* Vol. 37, pp. 547-558, 1995.

11. M. A. Jensen and Y. Rahmat-Samii, "EM Interaction in Handset Antennas and a Human in Personal Communications," *Proc. IEEE,* Vol. 83, pp. 7-17, 1995.

12. M. Okoniewski and M. A. Stuchly, "A Study of Handset Antenna and Human Body Interaction, *IEEE Trans. on Microwave Theory and Tech,* Vol.. 44, pp. 1855-1864, 1996.

13. M. A. Stuchly and S. S. Stuchly, "Experimental Radio and Microwave Dosimetry, " in *Handbook of Biological Effects of Electromagnetic Fields,*, 2nd ed., C. Polk and E. Postow, Eds. Boca Raton, FL: CRC, pp. 295-336, 1996.

14. H. I. Bassen and G. S. Smith, "Electric Field Probes -- a Review," *IEEE Trans. Antennas Propagat.,* Vol. AP-31, pp. 710-718, September 1983.

15. D. Hill, "Waveguide Techniques for the Calibration of Miniature Electric Field Probes for Use in Microwave Bioeffects Studies," *IEEE Trans. Microwave Theory Tech.,* Vol. MTT-30, pp. 92-94, 1982.

16. N. Kuster and Q. Balzano, "Energy Absorption Mechanism by Biological Bodies in the Near Field of Dipole Antennas Above 300 MHz," *IEEE Trans. Veh. Technol.,* Vol. 41, pp. 17-23, February 1992.

17. M. A. Stuchly, S. S. Stuchly, and A. Kraszewski, "Implantable Electric Field Probes – Some Performance Characteristics," *IEEE Trans. Biomed. Eng.,* Vol. BME-31, pp. 526-531, July 1984.

18. C. M. Furse, Q. S. Yu, and O. P. Gandhi, "Validation of the Finite-Difference Time-Domain Method for Near-Field Bioelectromagnetic Simulations," *Microwave and Optical Technology Letters*, Vol. 16, pp. 341-345, 1997.

APPENDIX E

EFFECT OF DIELECTRIC PROPERTIES ON THE PEAK 1- AND 10-G SAR FOR 802.11 a/b/g FREQUENCIES 2.45 AND 5.15 TO 5.85 GHz

Gang Kang, Senior Member, IEEE and Om P. Gandhi, Life Fellow, IEEE
Department of Electrical and Computer Engineering
University of Utah
Salt Lake City, Utah 84112, U.S.A.

Abstract

Compliance with 1- or 10-g SAR safety guidelines is required in various countries for all newly-introduced personal wireless devices such as Wi-Fi PCs. Even though the dielectric properties of the human tissues are known to be nonuniform and highly variable, relatively rigid adherence to prescribed dielectric properties (ε_r, σ) is required for compliance testing of such devices. Using some typical near-field irradiators, we have examined the effect of dielectric properties for SAR measurement fluids with conductivities varying by 2:1 to show that both 1- and 10-g SARs vary by less than ± 2-4% for the 802.11a band 5.15 to 5.825 GHz and only slightly more at the lower 802.11 b/g frequency of 2.45 GHz. This is due to higher surface SAR but shallower depth of penetration of EM fields for the higher conductivity media resulting in nearly identical SARs for cubical volumes associated with 1- or 10-g of tissue, respectively. Also studied is the effect of lower ε_r fluids recommended in some standards which results in slightly higher and thus a conservative assessment of SAR.

Accepted for publication in *IEEE Transactions on Electromagnetic Compatibility.*

EFFECT OF DIELECTRIC PROPERTIES ON THE PEAK 1- AND 10-G SAR FOR 802.11 a/b/g FREQUENCIES 2.45 AND 5.15 TO 5.85 GHz

Gang Kang, Senior Member, IEEE and Om P. Gandhi, Life Fellow, IEEE

I. Introduction

Compliance with the safety guidelines such as those proposed by IEEE [1] ICNIRP [2], etc. is required by regulatory agencies in the United States and elsewhere for all newly-introduced personal wireless devices such as Wi-Fi PCs, cellular telephones, etc. These safety guidelines are set in terms of maximum 1- or 10-g mass-normalized rates of electromagnetic energy deposition (specific absorption rates or SARs) for any 1- or 10-g of tissue. The two most commonly-used SAR limits today are those of IEEE [1] – 1.6 W/kg for any 1 g of tissue, and ICNIRP [2] – 2 W/kg for any 10 g of tissue, excluding extremities such as hands, wrists, feet, and ankles where higher SARs up to 4 W/kg for any 10 g of tissue are permitted in both of these standards. Experimental and numerical techniques using planar or head-shaped phantoms have been proposed for determining compliance with the SAR limits [3-5]. Dielectric properties (dielectric constant ε_r and conductivity σ) for the tissue-simulant fluids have been prescribed in three standards based on the properties measured for the various tissues for humans and other mammals [6] and equivalency with the properties needed for a homogeneous planar model to properly represent absorption of incident plane waves to that for a skin-fat-muscle-skull-sclera-CSF-brain layered planar model of a human [7].

In reality, the dielectric properties of the human tissues are highly nonuniform and likely variable with age as well [8]. Thus, dielectric constants and conductivities reported for the various tissues are highly variable and may vary by factors of 2:1 or more for some of the tissues [9]. This paper focuses on the effect of the dielectric properties of the SAR measurement fluids on the peak 1- and 10-g SARs for a planar phantom typically used for compliance testing of wireless PCs and other body- or torso-mounted devices that typically operate at frequencies of 2.4-2.484 GHz (802.11 b/g systems) and in the 5 GHz band for frequencies of 5.15 to 5.35 and 5.745 to 5.825 GHz (802.11a systems). For a 2:1 or 100% variability in conductivity of the tissue-simulant fluid, the variation in peak 1- and 10-g SAR is less than ± 2-4% for the higher frequency band 5.15 to 5.825 GHz and only slightly higher for the lower 802.11 b/g wireless systems band of 2.45 GHz. The reason for this is the higher surface SAR but shallower depth of penetration of electromagnetic fields for the higher conductivity media which has the net effect of providing nearly identical SAR for volumes in the shape of a cube, of dimensions 1 or 2.154 cm associated with 1- or 10-g of tissue, respectively. Though relatively negligible at 2.45 GHz, it is shown that the effect of the changing dielectric constant ε_r (instead of conductivity) is somewhat larger on both 1- and 10-g SARs for the 5-6 GHz band with the lower ε_r phantom materials resulting in 10-12 percent higher SARs. Thus the lower ε_r media recommended by IEC PT62209 [5] for the 5-6 GHz band may be used if a conservative determination of SAR is of interest.

II. Assumed EM Sources

The sources of microwave radiation typically used in wireless PCs are one or two dual band microstrip antennas either fabricated on an insertable wireless card or built into the base or at times behind the display screen of the PC. A wide variety of antenna dimensions and locations are typically used. For the purpose of calculations of peak 1- or 10-g SARs, we have assumed a typical microstrip antenna (see Fig. 1) and a couple of additional sources of EM radiation that are recommended in the compliance standards [3-5] for SAR measurement system validation. The three EM sources thus selected are: a square microstrip antenna of dimensions 30 × 30 mm placed with a spacing of 4 mm above a ground plane of dimensions 40 × 40 mm, a nominal half wave dipole of length 51.5 mm and diameter 3.6 mm recommended for 2.45 GHz in [3, 4] and a WR187 open-ended rectangular waveguide of internal dimensions 4.75 × 2.21 cm that may be used in the frequency band 5.1 to 5.8 GHz for SAR system validation. As recommended in the compliance standards [3-5], these sources are assumed to be placed under a planar phantom of a relatively thin base of thickness 2.0 mm made of a lossless dielectric and of sufficiently large lateral dimensions to be able to ignore scattering from the edges of the planar box or the tissue-simulant lossy fluid used to fill this box to a depth of 15 cm (several times the depth of penetration of fields in the fluid so as to present a nearly infinitely deep medium to neglect reflections). For the present calculations using the finite-difference time-domain (FDTD) numerical technique, we have used a planar phantom box of inside dimensions 30.5 × 41.9 × 20 cm made of acrylic ($\varepsilon_r = 2.56$) of base thickness 2.0 mm that is assumed to be filled with a tissue-simulant fluid of different dielectric properties (ε_r, σ) up to a depth of 15 cm. As recommended in the compliance standards [3-5], each of the three aforementioned sources of EM fields; namely, the microstrip antenna, the half-wave dipole or the open-ended rectangular waveguide, are assumed to be placed at a distance of 8.0 mm below the base of the planar phantom, resulting in a separation of 10 mm to the bottom level of the tissue-simulant fluid. A microstrip antenna is generally mounted in the base of a wireless portable computer (PC) which is tested for above-lap placement for one of the configurations. Thus, the ground plate of dimensions 40 × 40 mm for the assumed microstrip antenna is placed at a distance of 8 mm below the base of the planar phantom. The microstrip of dimensions 30 × 30 mm is assumed to be printed on a substrate of dielectric constant $\varepsilon_r = 2.56$ and thickness 4 mm.

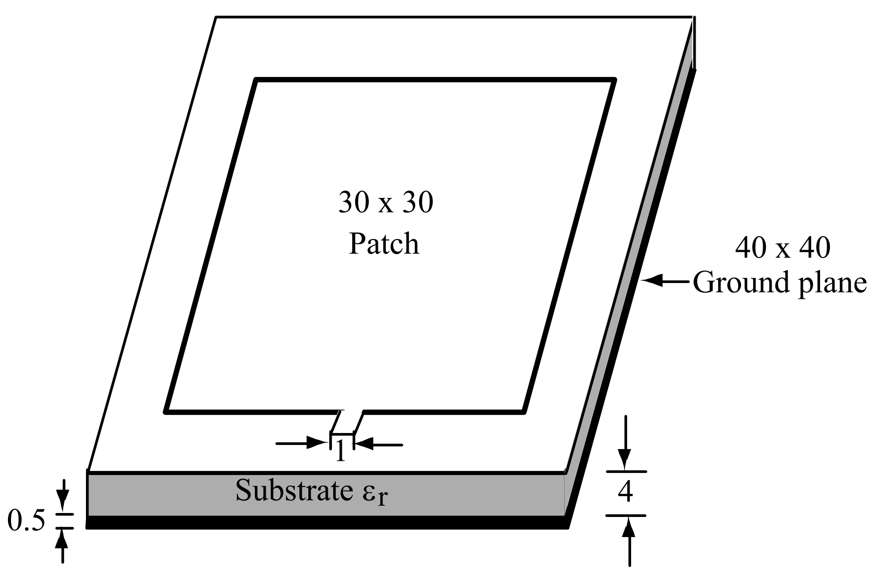

Fig. 1. A square patch microstrip antenna typical of wireless PCs. All dimensions are in mm.

III. The Finite-Difference Time-Domain Method

The method used for SAR distributions is the well-established finite-difference time-domain (FDTD) method. This method described in several texts [10, 11] has been used successfully by various researchers [12-15] and, therefore, would not be described here in any detail. For the FDTD calculations, we used a cell size 0.5 × 0.5 × 0.5 mm both at 2.45 GHz and for the two representative frequencies of 5.25 and 5.80 GHz in the 5-6 GHz band. This was done to meet the requirement $\delta \leq \lambda_\varepsilon / 10$ in the lossy tissue-simulant fluid as well as in recognition of the fact that the depth of penetration δ_s in the fluid is fairly small being on the order of 13-26 mm at 2450 MHz and less than 5-9 mm for the 5 GHz band. The dielectric properties (ε_r, σ) assumed for the "tissue-simulant" fluids for the two calculation bands are those given in the various compliance standards and conductivities that are 75% or 150% of those suggested in the various standards [3-5].

The values of ε_r, σ taken for various frequencies are given in Table 1. The dielectric properties are those suggested by the FCC OET Bulletin 65 Supplement C [16] and IEC TC 106/PT62209 [5] and SAR measurement fluids that may have conductivities that are 0.75 or 1.5 times those suggested for the flat body-simulant phantom in [5, 16]. Thus a 2:1 variation of conductivities is assumed for the SAR measuring fluid of the flat phantom.

IV. Calculated 1- and 10-g SARs

As recommended in the IEEE [1] and CENELEC [4] Standards, the peak 1- and 10-g SARs are calculated using cubes of dimensions 10 or 21.5 mm, respectively. Given in Tables 1 and 2 also are the peak 1- or 10-g SARs thus calculated for the various tissue-simulant fluids and several near-field irradiation systems at a number of frequencies typical of Wi-Fi PCs. Important points to note from the results of Tables 1 and 2 are as follows:

1. For a 2:1 variation in conductivity of the tissue-simulant fluids, the variation in peak 1- and 10-g SARs is within ± 2-4% for frequencies in the 802.11a 5 GHz band e.g. 5.25 and 5.8 GHz. The variation in peak 1- or 10-g SAR is higher at the lower frequency of 2.45 GHz. However, there is a move to harmonize the various compliance standards in terms of the peak 10- rather than 1-g SARs. For a 2:1 variation in the conductivity, the variation in peak 10-g SAR at 2.45 GHz is within ± 10%.

2. The effect of lower dielectric constant ε_r recommended by IEC PT62209 [5] is relatively small at 2.45 GHz ($\leq 4\,\%$) but is somewhat higher for the 5-6 GHz band. Both the 1- and 10-g SARs are higher by up to 10-12 percent for the 5 GHz band for the lower dielectric constant tissue-simulant fluids recommended by IEC PT62209 [5] as compared to those suggested in FCC OET Bulletin 65 [14].

The result of a relatively negligible variation of peak 1- and 10-g SAR in spite of a 2:1 change in conductivity is very surprising, since as expected, there is a highly variable penetration of EM energy into the different conductivity tissue-simulant fluids as seen in Tables 1, 2 and Figs. 2-5, respectively. As expected, somewhat deeper penetration is observed for lower conductivity fluids and increasingly shallower penetration is observed as the conductivity is increased both at 2.45 GHz and at frequencies in the 5-6 GHz band (see Tables 1, 2). Also to be noticed in Figs. 2-5 are the higher surface SARs for the higher conductivity fluids which tend to compensate for the shallower penetration of fields in such fluids. This is the reason for relatively constant 1- and 10-g SARs in spite of the wide variation of the conductivity of the media.

Table 1. Assumed dielectric properties (ε_r , σ) taken for frequencies 2.45, 5.25, and 5.80 GHz and the FDTD-calculated peak 1- and 10-g SARs for some typical near-field radiators. The irradiators are assumed to be placed 10 mm below the bottom surface of the tissue-simulant fluid in a flat phantom of base thickness 2 mm with (ε_r = 2.56). Radiated Power = 100 mW.

Frequency GHz	Near Field Radiator	Assumed Dielectric Properties			$1/e^2$ Depth of Power Penetration (mm)	1-g SAR (W/kg)	10-g SAR (W/kg)
		ε_r	σ (S/m)	Reference			
2.45	Dipole	52.7	1.46	Lower σ @ 75% of FCC	18.1	4.34	2.12
			1.95	FCC, body [16]	14.6	5.13	2.32
			2.93	Higher σ @ 150% of FCC	10.7	6.13	2.48
		39.2	1.35	Lower σ @ 75% of IEC	16.9	4.41	2.16
			1.80	IEC/FCC, head [5]	13.7	5.18	2.35
			2.70	Higher σ @ 150% of IEC	10.1	6.14	2.49
5.25	Waveguide	48.9	4.02	Lower σ @ 75% of FCC	8.9	3.37	1.44
			5.36	FCC, body [16]	6.8	3.57	1.44
			8.04	Higher σ @ 150% of FCC	4.6	3.63	1.42
		35.9	3.53	Lower σ @ 75% of IEC	8.7	3.79	1.61
			4.71	IEC/FCC, head [5]	6.7	3.99	1.61
			7.07	Higher σ @ 150% of IEC	4.6	4.02	1.57
5.80	Waveguide	48.2	4.50	Lower σ @ 75% of FCC	7.9	3.79	1.59
			6.00	FCC, body [16]	6.0	3.95	1.58
			9.00	Higher σ @ 150% of FCC	4.1	3.94	1.54
		35.3	3.95	Lower σ @ 75% of IEC	7.7	4.26	1.77
			5.27	IEC/FCC, head [5]	5.9	4.42	1.76
			7.91	Higher σ @ 150% of IEC	4.1	4.36	1.70

Table 2. Assumed dielectric properties (ε_r, σ) taken for frequencies 2.45, 5.25, and 5.80 GHz and the FDTD-calculated peak 1- and 10-g SARs for a typical microstrip antenna of dimensions 30 × 30 mm placed 4 mm above a ground plane of dimensions 40 × 40 mm (see Fig. 1). As required by the compliance standards [5, 16], the ground plane of the microstrip antenna is assumed to be 10 mm below the bottom surface of the tissue-simulant fluid (microstrip at 14.5 mm below the fluid). Radiated Power = 100 mW.

Frequency GHz	Assumed Dielectric Properties		$1/e^2$ Depth of Power Penetration (mm)	1-g SAR (W/kg)	10-g SAR (W/kg)
	ε_r	σ (S/m)			
2.45	52.7	1.46	25.2	2.26	1.43
		1.95	19.0	2.71	1.57
		2.93	13.2	3.37	1.72
	39.2	1.35	23.4	2.36	1.47
		1.80	18.3	2.82	1.61
		2.70	11.6	3.60	1.77
5.25	48.9	4.02	9.2	1.52	0.52
		5.36	7.0	1.60	0.51
		8.04	4.7	1.62	0.50
	35.9	3.53	9.0	1.57	0.53
		4.71	6.8	1.64	0.53
		7.07	4.6	1.66	0.51
5.80	48.2	4.50	8.0	1.96	0.57
		6.00	6.0	2.03	0.56
		9.00	4.1	2.03	0.54
	35.3	3.95	7.7	2.03	0.60
		5.27	5.9	2.10	0.59
		7.91	4.1	2.09	0.56

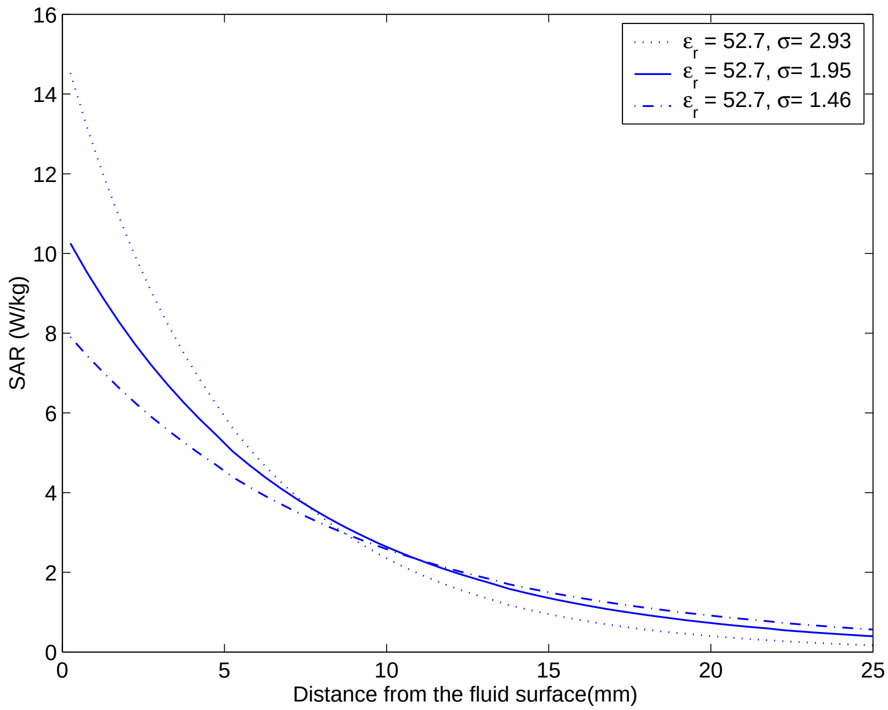

Fig. 2. **The dipole antenna.** Comparison of the FDTD-calculated variation of the SAR with depth for the various tissue-simulant media at 2.45 GHz.

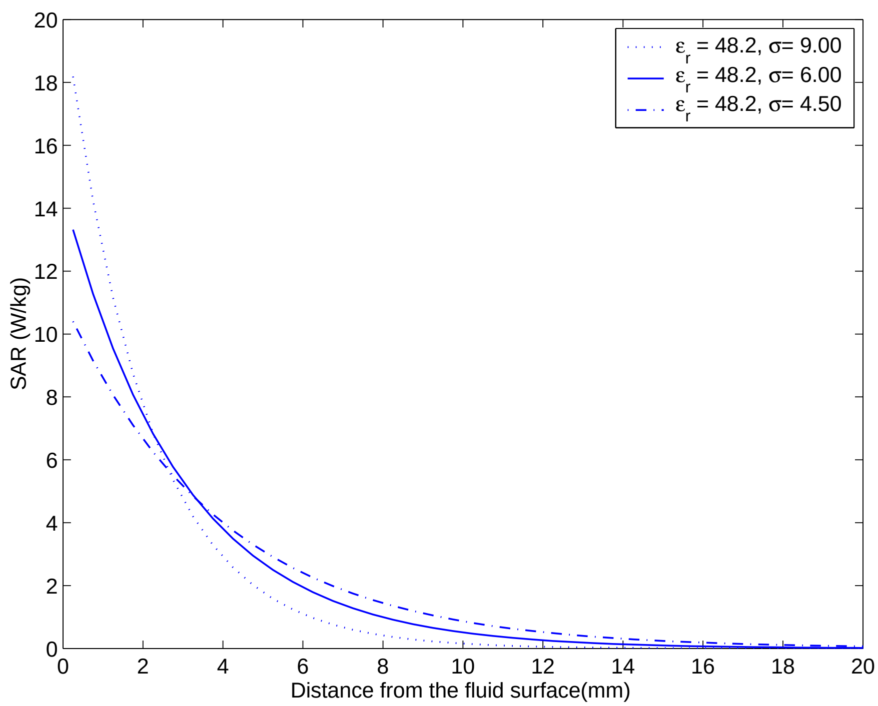

Fig. 3. **The rectangular waveguide radiator.** Comparison of the FDTD-calculated variation of the SAR with depth for the various tissue-simulant media at 5.8 GHz.

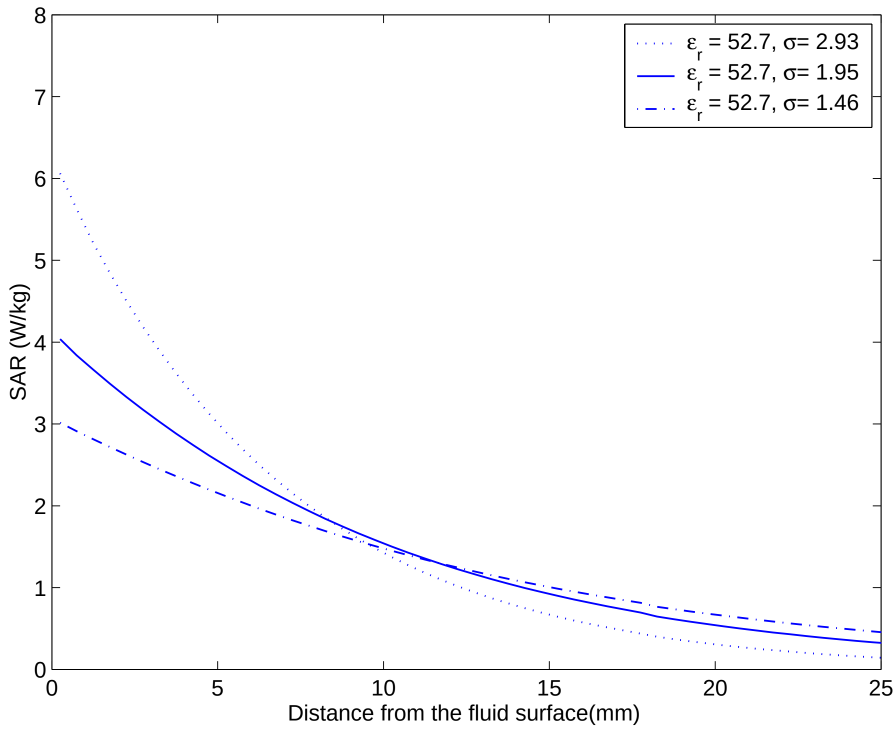

Fig. 4. **The microstrip antenna.** Comparison of the FDTD-calculated variation of the SAR with depth for the various tissue-simulant media at 2.45 GHz.

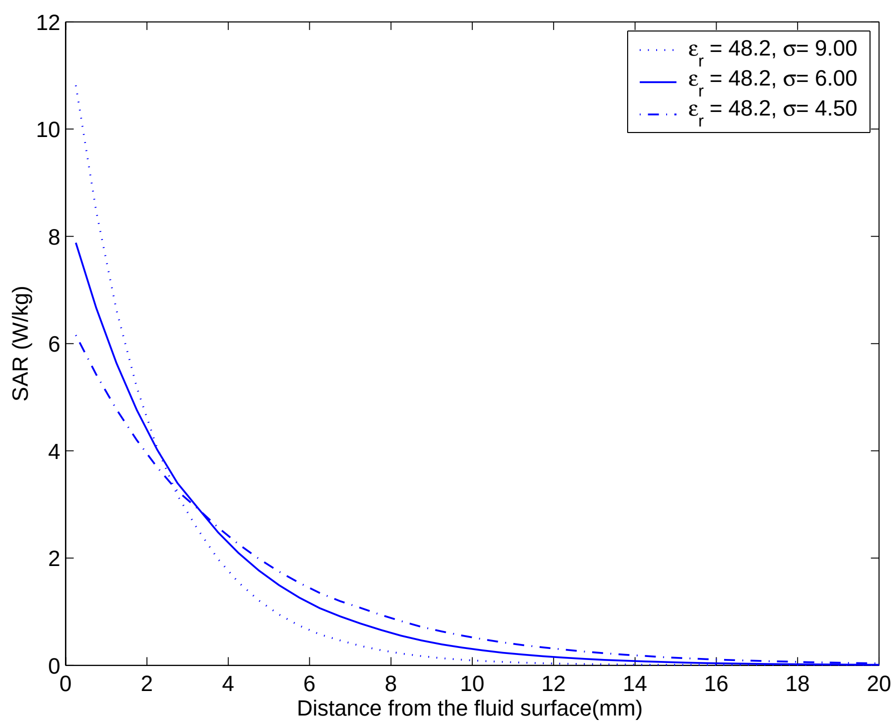

Fig. 5. **The microstrip antenna.** Comparison of the FDTD-calculated variation of the SAR with depth for the various tissue-simulant media at 5.8 GHz.

V. Comparison with Plane Wave Exposures

The above results are easy to understand when one looks at the peak 1- and 10-g SARs for plane waves incident normally at a semi-infinite slab of tissue-simulant fluid of variable dielectric properties. Given in Table 3 are some of the salient parameters and the peak 1- and 10-g SARs calculated for plane waves that are incident normal to a semi-infinite slab of dielectric properties similar to those of tissue-simulant media. Unlike the case of near-field exposure systems in Tables 1 and 2, closed-form analytical expressions given in the following may be used for this case of plane waves.

Table 3. Calculated skin depths, power transmission coefficients, and peak 1- and 10-g SARs for plane waves of power density 1 mW/cm^2 for normal incidence on a semi-infinite slab of tissue-simulant media of different assumed dielectric properties at 2.45, 5.25 and 5.80 GHz.

Frequency GHz	Assumed Dielectric Properties		Skin Depth (mm)	Power Transmission Coefficient TT*	1-g SAR (W/kg)	10-g SAR (W/kg)
	ε_r	σ (S/m)				
2.45	52.7	1.46	26.5	0.42	0.22	0.16
		1.95	19.9	0.42	0.26	0.17
		2.93	13.4	0.41	0.32	0.18
	39.2	1.35	24.8	0.47	0.26	0.18
		1.80	18.7	0.46	0.30	0.19
		2.70	12.7	0.45	0.35	0.20
5.25	48.9	4.02	9.3	0.43	0.38	0.20
		5.36	7.0	0.42	0.40	0.20
		8.04	4.8	0.41	0.40	0.19
	35.9	3.53	9.1	0.48	0.42	0.22
		4.71	6.9	0.47	0.44	0.22
		7.07	4.7	0.44	0.44	0.22
5.80	48.2	4.50	8.3	0.43	0.39	0.20
		6.00	6.3	0.42	0.41	0.20
		9.00	4.3	0.41	0.40	0.19
	35.3	3.95	8.1	0.48	0.44	0.22
		5.27	6.1	0.47	0.45	0.22
		7.91	4.2	0.44	0.44	0.21

For a lossy slab of dielectric constant ε_r and conductivity σ, the complex dielectric constant ε^* at radian frequency ω can be written as:

$$\varepsilon^* = \varepsilon_r - j\frac{\sigma}{\omega\varepsilon_o} = \varepsilon_r - j\varepsilon'' \tag{1}$$

The propagation constant γ in the lossy medium can be written as $\gamma = \alpha + j\beta$ where the attenuation constant α and propagation constant β can be written as follows [17]:

$$\alpha = \omega\sqrt{\frac{\mu\varepsilon_o\varepsilon_r}{2}}\left[\sqrt{1+\left(\frac{\varepsilon''}{\varepsilon_r}\right)^2} - 1\right]^{1/2} \tag{2}$$

$$\beta = \omega\sqrt{\frac{\mu\varepsilon_o\varepsilon_r}{2}}\left[\sqrt{1+\left(\frac{\varepsilon''}{\varepsilon_r}\right)^2} + 1\right]^{1/2} \tag{3}$$

The skin depth δ_s is given by $1/\alpha$ and the complex reflection coefficient ρ at the air-slab interface is given by

$$\rho = \frac{1-\sqrt{\varepsilon^*}}{1+\sqrt{\varepsilon^*}} \tag{4}$$

The power transmission coefficient is given by $TT^* = (1-\rho\rho^*)$.

For an incident power density $S_{inc}\ \mathrm{mW/cm^2}$, the peak 1- and 10-g SARs in mW/g or W/kg are given by the following equations:

$$\text{Peak 1-g SAR} = \left[1-e^{-2/\delta_s}\right]\left(TT^*\right)S_{inc} \qquad \text{W/kg} \tag{5}$$

$$\text{Peak 10-g SAR} = \frac{4.64}{10}\left[1-e^{-4.309/\delta_s}\right]\left(TT^*\right)S_{inc} \qquad \text{W/kg} \tag{6}$$

As for the case of the assumed near-field irradiators, here too, the results are very similar with an advantage that a physical insight into the results is now possible.

1. For a 2:1 increase in conductivity of the SAR measurement fluid, the variation in peak 10-g SAR is relatively small and generally within ± 2.5% for all of the frequencies in the band 5.25 to 5.8 GHz (see Table 3). However, for the lower frequency of 2.45 GHz, there is a somewhat higher variation in peak 1-g SAR (± 23%) and a considerably lower variation on the order of ± 5-6% for the peak 10-g SAR. The reason for such a small variation is that the power transmission coefficient varies very little with conductivity of the fluid particularly for the higher dielectric constant media. All of the power thus coupled into the tissue-simulant medium is absorbed by the 10-g averaging volume, particularly for the 5-6 GHz band, since the depth of penetration is only on the order of 4-9 mm as seen in Table 3. In fact, the peak 10-g SAR given in the last column of Table 3

at the higher frequencies of 5.25 and 5.8 GHz is nothing but the power coupled into a surface area of 2.154 cm × 2.154 cm or 4.64 cm^2 divided by 10 g.

2. Similar to the cases of the near-field irradiators of Tables 1 and 2, the peak 1- and 10-g SARs for plane waves for the lower dielectric constant (ε_r) media recommended by IEC TC 106/PT62209 are slightly higher than those for the higher ε_r media recommended in FCC OET Bulletin 65 [16]. As seen in Table 3, this is due to somewhat higher power transmission coefficients for the media with lower dielectric constants.

VI. Conclusions

We have examined the effect of dielectric properties (ε_r, σ) of SAR measuring tissue-simulant media on the peak 1- and 10-g SARs both for near-field sources and for plane waves since the dielectric properties reported for the various tissues are highly variable. For a 2:1 variability in the conductivity of tissue-simulant fluid, the variation in peak 1- and 10-g SAR is negligible within ± 2-4% for the 5 to 6 GHz band and only slightly larger on the order of ± 10% for the 2.45 GHz band, particularly for the all-important 10-g SAR. Thus, an exact match to the conductivities or the dielectric constant recommended in the various compliance standards is not really necessary as far as determination of 1- or 10-g SARs is concerned. This is important since tissue dielectric properties are known to be highly nonuniform and considerably variable between individuals [9]. Both the 1- and 10-g SARs are, however, higher by about 10-12% for the lower ε_r media recommended by IEC TC 106/PT62209 [5], which may, therefore, be used if a conservative determination of SAR is of interest.

REFERENCES

1. IEEE Std. C95.1, "IEEE Standard for Safety Levels with Respect to Human Exposure to Radiofrequency Electromagnetic Fields, 3 kHz to 300 GHz," Institute of Electrical and Electronics Engineers, Piscataway, NJ, 1999.

2. ICNIRP (International Commission on Non-Ionizing Radiation Protection), "Guidelines for limiting exposure to time-varying electric, magnetic, and electromagnetic fields (up to 300 GHz)", *Health Physics*, Vol. 74, pp. 494-522, 1998.

3. IEEE Standards Coordinating Committee 34, "Recommended Practice for Determining the Peak Spatial-Average Specific Absorption Rate (SAR) in the Human Body Due to Wireless Communications Devices: Experimental Techniques," Institute of Electrical and Electronics Engineers, Draft Standard, 2003.

4. CENELEC EN50361, "Basic Standard for Measurement of Specific Absorption Rate Related to Human Exposure to Electromagnetic Fields from Mobile Telephones (300-MHz-3 GHz), CENELEC European Committee for Electrotechnical Standardization, rue de Stassart 35, B-1050, Brussels, Belgium, 2001.

5. IEC TC 106/PT62209, "Evaluation of Human Exposure to Radiofrequency Fields from Handheld and Body-Mounted Wireless Communications Devices in the Frequency Range of 30 MHz to 6 GHz: Human Models, Instrumentation Procedures," Draft Standard in preparation, 2003.

6. C. Gabriel, "Compilation of the Dielectric Properties of Body Tissues at RF and Microwave Frequencies," Report AL/OE-TR-1996-0037, Armstrong Laboratory (AFMC), Radiofrequency Radiation Division, Brooks AFB, TX (www.brooks.af.mil/AFRL/HED/hedr/reports/dielectric/home.html).

7. A. Drossos, V. Santomaa, and N. Kuster, "The Dependence of Electromagnetic Energy Absorption Upon Human Head Tissue Composition in the Frequency Range of 300-3000 MHz," *IEEE Transactions on Microwave Theory and Techniques,* Vol. 48(11), pp. 1988-1995, November 2000.

8. A Peyman, A. A. Rezazadeh, and C. Gabriel, "Changes in the Dielectric Properties of Rat Tissue as a Function of Age at Microwave Frequencies," *Physics in Medicine and Biology,* Vol. 46, pp. 1617-1629, 2001.

9. M. A. Stuchly and S. S. Stuchly, "Dielectric Properties of Biological Substances – Tabulated," *Jour. Microwave Power*, Vol. 15, pp. 19-26, 1980.

10. A. Taflove (Ed.), *Advances in Computational Electrodynamics: The Finite-Difference Time-Domain Method,* Artech House, Boston, MA, 1998.

11. A. Taflove and S. C. Hagness, *Computational Electrodynamics: The Finite-Difference Time-Domain Method*, Artech House, Boston, MA, 2000.

12. P. J. Dimbylow and S. M. Mann, "SAR Calculations in an Anatomically-Based Realistic Model of the Head for Mobile Communication Transceivers at 900 MHz and 1.8 GHz," *Physics in Med. and Biol.,* Vol. 39**,** pp. 1537-1553, 1994.

13. O. P. Gandhi and J. Y. Chen, "Electromagnetic Absorption in the Human Head from Experimental 6 GHz Handheld Transceivers," *IEEE Trans. on Electromag. Compat.,* Vol. 37, pp. 547-558, 1995.

14. M. A. Jensen and Y. Rahmat-Samii, "EM Interaction in Handset Antennas and a Human in Personal Communications," *Proc. IEEE,* Vol. 83, pp. 7-17, 1995.

15. M. Okoniewski and M. A. Stuchly, "A Study of Handset Antenna and Human Body Interaction, *IEEE Trans. on Microwave Theory and Tech,* Vol.. 44, pp. 1855-1864, 1996.

16. U.S. Federal Communications Commission (FCC), Supplement C (Edition 01-01) to OET Bulletin 65 (Edition 97-01), "Additional Information for Evaluating Compliance of Mobile and Portable Devices with FCC Limits for Human Exposure to Radiofrequency Radiation," June 2001 (www.fcc.gov/oet/info/documents/bulletins/#65)

17. C. A. Balanis, *Advanced Engineering Electromagnetics,* John Wiley & Sons, 1989.

APPENDIX F

Uncertainty Analysis

The uncertainty analysis of the University of Utah SAR Measurement System is given in Table F.1. Several of the numbers on tolerances are obtained by following procedures similar to those detailed in [3], while others have been obtained using methods suggested in [5].

Table F.1. Uncertainty analysis of the University of Utah SAR Measurement System.

Uncertainty Component	Uncertainty Value ± %	Probability Distribution	Divisor	C_i 1-g	Standard Unc. u_i ± %	ν_i
Measurement System						
Probe calibration	2.0	N	1	1	2.0	∞
Axial isotropy of the probe	4.0	R	√3	$(1-cp)^{1/2}$	1.6	∞
Hemispherical isotropy of the probe	5.5	R	√3	$\sqrt{c_p}$	0.0	∞
Boundary effect	0.8	R	√3	1	0.5	∞
Probe linearity	3.0	R	√3	1	1.7	∞
System detection limits	1.0	R	√3	1	0.6	∞
Readout electronics	1.0	N	1	1	1.0	∞
Response time	0.0	R	√3	1	0.0	∞
Integration time	0.5	R	√3	1	0.3	∞
RF ambient conditions	0	R	√3	1	0	∞
Probe positioner mechanical tolerance	0.5	R	√3	1	0.3	∞
Probe positioning with respect to phantom shell	2.0	R	√3	1	1.2	∞
Extrapolation, interpolation, & integration algorithms for maximum SAR evaluation	5.0	R	√3	1	2.9	∞
Test Sample Related						
Device positioning	3	R	√3	1	1.7	11
Device holder uncertainty	3	R	√3	1	1.7	7
Output power variation – SAR drift measurement	5	R	√3	1	2.9	∞
Phantom and Tissue Parameters						
Phantom uncertainty – base thickness tolerance	10.0	R	√3	1	5.8	∞
Liquid conductivity – deviation from target values	0.4	R	√3	0.7	0.2	∞
Liquid conductivity – measurement uncertainty	1.5	R	√3	0.7	0.6	∞
Liquid permittivity – deviation from target values	0.8	R	√3	0.6	0.3	∞
Liquid permittivity – measurement uncertainty	3.5	R	√3	0.6	1.2	∞
Combined Standard Uncertainty		RSS			8.3	
Expanded Uncertainty (95% Confidence Level)					± 16.6	

APPENDIX G

COARSE SCANS FOR THE HIGHEST SAR REGION FOR THE RF MICRO DEVICES CARDBUS CARD MODEL DK5405 WITH TOSHIBA MODEL 1415-S173 HOST COMPUTER (FCC ID# RFN5405RDK0401)

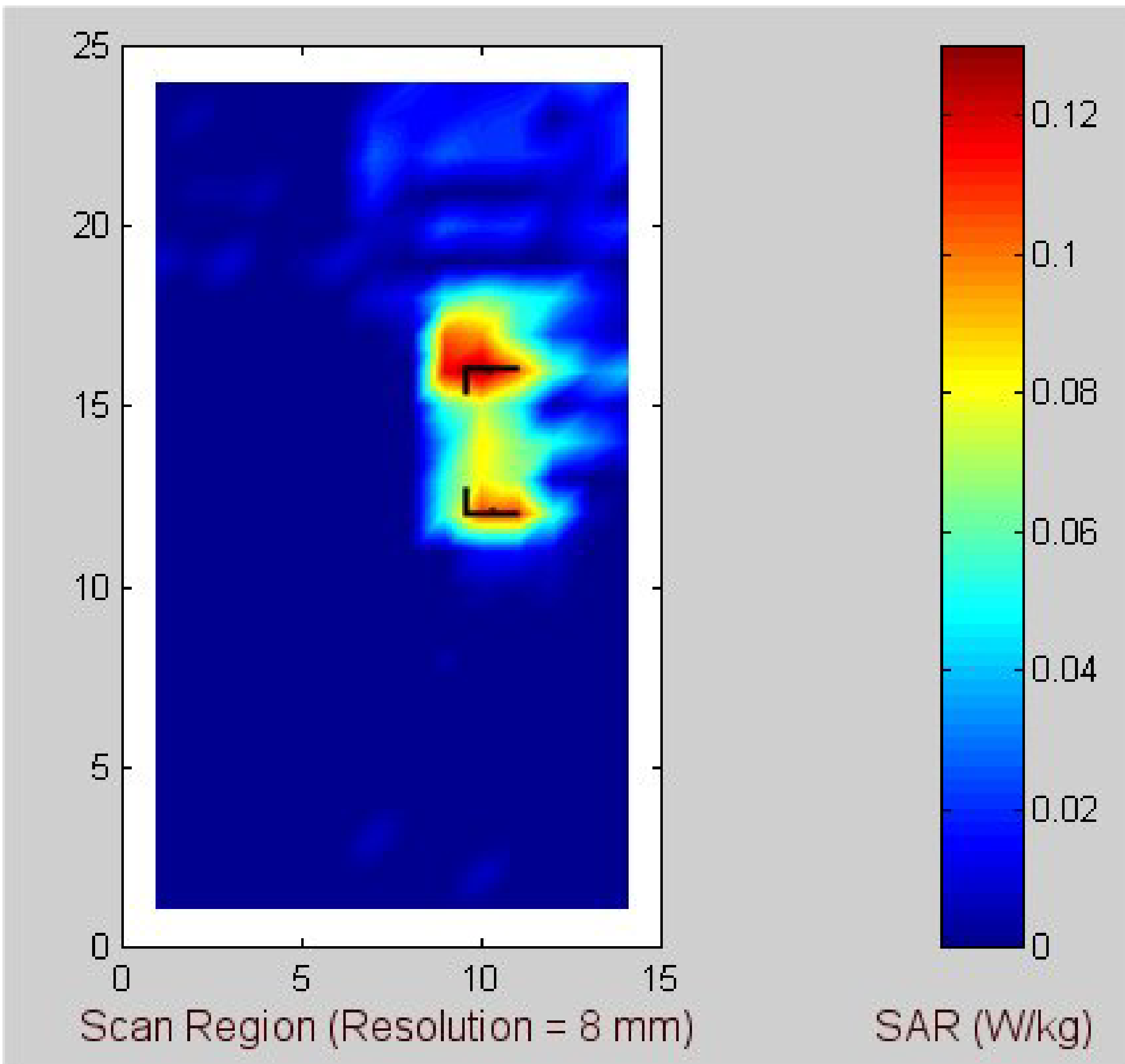

Fig. G.1. **Above-lap position (Configuration 1).** Coarse scan for the highest SAR region for the RF Micro Devices Cardbus Card Model DK5405. **Frequency = 5.18 GHz, normal mode.**

Table G.1. **Above-lap position (Configuration 1). Normal mode at 5.18 GHz**. The SARs measured for the RF Micro Devices Cardbus Card Model DK5405 inserted into Toshiba Model 1415-S173 Host Computer.

1-g SAR = 0.122 W/kg

a. At depth of 1 mm

0.229	0.141	0.196	0.157	0.103
0.172	0.212	0.191	0.241	0.129
0.165	0.225	0.167	0.197	0.160
0.149	0.118	0.189	0.167	0.145
0.199	0.167	0.188	0.129	0.178

b. At depth of 3 mm

0.140	0.126	0.134	0.128	0.106
0.135	0.144	0.135	0.144	0.120
0.137	0.139	0.125	0.125	0.128
0.124	0.123	0.133	0.126	0.120
0.143	0.140	0.146	0.131	0.140

c. At depth of 5 mm

0.104	0.112	0.109	0.108	0.103
0.114	0.117	0.108	0.112	0.108
0.116	0.104	0.103	0.095	0.105
0.108	0.115	0.106	0.107	0.108
0.115	0.124	0.122	0.123	0.125

d. At depth of 7 mm

0.096	0.100	0.100	0.097	0.097
0.102	0.109	0.098	0.106	0.099
0.101	0.095	0.092	0.087	0.091
0.097	0.103	0.094	0.100	0.102
0.103	0.112	0.109	0.113	0.119

e. At depth of 9 mm

0.095	0.091	0.095	0.090	0.092
0.097	0.104	0.094	0.104	0.095
0.091	0.094	0.085	0.085	0.085
0.091	0.094	0.088	0.098	0.097
0.099	0.104	0.103	0.105	0.115

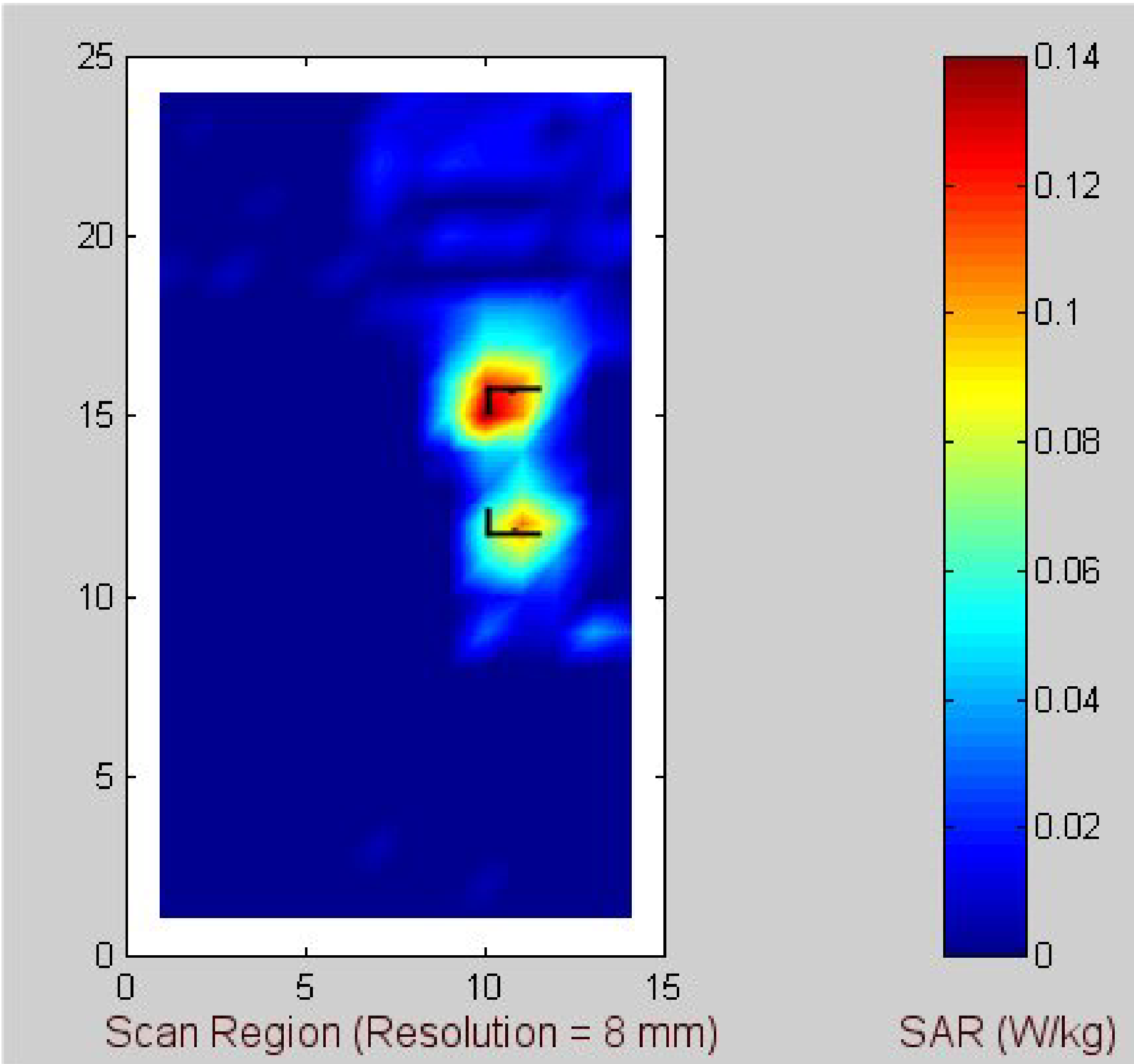

Fig. G.2. **Above-lap position (Configuration 1).** Coarse scan for the highest SAR region for the RF Micro Devices Cardbus Card Model DK5405. **Frequency = 5.26 GHz, normal mode.**

Table G.2. **Above-lap position (Configuration 1). Normal mode at 5.26 GHz**. The SARs measured for the RF Micro Devices Cardbus Card Model DK5405 inserted into Toshiba Model 1415-S173 Host Computer.

1-g SAR = 0.148 W/kg

a. At depth of 1 mm

0.339	0.302	0.294	0.334	0.292
0.297	0.362	0.314	0.397	0.304
0.288	0.316	0.313	0.286	0.299
0.346	0.384	0.334	0.318	0.244
0.311	0.337	0.255	0.323	0.323

b. At depth of 3 mm

0.166	0.161	0.166	0.175	0.161
0.171	0.187	0.183	0.182	0.162
0.164	0.176	0.185	0.179	0.159
0.171	0.190	0.185	0.176	0.156
0.173	0.176	0.180	0.193	0.183

c. At depth of 5 mm

0.089	0.094	0.105	0.100	0.096
0.107	0.110	0.112	0.093	0.095
0.097	0.108	0.113	0.116	0.092
0.098	0.104	0.115	0.106	0.106
0.107	0.105	0.127	0.125	0.120

d. At depth of 7 mm

0.061	0.066	0.078	0.070	0.069
0.077	0.083	0.078	0.069	0.068
0.067	0.079	0.078	0.082	0.065
0.074	0.075	0.086	0.075	0.078
0.080	0.080	0.095	0.095	0.096

e. At depth of 9 mm

0.052	0.055	0.065	0.058	0.058
0.065	0.074	0.062	0.066	0.056
0.056	0.068	0.062	0.065	0.054
0.067	0.066	0.074	0.062	0.064
0.068	0.073	0.081	0.085	0.086

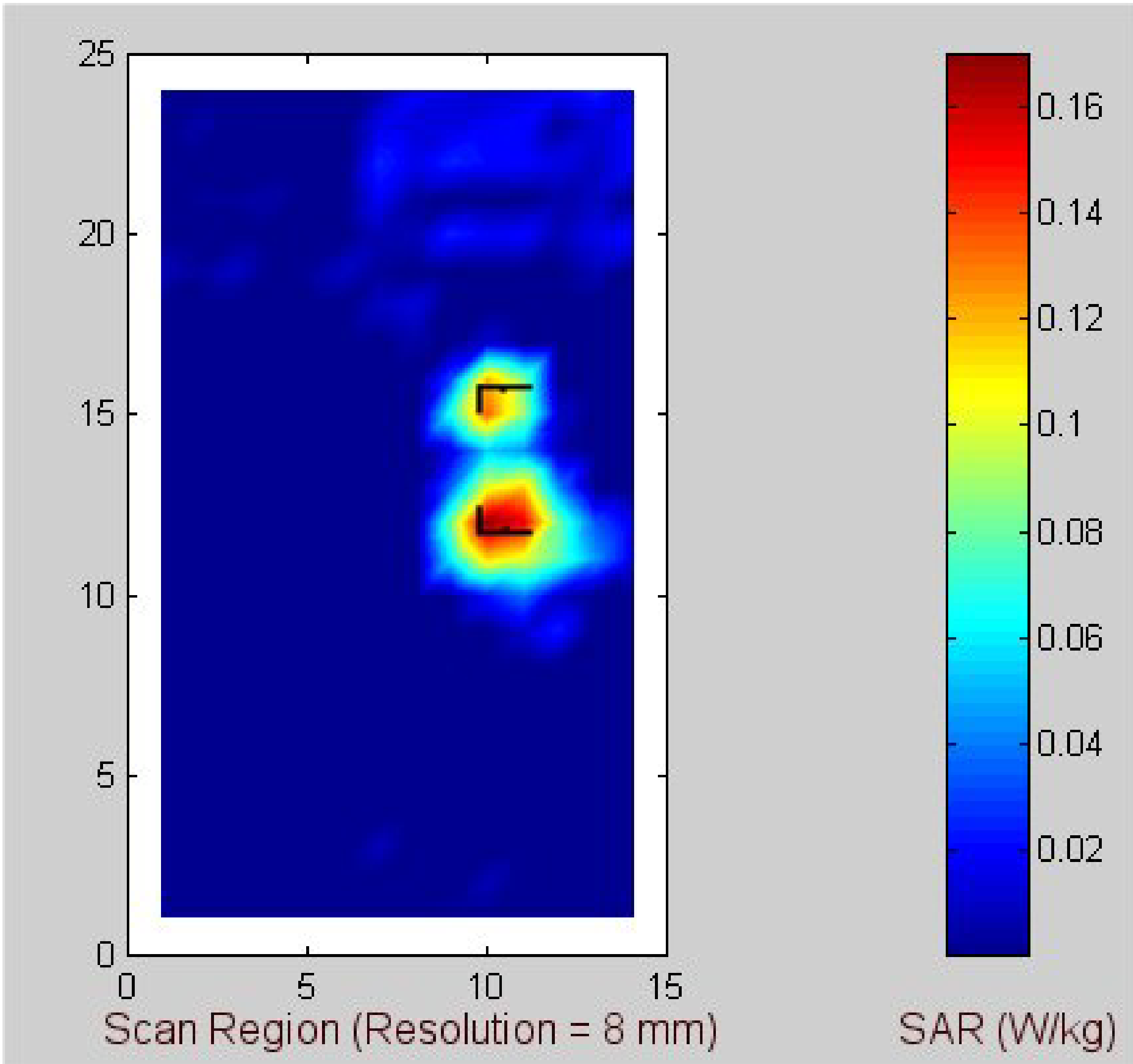

Fig. G.3. **Above-lap position (Configuration 1).** Coarse scan for the highest SAR region for the RF Micro Devices Cardbus Card Model DK5405. **Frequency = 5.32 GHz, normal mode.**

Table G.3. **Above-lap position (Configuration 1). Normal mode at 5.32 GHz**. The SARs measured for the RF Micro Devices Cardbus Card Model DK5405 inserted into Toshiba Model 1415-S173 Host Computer.

1-g SAR = 0.157 W/kg

a. At depth of 1 mm

0.305	0.311	0.310	0.310	0.340
0.259	0.369	0.298	0.268	0.290
0.341	0.353	0.230	0.288	0.273
0.260	0.298	0.354	0.251	0.289
0.355	0.303	0.280	0.319	0.217

b. At depth of 3 mm

0.192	0.195	0.187	0.184	0.175
0.179	0.206	0.194	0.180	0.177
0.206	0.202	0.178	0.182	0.172
0.178	0.188	0.197	0.179	0.180
0.199	0.193	0.185	0.180	0.152

c. At depth of 5 mm

0.128	0.133	0.125	0.122	0.106
0.123	0.130	0.131	0.125	0.119
0.133	0.127	0.132	0.122	0.117
0.124	0.126	0.126	0.127	0.120
0.127	0.135	0.129	0.116	0.107

d. At depth of 7 mm

0.096	0.103	0.097	0.094	0.085
0.088	0.099	0.096	0.093	0.092
0.100	0.094	0.100	0.092	0.090
0.093	0.092	0.099	0.094	0.091
0.101	0.105	0.098	0.092	0.079

e. At depth of 9 mm

0.081	0.086	0.084	0.079	0.077
0.070	0.085	0.079	0.074	0.078
0.089	0.081	0.083	0.077	0.077
0.077	0.075	0.087	0.078	0.077
0.092	0.090	0.082	0.083	0.065

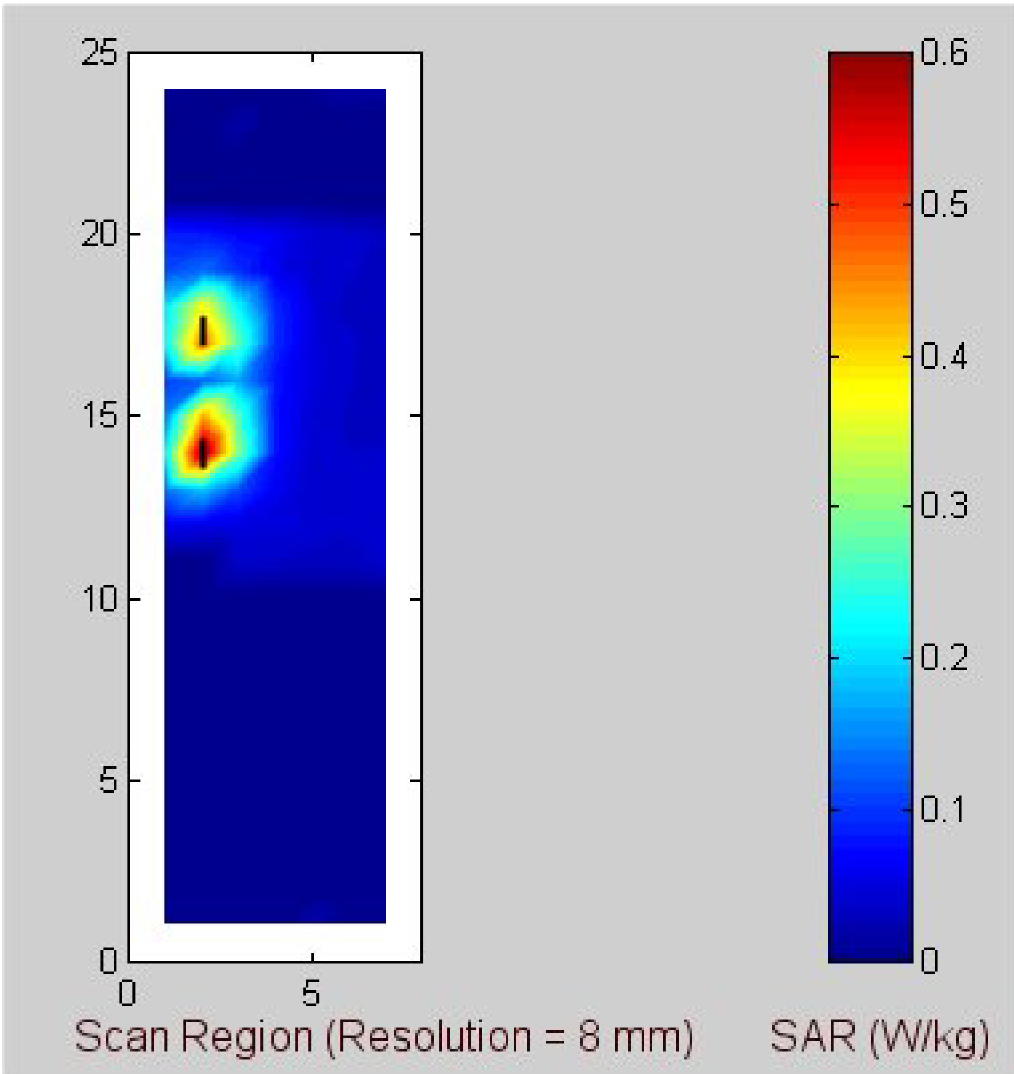

Fig. G.4. **Edge-on position (Configuration 2).** Coarse scan for the highest SAR region for the RF Micro Devices Cardbus Card Model DK5405. **Frequency = 5.18 GHz, normal mode.**

Table G.4. **Edge-on position (Configuration 2). Normal mode at 5.18 GHz**. The SARs measured for the RF Micro Devices Cardbus Card Model DK5405 inserted into Toshiba Model 1415-S173 Host Computer.

1-g SAR = 0.491 W/kg

a. At depth of 1 mm

0.951	1.201	1.431	1.363	1.209
0.991	1.386	1.487	1.586	1.343
1.051	1.448	1.769	1.636	1.447
0.997	1.328	1.382	1.330	1.229
0.792	1.008	1.193	1.272	1.044

b. At depth of 3 mm

0.498	0.631	0.717	0.669	0.572
0.531	0.703	0.768	0.766	0.643
0.550	0.724	0.835	0.802	0.701
0.509	0.648	0.691	0.658	0.596
0.406	0.510	0.594	0.616	0.542

c. At depth of 5 mm

0.256	0.317	0.346	0.314	0.259
0.277	0.340	0.376	0.352	0.291
0.275	0.346	0.375	0.373	0.325
0.252	0.305	0.332	0.314	0.280
0.204	0.251	0.288	0.296	0.273

d. At depth of 7 mm

0.137	0.162	0.174	0.155	0.126
0.148	0.167	0.185	0.168	0.138
0.138	0.170	0.179	0.179	0.159
0.130	0.155	0.166	0.157	0.144
0.110	0.132	0.153	0.160	0.145

e. At depth of 9 mm

0.078	0.092	0.098	0.087	0.073
0.086	0.090	0.100	0.093	0.076
0.075	0.093	0.101	0.098	0.088
0.076	0.092	0.093	0.086	0.089
0.070	0.082	0.099	0.105	0.091

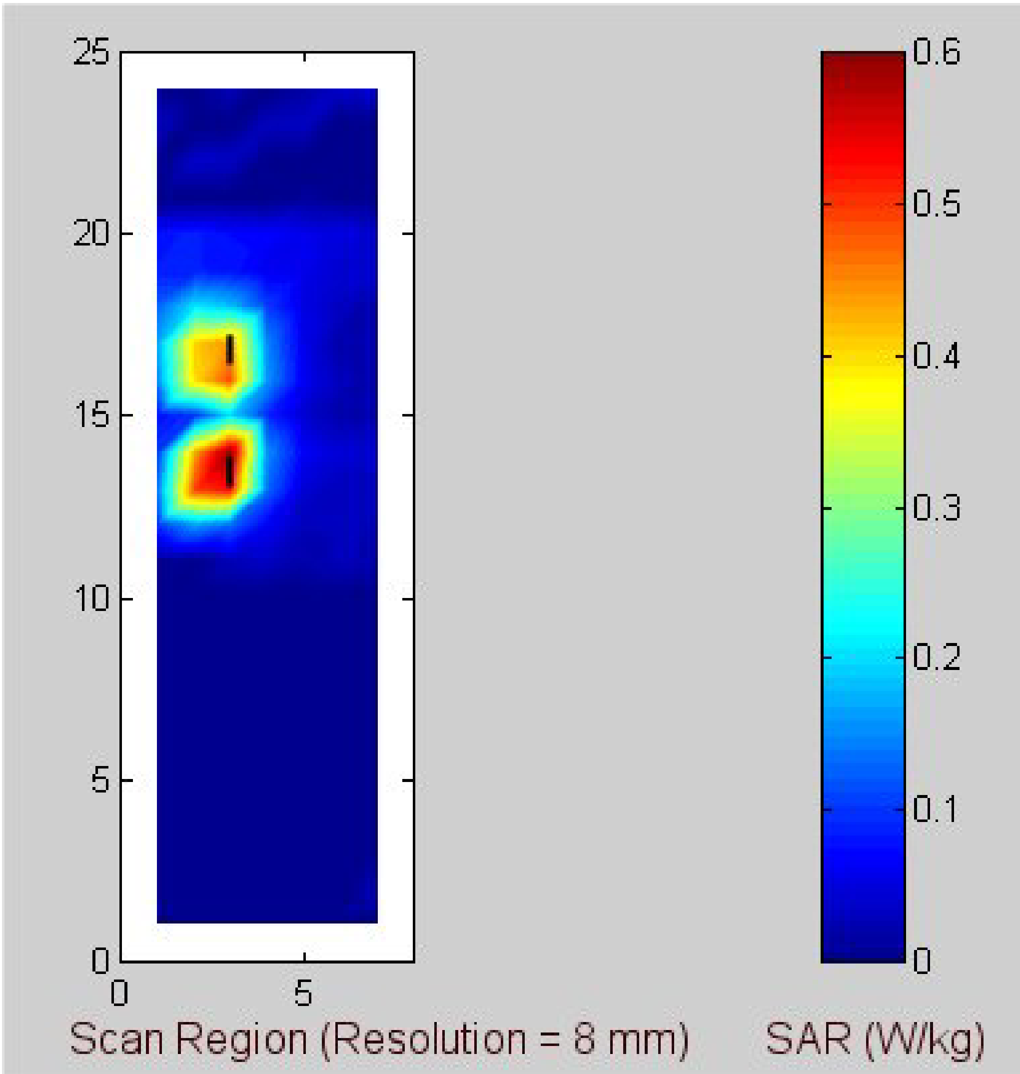

Fig. G.5. **Edge-on position (Configuration 2).** Coarse scan for the highest SAR region for the RF Micro Devices Cardbus Card Model DK5405. **Frequency = 5.26 GHz, normal mode.**

Table G.5. **Edge-on position (Configuration 2). Normal mode at 5.26 GHz**. The SARs measured for the RF Micro Devices Cardbus Card Model DK5405 inserted into Toshiba Model 1415-S173 Host Computer.

1-g SAR = 0.468 W/kg

a. At depth of 1 mm

0.873	1.167	1.368	1.412	1.126
0.990	1.244	1.522	1.584	1.284
0.886	1.219	1.510	1.524	1.437
0.893	1.190	1.435	1.506	1.366
0.705	0.953	1.159	1.206	1.182

b. At depth of 3 mm

0.419	0.557	0.647	0.646	0.546
0.477	0.610	0.714	0.727	0.607
0.434	0.590	0.713	0.732	0.675
0.430	0.579	0.686	0.714	0.647
0.351	0.465	0.563	0.600	0.582

c. At depth of 5 mm

0.201	0.264	0.300	0.284	0.256
0.231	0.290	0.324	0.326	0.273
0.213	0.280	0.326	0.340	0.310
0.213	0.279	0.319	0.329	0.302
0.181	0.230	0.280	0.297	0.295

d. At depth of 7 mm

0.111	0.142	0.154	0.139	0.129
0.130	0.150	0.163	0.167	0.131
0.119	0.148	0.164	0.170	0.160
0.126	0.152	0.166	0.170	0.162
0.111	0.133	0.165	0.170	0.179

e. At depth of 9 mm

0.074	0.090	0.093	0.085	0.079
0.089	0.093	0.101	0.104	0.077
0.080	0.094	0.100	0.100	0.099
0.090	0.102	0.106	0.110	0.107
0.081	0.096	0.119	0.123	0.137

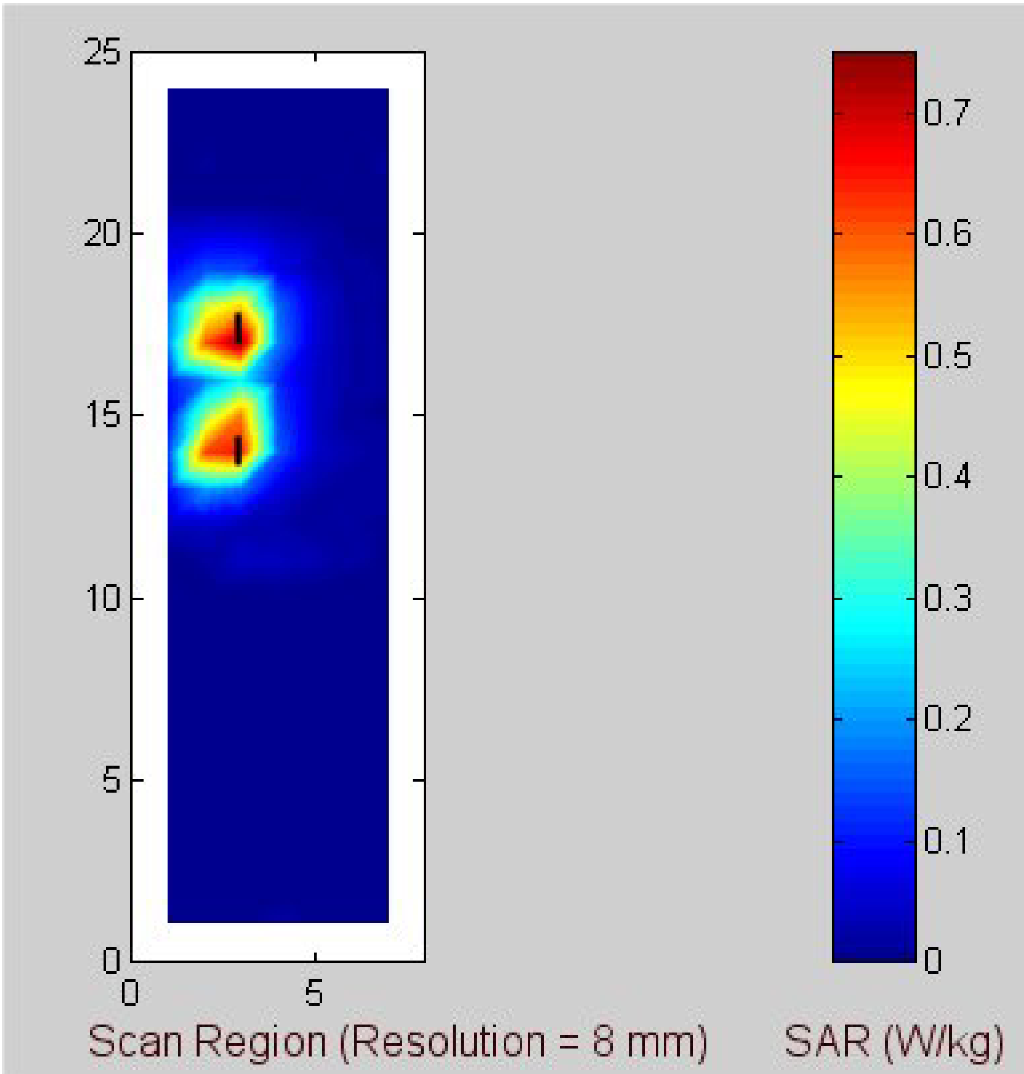

Fig. G.6. **Edge-on position (Configuration 2).** Coarse scan for the highest SAR region for the RF Micro Devices Cardbus Card Model DK5405. **Frequency = 5.32 GHz, normal mode.**

Table G.6. **Edge-on position (Configuration 2). Normal mode at 5.32 GHz**. The SARs measured for the RF Micro Devices Cardbus Card Model DK5405 inserted into Toshiba Model 1415-S173 Host Computer.

1-g SAR = 0.610 W/kg

a. At depth of 1 mm

1.284	1.585	1.744	1.544	1.436
1.343	1.791	2.021	1.869	1.615
1.450	1.919	2.175	2.009	1.693
1.332	1.717	1.907	1.863	1.660
1.220	1.554	1.774	1.728	1.518

b. At depth of 3 mm

0.578	0.719	0.798	0.750	0.705
0.619	0.815	0.931	0.899	0.800
0.675	0.885	1.011	0.954	0.824
0.628	0.802	0.908	0.892	0.799
0.571	0.733	0.826	0.811	0.727

c. At depth of 5 mm

0.243	0.301	0.338	0.342	0.326
0.268	0.346	0.398	0.405	0.373
0.298	0.380	0.436	0.421	0.374
0.280	0.351	0.402	0.398	0.359
0.254	0.328	0.363	0.359	0.330

d. At depth of 7 mm

0.110	0.132	0.149	0.157	0.152
0.126	0.157	0.177	0.184	0.173
0.142	0.171	0.193	0.187	0.169
0.132	0.160	0.181	0.179	0.164
0.122	0.156	0.171	0.169	0.158

e. At depth of 9 mm

0.062	0.072	0.080	0.079	0.077
0.074	0.087	0.094	0.094	0.089
0.083	0.095	0.102	0.094	0.085
0.074	0.088	0.096	0.092	0.087
0.073	0.090	0.100	0.099	0.091

APPENDIX H

VARIATION OF SAR AS A FUNCTION OF DEPTH Z IN THE LIQUID FOR LOCATIONS OF THE HIGHEST SAR (FROM TABLES G.1 TO G.6)

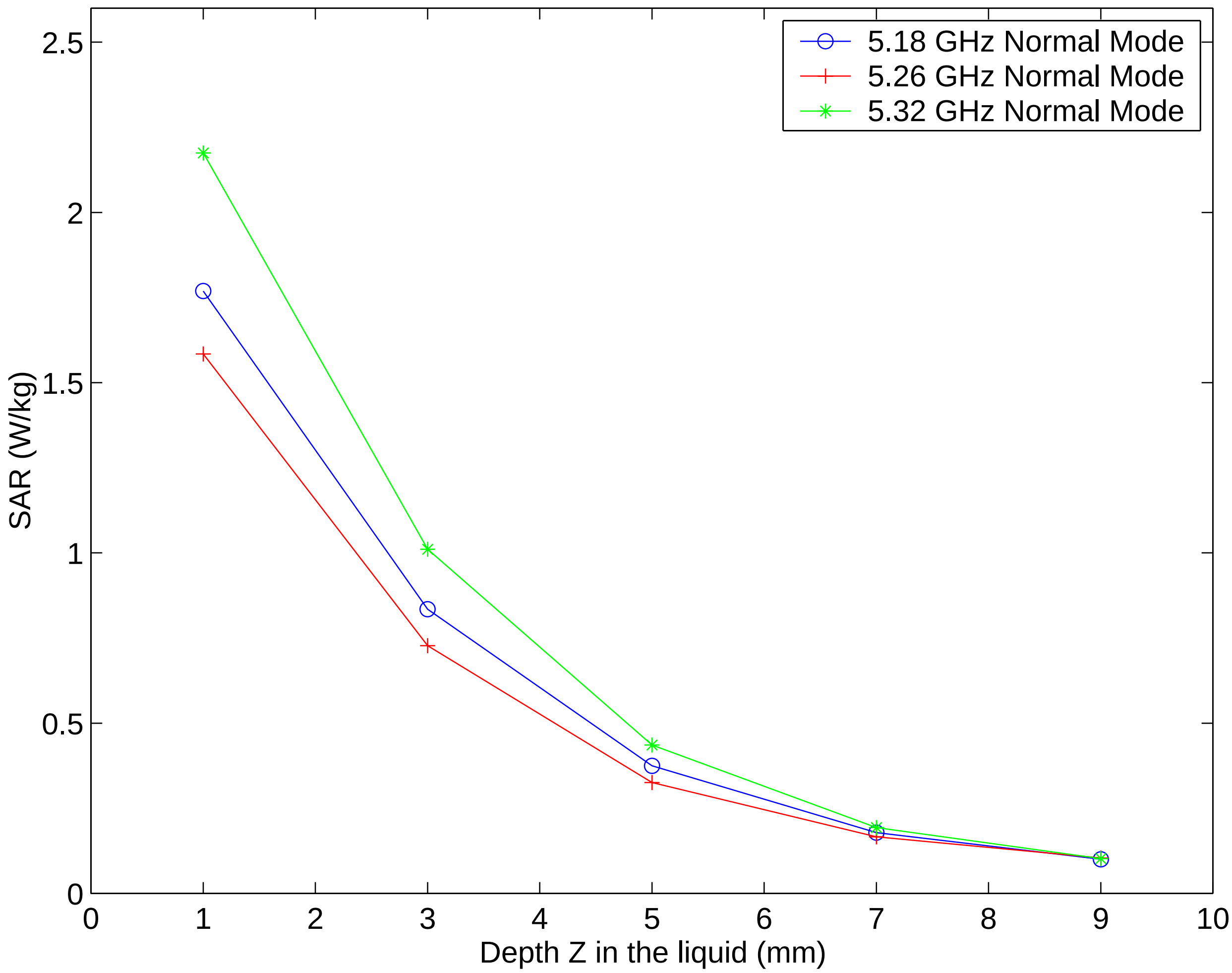

Fig. H.1. **Above-lap, Configuration 1.** Plot of the SAR variation as a function of depth Z in the liquid for locations of the highest SAR for the RF Micro Devices Cardbus Card Model DK5405 inserted into Toshiba Model 1415-S173 Host Computer (from Tables G.1 to G.3).

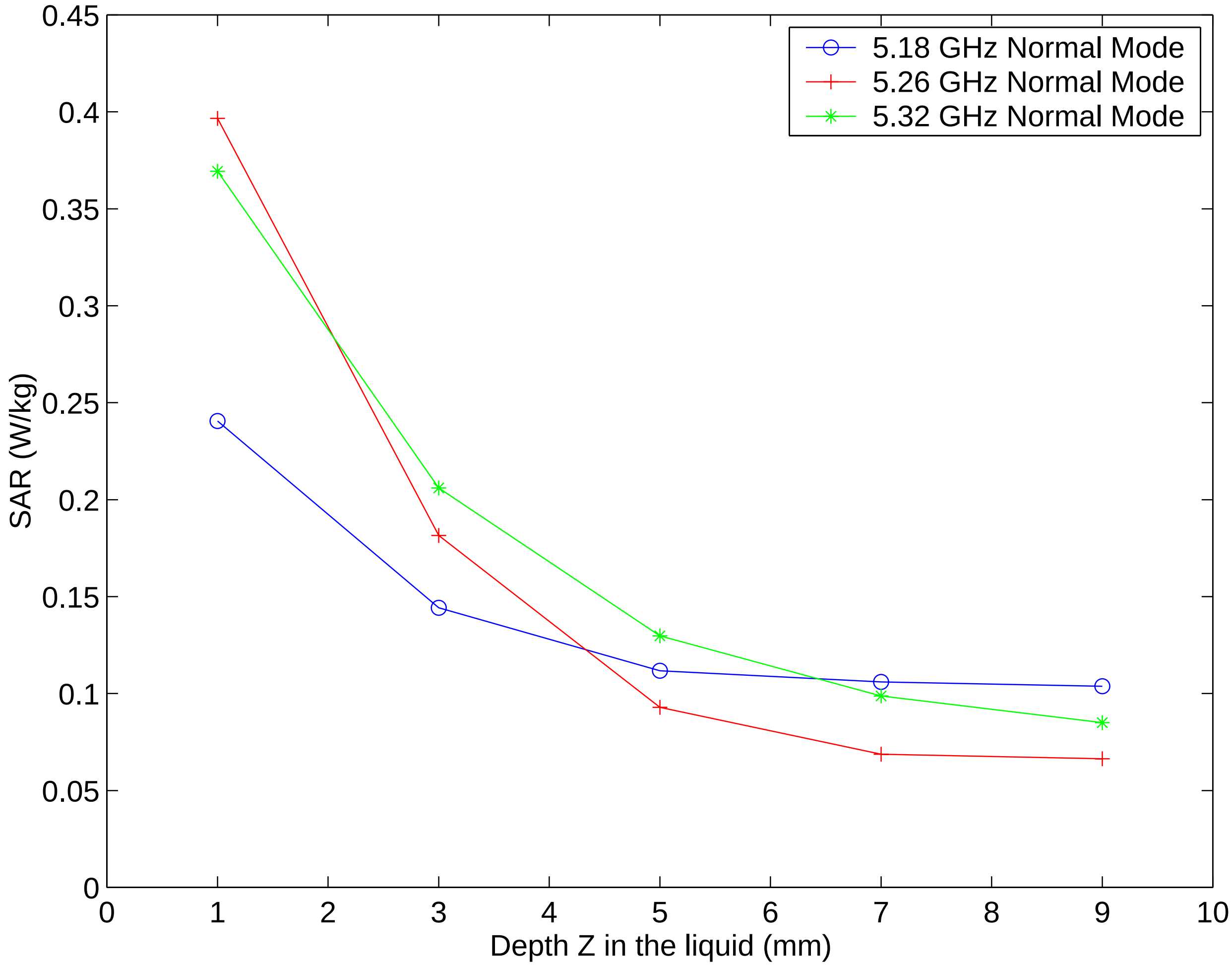

Fig. H.2. **Edge-on, Configuration 2.** Plot of the SAR variation as a function of depth Z in the liquid for locations of the highest SAR for the RF Micro Devices Cardbus Card Model DK5405 inserted into Toshiba Model 1415-S173 Host Computer (from Tables G.4 to G.6).